

LOGISTICS and PROCESSING REPORT

**of the
AIRBORNE MAGNETIC AND GEOTEM ELECTROMAGNETIC
MULTICOIL SURVEY**

**in
BERNALILLO, SANDOVAL and SANTA FE counties, NEW MEXICO**

**for the
U.S. GEOLOGICAL SURVEY**

*Job N° 319
August, 1997
Ottawa, Ontario*

geoterrex-dighem

TABLE OF CONTENTS

INTRODUCTION.....	1
SURVEY OPERATIONS.....	2
Location of the Survey Area	2
Aircraft and Geophysical On-Board Equipment	2
Base Station Equipment	4
Field Office Equipment	4
Survey Specifications	4
Survey Coverage	5
Tests and Calibrations.....	5
Field Crew	7
Production Statistics	7
QUALITY CONTROL AND COMPILATION PROCEDURES	8
In the Field	8
DATA PROCESSING IN THE OFFICE	9
Flight Path Recovery	9
Altitude Data (Radar and GPS).....	9
Diurnal Magnetism	9
Magnetism	10
Electromagnetism	10
FINAL PRODUCTS	13
Digital Archives	13
Profile Data	13
Maps.....	14

APPENDICES

- A** **Field Processing of the Data**
- B** **GEOTEM[®] Electromagnetic System**
- C** **GEOTEM[®] Interpretation Notes**
- D** **The Utility of Multicomponent Time-Domain
Electromagnetic Measurements**
- E** **Multicomponent GEOTEM[®] Modelling**
- F** **Archive Format Description**
- G** **Contents of CDT Grids**
- H** **Sample Parameter Table File**
- I** **Conversion of Data from pV/m^2 to ppm**
- J** **Production Log**



INTRODUCTION

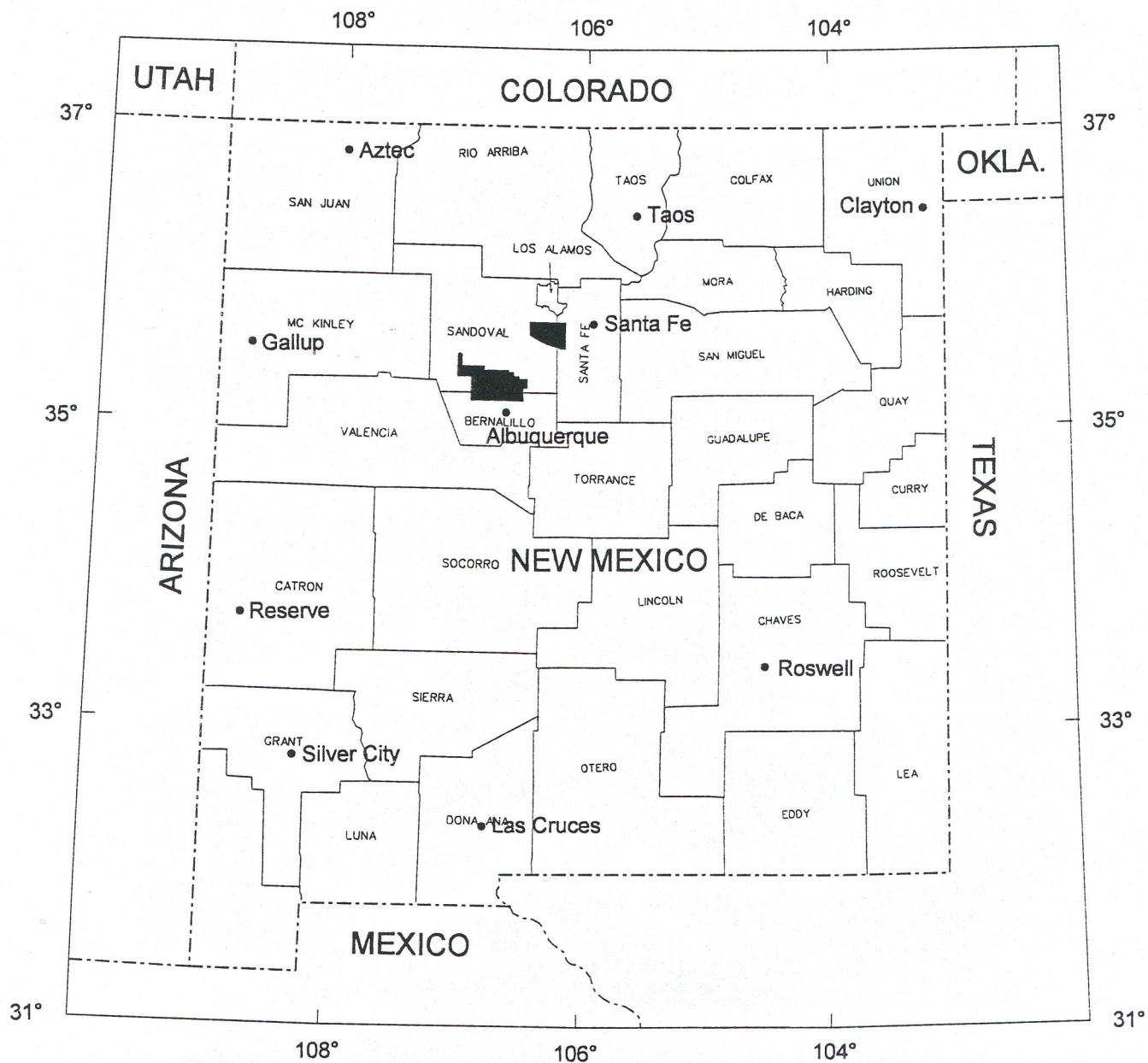
From February 18th to March 9th, 1997, an electromagnetic and magnetic survey was flown by Geoterrex-Dighem on behalf of the United States Geological Survey. Three areas were flown, namely the Cochiti Indian reservation, the Rio Rancho and the Rio Puerco blocks, in Bernalillo, Sandoval and Santa Fe counties, New Mexico. In all, 2338 line miles of data were collected.

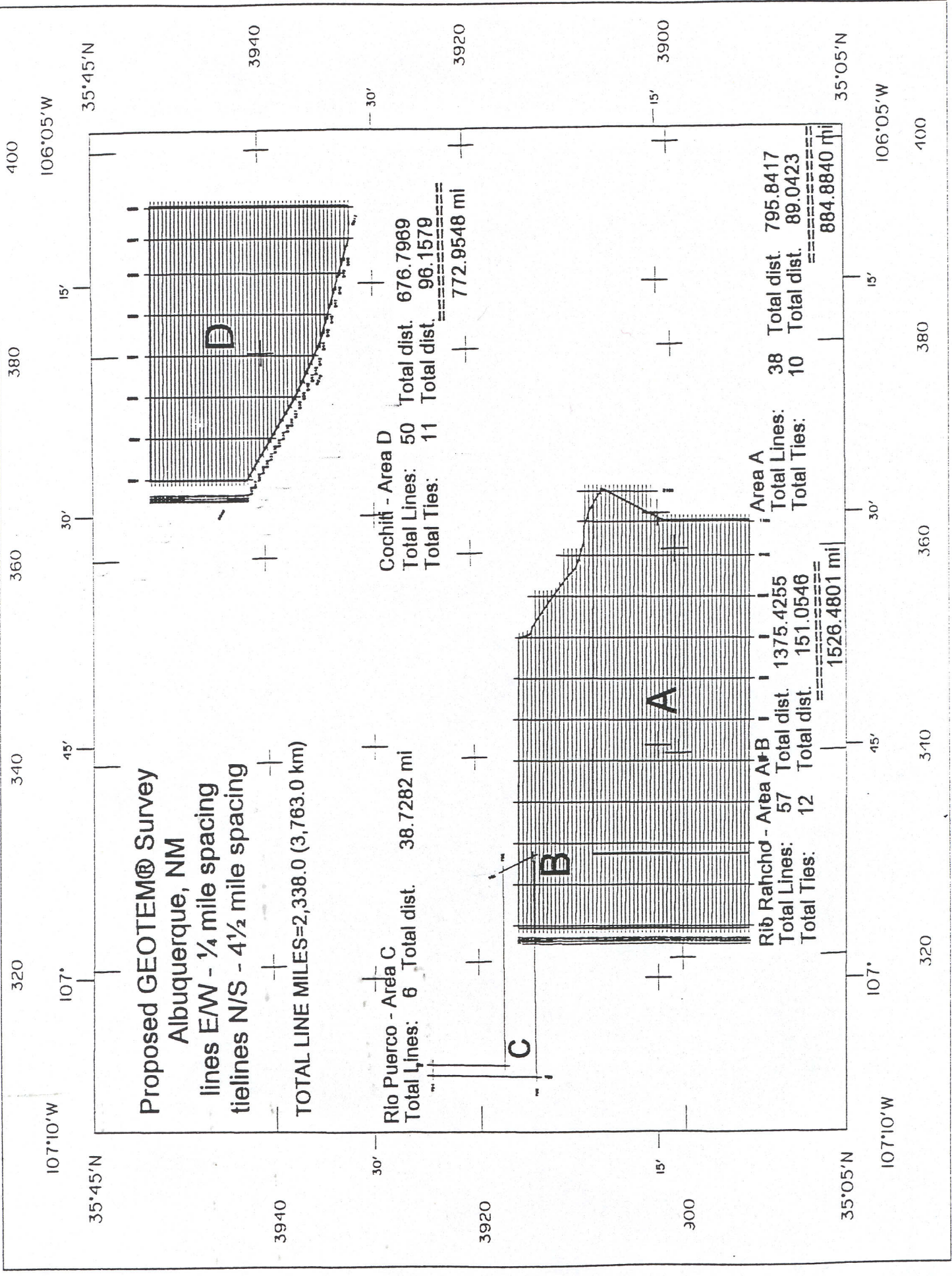
The survey data was compiled and processed in the Geoterrex-Dighem Ottawa office and is presented as maps of the total intensity magnetics with flight path, and the terrain clearance, multiparameter profiles, conductivity-depth-transform grids for each survey line and digital archive files.

SURVEY LOCATION

Cochiti Indian Reservation Rio Rancho area Rio Puerco reconnaissance lines

New Mexico







SURVEY OPERATIONS

Location of the Survey Area

The survey areas are in Bernalillo, Sandoval and Santa Fe counties, New Mexico. The Cochiti Indian reservation block is located west of Santa Fe; the Rio Rancho block is just north of Albuquerque; and the Rio Puerco test lines are located at the northwestern corner of the Rio Rancho block.

The base of operation was Albuquerque, New Mexico.

Aircraft and Geophysical On-Board Equipment

Aircraft	CASA C-212 twin turbo-prop.
Operator	Geoterrex-Dighem
Registration	C-FDPP
Survey Speed	125 knots/145 mph/65m/sec.
Magnetometer	Scintrex Cs-2 single cell cesium vapour, towed-bird installation, sensitivity = 0.01 nT ¹ , sampling rate = 0.1 sec., ambient range 20,000 to 100,000 nT. The general noise envelope was kept below 0.5 nT. Nominal sensor height of 73 metres above ground.
Electromagnetic system	GEOTEM multicoil system
	<u>System parameters</u>
	<i>Transmitter.</i> vertical axis loop of 232 m ² ,

¹ One gamma is equivalent to the S.I. unit nanotesla (nT).

metres.	<p>number of turns : 3, nominal height above ground of 120</p>																				
	<p><i>Receiver:</i> multicoil system (x, y and z) with a final recording rate of 4 samples/second, for the recording of 20 channels of x, y and z-coil data. Nominal height above ground of 70 metres, placed 125 m behind the centre of the transmitter loop.</p> <p><i>Base frequency:</i> 30 Hz</p> <p><i>Pulse width:</i> 4036 μs</p> <p><i>Pulse delay:</i> 130.2 μs</p> <p><i>Off-time:</i> 12501 μs</p> <p><i>Point value:</i> 130.2 μs</p> <p><i>Transmitter:</i> Current of 935 amperes, dipole moment of $6.5 \times 10^5 \text{Am}^2$.</p>																				
	<p><i>Receiver:</i> Window mean delay times in microseconds from the end of the pulse:</p> <table> <tr> <td>channel 1: 1106</td><td>channel 11: 9569</td></tr> <tr> <td>channel 2: 1432</td><td>channel 12: 11523</td></tr> <tr> <td>channel 3: 1822</td><td>channel 13: 846</td></tr> <tr> <td>channel 4: 2278</td><td>channel 14: 586</td></tr> <tr> <td>channel 5: 2864</td><td>channel 15: 390</td></tr> <tr> <td>channel 6: 3580</td><td>channel 16: 260</td></tr> <tr> <td>channel 7: 4427</td><td>channel 17: -455</td></tr> <tr> <td>channel 8: 5403</td><td>channel 18: -1757</td></tr> <tr> <td>channel 9: 6510</td><td>channel 19: -3059</td></tr> <tr> <td>channel 10: 7877</td><td>channel 20: -3841</td></tr> </table>	channel 1: 1106	channel 11: 9569	channel 2: 1432	channel 12: 11523	channel 3: 1822	channel 13: 846	channel 4: 2278	channel 14: 586	channel 5: 2864	channel 15: 390	channel 6: 3580	channel 16: 260	channel 7: 4427	channel 17: -455	channel 8: 5403	channel 18: -1757	channel 9: 6510	channel 19: -3059	channel 10: 7877	channel 20: -3841
channel 1: 1106	channel 11: 9569																				
channel 2: 1432	channel 12: 11523																				
channel 3: 1822	channel 13: 846																				
channel 4: 2278	channel 14: 586																				
channel 5: 2864	channel 15: 390																				
channel 6: 3580	channel 16: 260																				
channel 7: 4427	channel 17: -455																				
channel 8: 5403	channel 18: -1757																				
channel 9: 6510	channel 19: -3059																				
channel 10: 7877	channel 20: -3841																				
Digital Acquisition Analog Recorder	<p>Geoterrex-Dighem GEODAS.</p>																				
	<p>RMS GR-33, showing the total magnetic field at 2 vertical scales, the radar and barometric altimeters, the time-constant filtered traces of the x-coil channels 1 to 12 and the on-time channel 20, the raw traces of the x and z-coil channel 1 and 12, the EM primary field, the powerline monitor, the 4th difference of the magnetics, the x and z-coil earth's field monitors and the fiducials.</p>																				
Barometric Altimeter	<p>Rosemount 1241M, sensitivity 1 foot, 1 sec. recording interval.</p>																				

Radar Altimeter	TRT AHV-8, accuracy 2%, sensitivity one foot, range 0 to 2,500 feet, 1 sec. recording interval.
Camera	Panasonic colour video, super VHS, model WV-CL302.
Electronic Navigation	Sercel GPS receiver NR103, 1 sec. recording interval, with a resolution of 0.00001 degree and an accuracy of ± 10 m.

Base Station Equipment

Magnetometer:	Scintrex H8 single cell split beam cesium vapour, mounted in a magnetically quiet area, measuring the total intensity of the earth's magnetic field in units of 0.01 nT at intervals of 1 second, within a noise envelope of 0.10 nT.
GPS Receiver:	SERCEL NR103 V2.3, measuring all GPS channels, for up to 10 satellites.
Computer:	Toshiba laptop, model T4600, 33 MHz, 486.
Converter:	Picodas, model MEP710 3/10901 GTS 780008.
Printer:	Kodak Diconix 150 plus.
Battery Backup:	

Field Office Equipment

Video Playback:	Panasonic Super VHS with an 8" BRULE Colour Monitor.
Computer:	Dell Latitude LM laptop with 800 MB hard drive.
Plotter:	Design Mate 24" Calcomp with multiple colours and pen types, quality - 2000 steps/inch.
Printer:	Hewlett Packard Deskjet 660C.
DAT Tape Drive:	Conner, 90 metre tapes (1300 MG).
Hard Drive:	Seagate 4 gigabyte

Survey Specifications

Altitude:	The survey was flown at a mean terrain clearance of 120 metres.
------------------	---

The altitude tolerance was limited to ± 15 m, not to be exceeded over a distance greater than 3 km, unless required for safety or air regulations.

Traverse Lines: Spacing of 400 m, direction E-W.

The separation between flight lines was not to exceed 600 m over a distance greater than 4500 m.

Control lines: Spacing of 7250 m, direction N-S.

Diurnal variation: Acceptable variations were limited to 7.5 nT deviations from a one minute chord.

Noise levels: The noise level on the magnetic data was not to exceed ± 0.25 nT over a distance greater than 3 km.
The noise level on the electromagnetic data was not to exceed ± 30 ppm over a distance greater than 3 km, as displayed on the analogue traces of the late-time x-coil channels.

Lines or portions of lines flown during any of the above deviations were reflown. These reflights began and ended by crossing control lines and overlapping good data.

Survey Coverage

In the Cochiti area, 773 line miles of data were collected.

In the Rio Rancho area, 1526 line miles of data were collected.

In the Rio Puerco area, only 39 line miles of data were collected. These were for general reconnaissance purposes.

Tests and Calibrations (flown from the Sierra Vista airport, March 14, 1997)

System lag for the Magnetic and Electromagnetic response

A suite of lines were flown over a bridge, near the airport, along bearings 140° and 320° , and checked against the video positions to verify the system lag of the magnetic and EM response.

The average system lag from all passes were as follows:

Magnetics: 3.6 seconds

Electromagnetics: 4.0 seconds

A sample of the response over the bridge is provided in figure 1.

GPS Accuracy check (cloverleaf)

The accuracy of the GPS navigation system and its synchronization with the on-board video system was verified by flying a cloverleaf pattern at survey altitude over the basestation GPS antenna, set-up at the Sierra Vista airport (Easting of 563741, Northing of 3495176, datum Clarke 1866).

Control from the video:

<u>Pass</u>	<u>Dir</u>	<u>Altitude</u>	<u>Eiducial</u>	<u>Video Position</u>
1	W	380 ft	61181.55	3 m N of mark
2	E	381 ft	61319.75	1 m N of mark
3	W	380 ft	61491.85	4 m N of mark
4	E	383 ft	61624.85	1 m S of mark
5	S	383 ft	61841.35	8 m W of mark
6	N	431 ft	61959.98	7 m E of mark
7	S	392 ft	62171.50	5 m W of mark
8	N	406 ft	62329.35	5 m E of mark

Results after post flight differential corrections applied:

Scatter of solutions inside an error box of 15 x 20 metres.

Offset of mean position from all passes relative to the mark is less than one metre.

Synchronization difference of the GPS position and the video image is 0.5 second.

Figure 2: Sketch of the calibration site

Figure 3: Trajectory of the aircraft over the calibration site

Altimeter Calibration

A series of altitude passes were flown over the runway (elevation of 4612 feet above sea level), ranging from 300 to 800 feet terrain clearance, as monitored by the on-board radar altimeter.

Figure 4 shows the relationship of the barometric elevation (as measured by the GPS receiver) and the radar altitude (adjusted for the runway elevation). The plot shows a good linear relationship with a correlation factor of 0.913. The increased spreading of points with the increase in altitude reflects the apparent shift between the radar and barometric altimeters when the aircraft is banked and turning. The barometric information displays true information,

while the radar indicates an exaggerated height since the beam is no longer focused directly beneath the aircraft, but at an angle away from it.

Figure 5 explains this discrepancy between the radar and barometric altitudes more clearly. The "peaks" represent the aircraft in turnarounds, with the radar trace displaying a greater deviation; the "troughs" represent the aircraft returning to straight and level flying over the runway between turnarounds. The areas of straight and level flying (troughs) are the only regions where the direct comparison of the radar and barometric elevation is valid.

Field Crew

The base of field operations was Albuquerque, New Mexico.

Pilots:	G. Stonehouse, G. Mueller, D. Wiens, M. Mellett
Electronics Operators:	D. Patzer, R. Penton, J. Moore
Engineer:	R. Constapel
Geophysicist:	R. Williams

Production Statistics

Flying was done between February 18th and March 9th, 1997.

- Total production: 3762 km
- Number of production flights: 16
- Hours of production flying: 42.7 hours
- Number of km/hour of production flying: 88.1 km/hr.
- Number of km/average production flight: 235 km
- Number of hours/average production flight: 2.7 hours
- Number of days lost to:
 - Equipment: 1
 - Weather: 4.5
 - Testing: 0.5
 - Pilot training and/or rest: 5

USGS Geotem Survey, Arizona

Mag & Em lag check

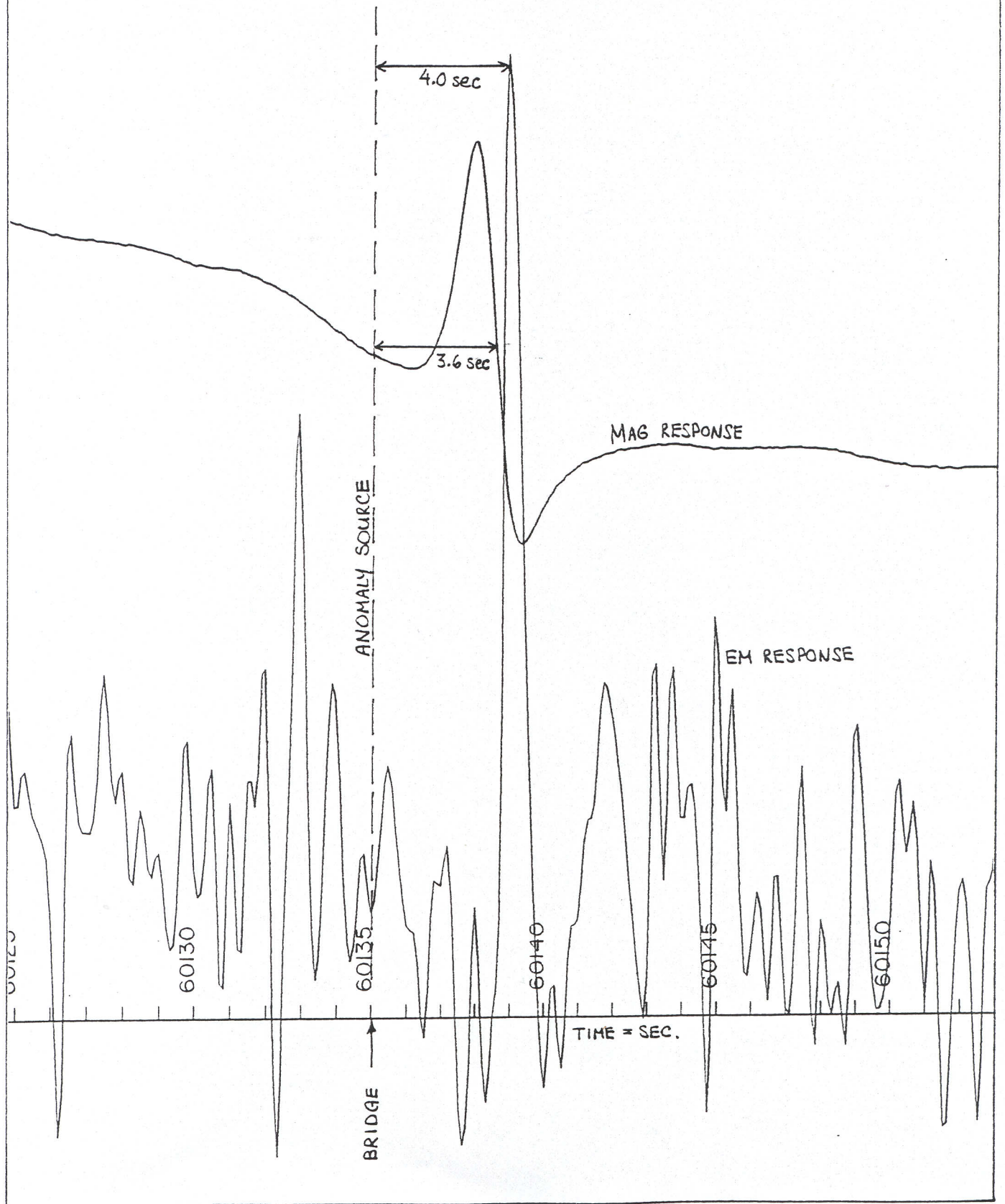


FIGURE 1

U.S.G.S Geotem Survey, Arizona

GPS ACCURACY CHECK Sierra Vista Airport

⊙ Location of mark (Clarke 1866)

UTM-X = 563741 metres

UTM-Y = 3495176 metres

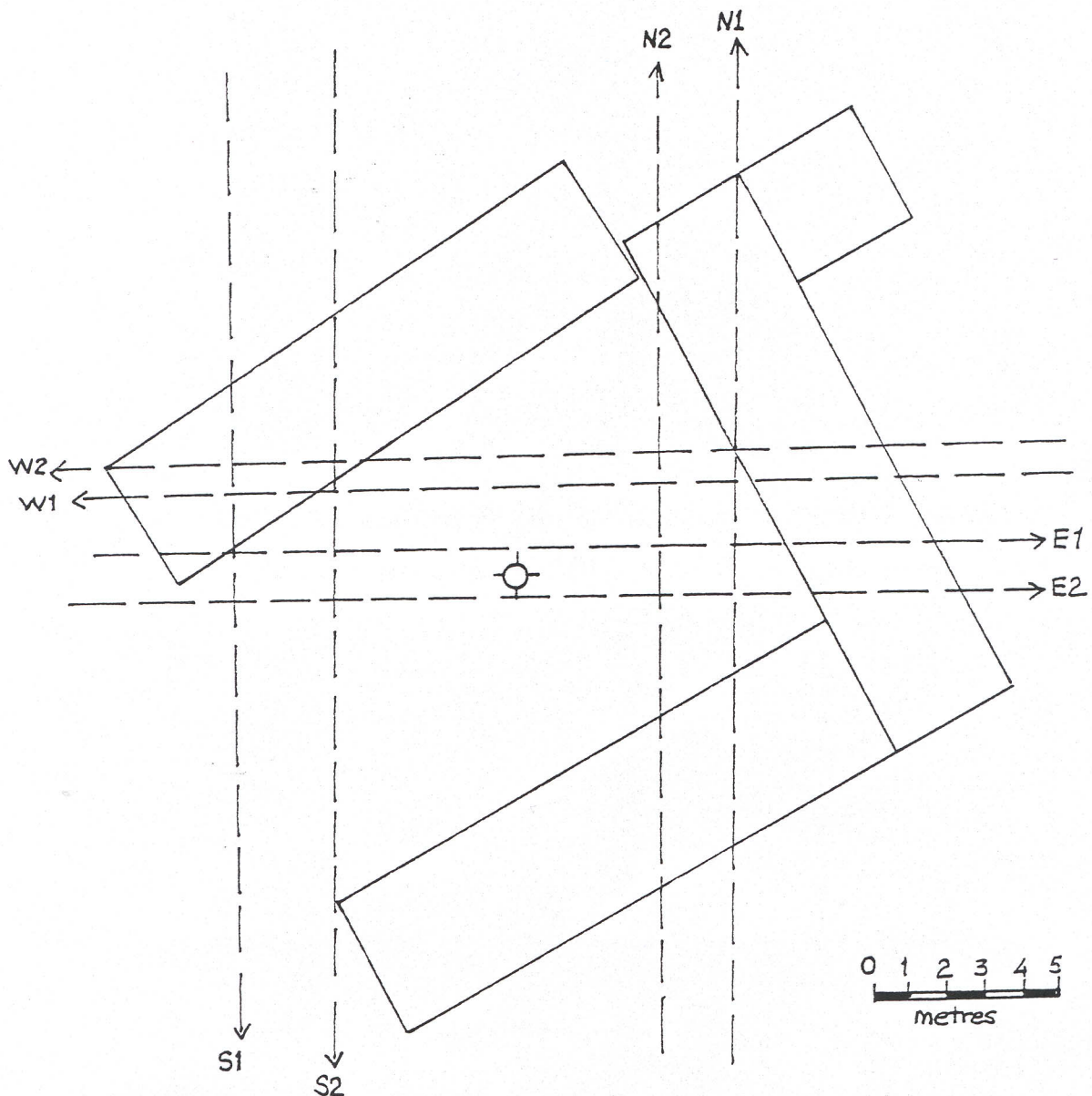


FIGURE 2

USGS Geotem Survey, Arizona

GPS ACCURACY CHECK Sierra Vista Airport

⊕ = Location of reference mark

• = Video position from each pass

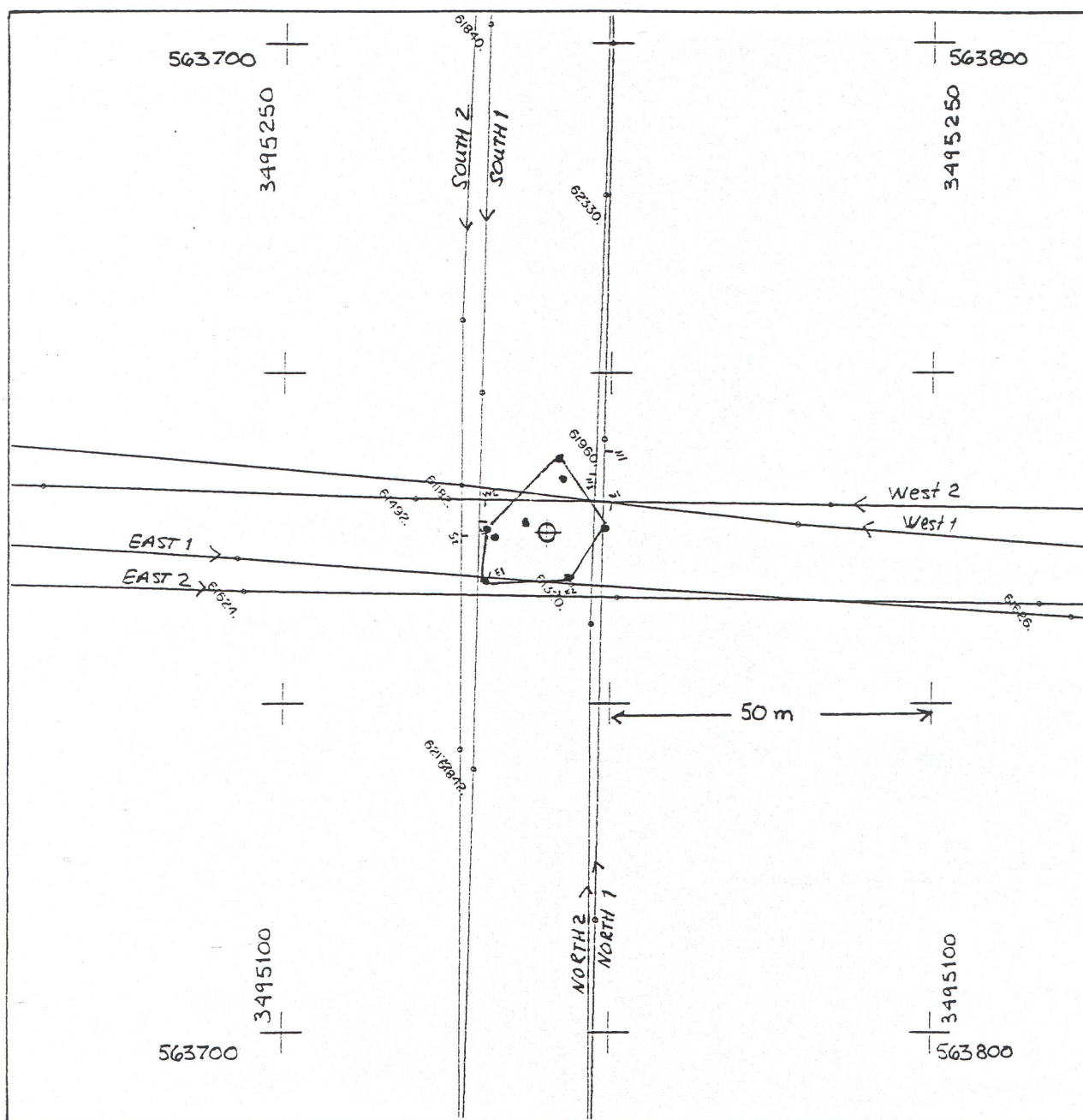


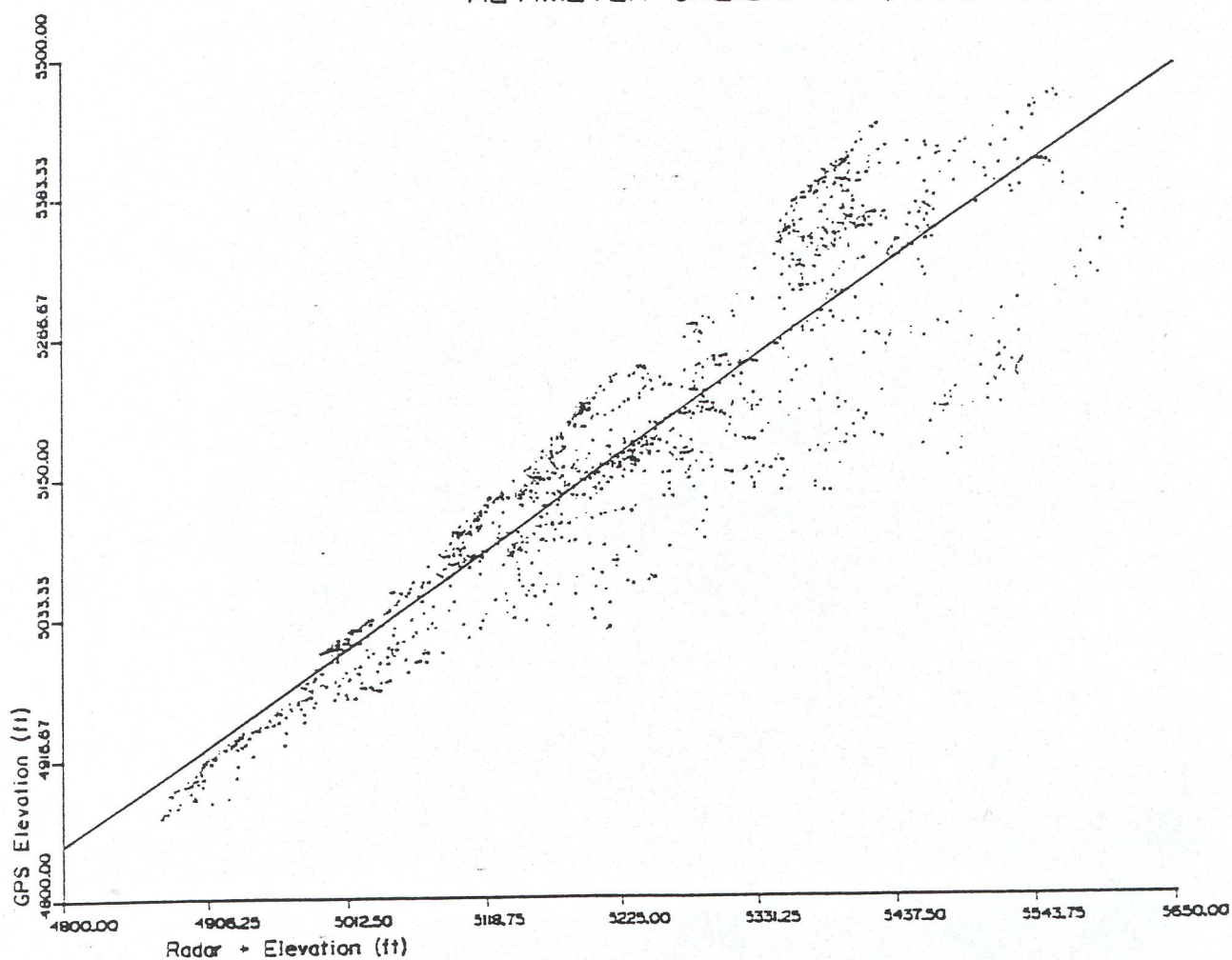
FIGURE 3

USGS Geotem Survey, Arizona

Altimeter Calibration Sierra Vista Airport

Runway elevation = 4612 feet

ALTIMETER CALIBRATION, JOB 356



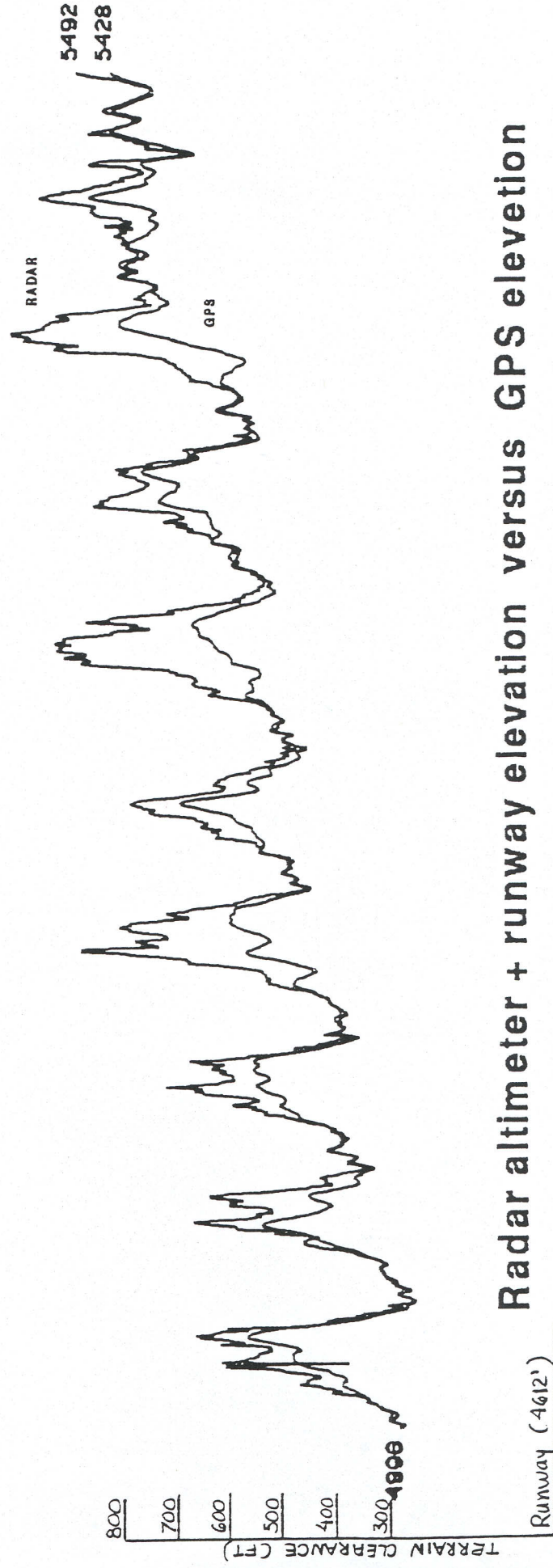
JOB NUMBER = 356
CORRELATION = 0.912692

SLOPE OF LINE = 0.7612
Y - INTERCEPT = 1192.16

FIGURE 4

ALTIMETER CALIBRATION

Sierra Vista, Arizona



Radar altimeter + runway elevation versus GPS elevation



QUALITY CONTROL AND COMPILATION PROCEDURES

In the Field

After each flight, all analog records were examined as a preliminary assessment of the noise level of the recorded data. Altimeter deviations from the prescribed flying altitudes were also closely examined as well as the general condition of the diurnal activity, as recorded on the base stations.

All digital data were verified for validity and continuity. The data from the aircraft and base station was transferred to the PC's hard disk. Basic statistics were generated for each parameter recorded; these included the minimum, maximum and mean values, the standard deviation and any null values located. Editing of all recorded parameters for spikes or datum shifts was done, followed by final data verification via an interactive graphics screen with on-screen editing and interpolation routines. Any of the recorded parameters could be plotted back at a suitable scale on the field pen plotter.

The quality of the navigation was controlled on a daily basis by recovering the flight path of the aircraft. The Trajecto correction procedure employs the raw ranges from the base station to create improved models of clock error, atmospheric error, satellite orbit, and selective availability. These models are used to improve the conversion of aircraft raw ranges to aircraft position. The Trajecto-corrected GPS was plotted back daily in the field on the pen plotter and checked for speed busts.

Checking all data for adherence to specifications was carried out in the field by the Geoterrex-Dighem field operations manager/data technician.

More details on the individual processing steps applied to each parameter are given in Appendix A of this report.

IV

DATA PROCESSING IN THE OFFICE

Flight Path Recovery

Data used: GPS positions recalculated from the recorded raw range data, differentially corrected and converted to UTM metres.

Final positions:

Projection: Universal Transverse Mercator

Central meridian: 109°W

False Easting: 500,000 metres

False Northing: 0 metres

Scale factor: 0.9996

Spheroid: Clarke 1866

Altitude Data (Radar and GPS)

Noise editing: Alfatrims median filter used to eliminate the 2 high and 2 low values from the statistical distribution of a 9 point sample window.

Noise filtering: Triangular filters set to remove radar wavelengths less than 6 seconds and amplitudes below 25 feet; and GPS wavelengths up to 4 seconds and amplitudes up to 2.5 metres.

Gridding: A grid of the terrain clearance was produced from the radar altimeter values, as a general reference for evaluation of the survey results.

Diurnal magnetics

Noise editing: Alfatrims median filter used to eliminate the 2 high and 2 low values from the statistical distribution of a 9 point sample window.

Culture editing: Polynomial interpolation via a graphic screen editor.

Noise filtering: Triangular filter set to remove wavelengths of less than 4 seconds and amplitudes up to 0.5 nT.

Extraction of long wavelength component: Low pass filter set to retain only wavelengths of greater than 50 seconds.

Magnetics

Lag correction: 3.6 seconds

Noise editing: 4th difference editing routine set to remove spikes of greater than 0.5 nT, followed by an alftrim median filter eliminating 2 high and 2 low value from its calculation over a 9 point window.

Noise filtering: Triangular filter set to remove noise events having a wavelength of less than 0.5 second and an amplitude of less than 0.3 nT.

Diurnal subtraction: The long wavelength component of the diurnal (greater than 50 seconds) was removed from the data, prior to the levelling analysis.

Levelling: The levelling consisted of applying a micro-levelling routine to the gridded data to remove small residual effects. The difference in the gridded datasets before and after the application of the micro-levelling routine were computed and extracted along the original survey lines to be stored in the final line dataset as the final magnetic compensation values.

Gridding: The data was gridded with a 25 m grid cell size, using a minimum curvature routine.

Regional: The regional values were computed from the 1995 coefficients for the date of 1997.16 at an elevation of 1900 m a.s.l.

Electromagnetics

Lag correction: 4.0 seconds

Data correction: The x, y and z-coil data were processed from the 20 raw channels recorded at 4 samples per second.

The EM data measured by the three coils, x, y and z, is collected in pv/m^2 which is an unnormalized value permitting a direct comparison of the signal between the three coil sets. The conversion of the data from pv/m^2 to ppm is a function of the effective area of each coil and the voltage of the primary signal received by each coil. The effective area of the coil is identical for all coils, but the value of the primary field voltage differs for each coil due to coupling effects such that the derived ppm value becomes a relative value for a particular coil set only. If quantitative analysis of the data is required, where the response from the different coil sets are to be referenced to each other, then the data should be left in unnormalized pv/m^2 units which is the true representation of the signal measured.

For the current configuration of 30 Hz with a 4 ms pulse, the correspondence between pv/m^2 and ppm is roughly:

- 28:1 for the x-coil;
- 16:1 for the z-coil; and
- 2:1 for the y-coil.

The final data is archived in pv/m^2 but the conversion factors to normalized the data back to ppm are given in a table in Appendix I. The conversion factors vary slightly from one flight to the next reflecting small variations in the received primary field from day to day.

The following processing steps were applied to the channel data from all coil sets:

- a) the data from channels 1 to 16 (off-time) and 20 (on-time) were corrected for drift in flight form (prior to cutting the recorded data back to the correct line limits) by passing a low order polynomial function through the baseline minima along each channel, via a graphic screen display;
- b) the data were edited for residual spheric spikes by examining the decay pattern of each individual EM transient. Bad decays (i.e. not fitting a normal exponential function) were deleted and replaced by interpolation;
- c) for the x and z-coils only, the data were initially corrected for incoherent, non-decaying low frequency noise events by analyzing the decay information through decay constant calculations, in order to separate the true signal from the low-frequency noise.
An adaptive filter was then applied to the data. This filter responds to local changes in the gradient in order to select and apply an appropriate time domain convolution ranging from very narrow to wide, depending on the local character of the anomaly. The suite of filters selected were aimed at noise frequencies ranging from 2 Hz to 0.18 Hz;
- d) for the y-coil data, spikes were removed using an alftrim median filter to isolate extreme high and low values. This was followed by the application of a small running average filter.
An adaptive filter was then applied to the data. This filter responds to local changes in the gradient in order to select and apply an appropriate time domain convolution ranging from very narrow to wide, depending on the local character of the anomaly;
- e) the filtered data from the x, y and z-coils were then re-sampled to a sample rate of 5 samples/sec and combined into a common file for archiving.

Decay constant calculation: An off-time decay constant was calculated by fitting the channel information to an exponential function. The decay constant was calculated using channels 2 to 12 from the z-coil data (mean delay times of 1432 to 11,523 μ sec). This parameter was provided in preliminary form only for the purpose of assessing the general EM response over the survey blocks.

Conductivity-Depth-Transform (CDT): Conductivity-Depth-Transforms were computed along each survey line, resulting in a vertical pseudo-section of resistivity values. In this calculation, the complete waveform (all 20 channels) is used, fitting the combined data from the x and z-coils to a layered earth model. The derived resistivity grid values are then adjusted such that the top of the grid reflects the true terrain topography.

For the **Cochiti block**, the maximum depth of investigation was set at 1300 m from a reference barometric elevation of 2500 m.

For the **Rio Rancho block**, the maximum depth of investigation was set at 1100 m from a reference barometric elevation of 2200 m.

For the **Rio Puerco reconnaissance lines**, the maximum depth of investigation was set at 1000 m from a reference barometric elevation of 2300 m.

Further description on the content of the CDT grids and their format is given in Appendix G.

Information on the CDT algorithm itself is given in the article published by P. Wolfgram and G. Karlik, in *Exploration Geophysics*, 1995, vol. 26, pp. 179-185.

Additional Reference grids: The following data grids were also generated for each survey block as a general reference when evaluating the dataset:

- amplitude of the x-coil channel 2;
- amplitude of the x-coil channel 6;
- amplitude of the x-coil channel 10;
- amplitude of the z-coil channel 2;
- amplitude of the z-coil channel 6;
- amplitude of the z-coil channel 10.

V

FINAL PRODUCTS

Digital Archives

The line data are archived in 3 files having standard ASCII format. The 1st file contains a flight line identification, eastings and northings and the 20 channels of processed x, y and z-coil data. The 2nd file is the same as the 1st except having the raw data. The 3rd file contains all the magnetic, altimeter and other secondary data as described in Appendix F (Archive Format Description).

The gridded data are archived in GEOSOFT ASCII format as a .GXF file. There are grids of channels 2, 6, 10, x and z-coil, magnetics, radar altimeter and the individual CDT grids for each survey line.

Profile Data

1 set of multiparameter profiles displaying the following information at a horizontal scale of 1:24,000, on paper.

- Radar altimeter
- EM Primary field
- Residual magnetics
- 12 off-time x-coil channels
- 12 off-time y-coil channels
- 12 off-time z-coil channels
- Hz monitor

Maps

1 set of maps at 1:100,000 scale, presented on a clear UTM base with flight path.

- Total Field magnetic contours; delivered as 3 mylars
- Terrain Clearance contours; delivered as 1 mylar

Note: Also delivered were the digital reference EM waveform (parameter table) for each flight (a sample is included in Appendix H) and the digital data from the pre-survey tests and calibration in GEOSOFT ASCII format.

Appendix A

Field Processing of the Data

Flight Path Recovery

1. Recover GPS data from base station.
2. Recover GPS data from aircraft file.
3. Combine base station and aircraft GPS data to a common file.
4. Apply differential corrections and compute Lat/Long fixes from the raw range data (TRAJECTOGRAPHY); GPS lag of 0.5 sec used.
5. Change spheroid from WGS84 to Clarke 1866 using the following offsets:
Dx = 8 m
Dy = -163 m
Dz = -180 m
6. Convert Lat/Long fixes to UTM metres, using the following:
Central meridian: 105°W
False Easting: 500,000
False Northing: 0
Scale factor: 0.9996
Ellipsoid: Clarke 1866
7. Compute speed from resulting positions to check for irregularities, time gaps, etc.

Correction of Altimeter Data

1. Recover altimeter data from aircraft file.
2. Convert radar and GPS altitude data to feet and cm respectively.
3. Remove spikes from the radar and GPS data using an alftrim median filter to isolate the 2 extreme values (high or low) of a statistical distribution based on a window of 9 points.
4. Apply triangular convolutions to the altimeter data; aimed at wavelengths of 4 seconds or less and amplitudes of 2.5 m, or less for the GPS and wavelengths of 6 seconds or less and amplitudes of 25 feet or less for the radar.

Processing of Magnetic Data from the Base Station

1. Recover magnetic data from the base station.
2. Edit the ground data for spikes, isolating the 2 extreme values out of a 9 point distribution (alfatrim median filter).
3. Remove culture events (when applicable) by polynomial interpolation via a graphic display/editing routine.
4. Apply a triangular smoothing convolution, aimed at removing wavelengths of 4 seconds or less with amplitudes of 0.5 nT or less.
5. Extract long wavelength component of the data (greater than 25 seconds) with a low pass filter, to be subtracted from the air data.

Processing of Magnetic Data from the Aircraft

1. Recover data at full 10 samples/sec.
2. Adjust readings for a system lag of 3.6 seconds (36 samples).
3. Edit data for spikes using a fourth difference routine, set for spikes of greater than 0.5 nT.
4. Apply triangular smoothing convolution, aimed at removing wavelength of less than 0.5 seconds with amplitudes less than 0.3 nT.
5. Remove the long wavelength component of the diurnal data (greater than 25 seconds).
6. Add back the mean value of the diurnal field.
7. Grid the resulting magnetic values, image and check for irregularities.

Processing of GEOTEM Multicoil Data

1. Recover x, y and z-coil data in full flight format; x and z-coil channels at 4 samples/second.
2. Adjust readings for a system lag of 4.0 seconds (16 samples).
3. Review baseline positions for every channel of x and z-coil data via a graphic screen display and remove any visible drift component when required by graphically reconstructing and subtracting a low order polynomial. This procedure is only followed in resistive terrains when background "no response" sections along lines can be observed.
4. Isolate and remove, by interpolation, spheric events which are located in the data by analyzing the decay pattern at each sample point. All bad samples identified are labelled in the flag field. A decay threshold of 400 ppm was used, with the correction of no more than 2 consecutive samples allowed.
5. Remove any remaining small spikes in the data (x and z-coil channels) by using an alftrim median filter to isolate the extreme value (high or low) of a statistical distribution based on a window of 5 sample points.
6. Correct the data for low frequency, incoherent noise elements (that do not correlate from channel to channel) in the data, by analyzing the decay patterns of channels 9 to 20 (OMEGA process). Decay threshold of 180 ppm used and the RMS error in fitting stored.
7. Noise filtering done using an adaptive filter technique based on time domain triangular

operators. Using a 2nd difference value to identify changes in gradient along each channel, minimal filtering (3 point convolution) is applied over the peaks of the anomalies, ranging in set increments up to a maximum amount of filtering in the resistive background areas (29 points for the z-coil data and 31 points for the x-coil data).

Creation of Final Files

1. Processed positioning, altimeter, magnetic and GEOTEM x, y and z-coil data is cut-back from flight form to survey line limits, re-sampled and combined into a common file at 5 samples/sec.
2. EM anomalies are automatically selected (using channel 6 as reference) and fitted to the vertical plate model to derive the conductivity-thickness product and the depth to source.
3. The automatic anomaly selection is reviewed and updated interactively via a graphic screen display/editing routine.

Field Products

1. Decay Constant from z-coil at 1:100,000 scale, deherringboned.
2. Preliminary total magnetic field contour map with flight path at 1:100,000 scale.

Appendix B

GEOTEM[®] EM System

GEOTEM® ELECTROMAGNETIC SYSTEM

General

The operation of a towed-bird time-domain electromagnetic system (EM) involves the measurement of decaying secondary electromagnetic fields induced in the ground by a series of short current pulses generated from an aircraft-mounted transmitter. Variations in the decay characteristics of the secondary field (sampled and displayed as channels) are analyzed and interpreted to provide information about the subsurface geology. The response of such a system utilising a vertical-axis transmitter dipole and a horizontal-axis receiver coil has been documented by various authors including Palacky and West (1973, *Geophysics*, v. 38, p. 1145-1158).

The principle of sampling the induced secondary field in the absence of the primary field (during the "off-time") gives rise to an excellent signal-to-noise ratio and an increased depth of penetration compared to conventional continuous wave (frequency domain) electromagnetic systems. Such a system is also relatively free of noise due to air turbulence.

Through free-air model studies using the University of Toronto's Plate and Layered Earth programs it may be shown that the "depth of investigation" depends upon the geometry of the target. Typical depth limits would be 250 m below surface for a homogeneous half-space, 350 m for an inductively thin sheet or 200 m for a large vertical-plate conductor. These depth estimates are based on the assumptions that a significant response is recorded 1.4 ms after the primary field is turned off and that the overlying or surrounding material is resistive. If a preselected range of channels is deemed adequate to detect or resolve a given target, then the depth of investigation increases significantly.

In addition to substantial penetration, time-domain systems respond to a wide range of conductors. With measurements taken during off-time, significant effects are seen for values of 0.8 s or greater, thus responding to the majority of geological features deemed relevant in most exploration projects and many mapping applications.

The method also offers very good discrimination of conductor geometry. This ability to distinguish between flat-lying and vertical conductors combined with excellent depth penetration results in good differentiation of bedrock conductors from surficial conductors.

Most of the preceding discussion concerns theoretical responses for all time-domain installations of similar geometry. The factor which distinguishes the various systems is their ability to faithfully and completely represent the secondary field response.

Equipment Procedure

GEOTEM® (GEOterrex Transient ElectroMagnetic system) is a time-domain towed-bird electromagnetic system incorporating a high-speed digital EM receiver. The primary electromagnetic pulses are created by a series of discontinuous sinusoidal current pulses fed into a three-turn transmitting loop surrounding the aircraft and fixed to the nose, tail and wing tips. The base frequency rate is selectable: 75, 90, 125, 150, 225 and 270 Hz. The standard system configuration (150 Hz, equivalent to 300 bipolar pulses per second) delivers a half-sine current pulse lasting 1030 μ s followed by 2303 μ s off-time. Present peak current through the loop is 600 A resulting in a primary magnetic dipole moment of $4.5 \times 10^6 \text{ A.m}^2$. Optionally, the system can be reconfigured to generate a half-sine pulse lasting up to 1700 μ s.

The receiver is an induction coil with a ferrite core. The receiving coil axis is aligned in the flight direction and mounted horizontally in a bird which is towed by the aircraft on a 135-metre cable. A non-magnetic tow cable is used to reduce noise levels. Mean terrain clearance for the aircraft is

120 m with the EM bird being situated nominally 56 m below and 123 m behind the aircraft.

For each primary pulse a secondary magnetic field is produced by decaying eddy currents in the ground. These in turn induce a voltage in the receiver coil which provides a measure of the electromagnetic field.

The measured signals pass through anti-aliasing filters and are then digitized with an analog-to-digital (A/D) converter at sampling rates of up to 40 kHz. The digital data flows from the A/D converter into an array processor where all the numerically intensive processing tasks, such as Fourier analysis, are carried out. The array processor is under the control of a multi-tasking minicomputer which provides all of the software management.

Operations which are carried out in the receiver are:

1. *Compensation:* During flight, the transmitter creates eddy currents within the structure of the aircraft that have a measurable effect at the bird. Compensation for this signal is implemented numerically within the receiver by a statistical analysis of the signal detected at the bird in absence of ground response (i.e., achieved by flying at an altitude such that no ground response is detectable). The observed signal is used to define a compensation signal which is removed from the observed signal to produce a null and thus effectively buck out any response due to the aircraft.
2. *Normalization:* All EM response channels are automatically calibrated and reduced to parts per million (ppm) of the primary field in the receiver. This is achieved by dividing the measured voltage by the voltage induced by the primary field at the bird.
3. *Transient Analysis:* Harmonic analysis permits the separation of specific types of noise from the signal in real time.
4. *Digital Stacking:* Stacking is carried out to reduce the effect of broadband noise on the data. Stacking time is 120 ms in areas where 50 Hz power lines are used and 133 ms where they are 60 Hz.
5. *Windowing of data:* The GEOTEM® digital receiver samples the secondary and primary electromagnetic field at 128 points per EM pulse and windows the signal in up to 20 time gates whose centres and widths are software selectable and which may be placed anywhere within or outside the transmitter pulse. This flexibility offers the advantage of arranging the gates to suit the goals of a particular survey, ensuring that the signal is appropriately sampled through its entire dynamic range.
6. *Power Line Filtering:* Digital comb filters are applied to the data during real-time processing to remove power line interference while leaving the EM signal undisturbed. The RMS power line voltage (at all harmonics in the receiver passband) are computed, displayed and recorded for each data stack.
7. *Primary Field:* The primary field at the towed sensor is measured for each stack and recorded as a separate data channel to assess the variation in coupling between the aircraft and the towed sensor induced by changes in system geometry.
8. *Earth Field Monitor:* A monitor of sensor coil motion noise induced by coil motion in the Earth's magnetic field is also extracted in the course of the real-time digital processing. This information is also displayed on the real-time chart as well as being recorded for post-survey diagnostic processes.

9. *Noise/Performance:* A monitor computes the RMS signal level on channel 3 over a running 10-second window. This monitor provides a measure of noise levels in areas of low ground response. This information is printed at regular intervals on the side of the flight record and is recorded for every data stack.

One of the major roles of the GEOTEM® digital receiver is to provide diagnostic information on system functions and to allow for identification of noise events, such as sferics, which may be selectively removed from the EM signal.

The receiver automatically calibrates its received signal with reference to the primary field in ppm and hence compensates for the transmitter drift. Due to the fact that the receiver is digital, receiver drift is minimal. These factors result in more reliable resistivity mapping where base level shifts can dramatically affect results.

GEOTEM®'s high digital sampling rate yields maximum resolution of the secondary field. The absence of an analog system time-constant filter results in minimal signal distortion and, therefore, superior representation of the anomaly amplitudes and shapes.

System Hardware

The GEOTEM® system is an integrated whole, consisting of the CASA 212 aircraft, the on-board hardware, and the software packages controlling the hardware.

The software packages in the GEODAS data acquisition system and in the HP1000-A600 GEOTEM® computer were developed in-house by Geoterrex. Likewise, certain elements of the hardware (GEOTEM® transmitter, system timing clock, towed-bird receiver system) were developed in-house.

Computer: Hewlett Packard HP1000-A600

The HP1000 is a rack-mounted minicomputer capable of one million instructions per second. It acts as a controlling host for the analogic array processor. Communication between the HP1000 and array processor is via DMA transfers. The software running on the HP1000 controls the actions of the array processor, and passes the resulting output data to the GEODAS for display and recording.

Analogic Array Processor: AP504

The array processor performs the real-time processing on the EM data. It is controlled by the HP1000. Receiver data comes to the AP504 from the ADC-510-60 analog-to-digital converter.

Analogic Analog-to-Digital Converter: ADC-510-60

The ADC-510-60 digitizes the receiver coil signal. It has 16-bit resolution and can digitize 2 differential input channels at sampling rates up to 52.5 kHz.

Transmitter System

The transmitter system drives high-current pulses of an appropriate shape and duration through the coils mounted on the CASA aircraft.

System Timing Clock

This subsystem provides appropriate timing signals to the transmitter, and also to the analog-to-digital converter, in order to produce output pulses and capture the ground response.

Towed-Bird Receiver System

A single coil is mounted inside a towed bird which typically is 56 metres below and 123 metres behind the aircraft. The coil axis is parallel to the longitudinal axis of the aircraft. (A second bird, housing the magnetometer sensor, is typically 47 metres below and 82 metres behind the aircraft.)

GEOTEM[®] III SYSTEM GEOMETRY

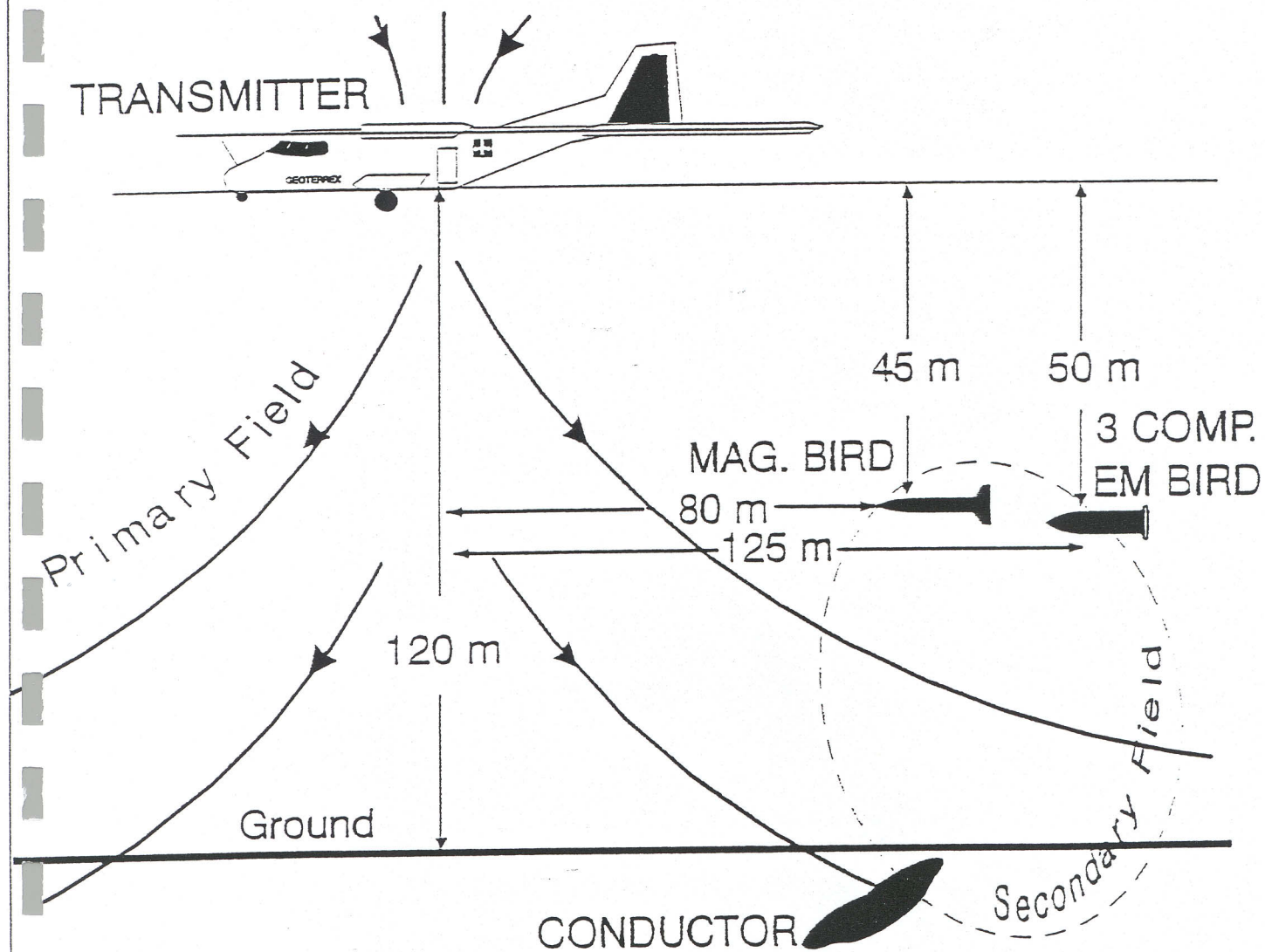


Figure 1

GEOTEM[®] SIGNAL

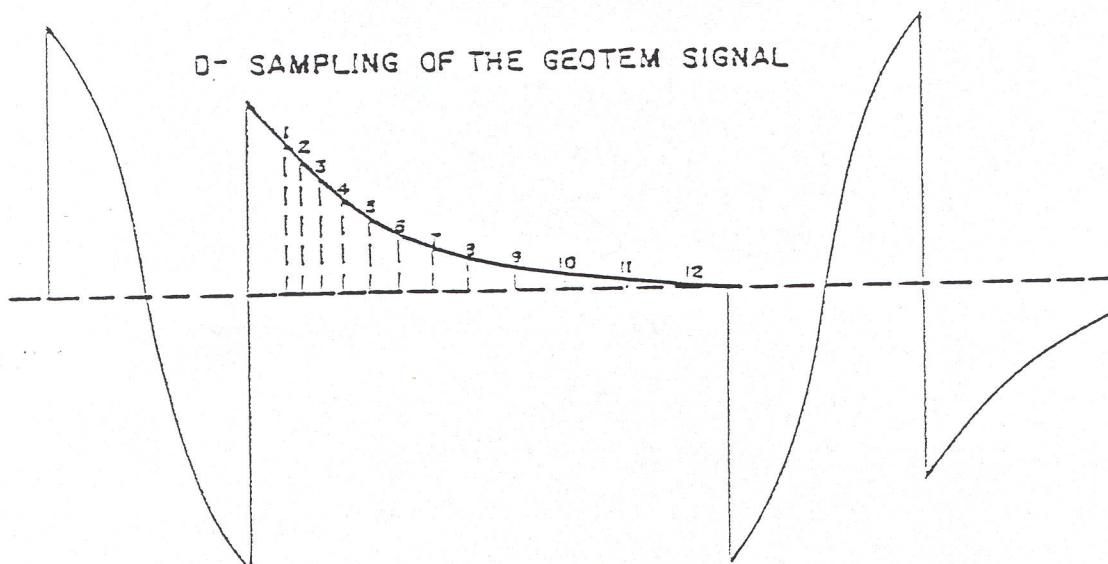
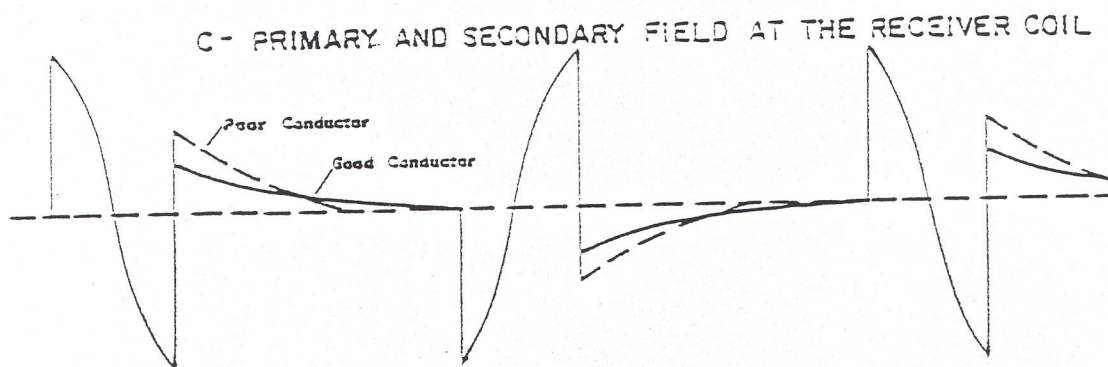
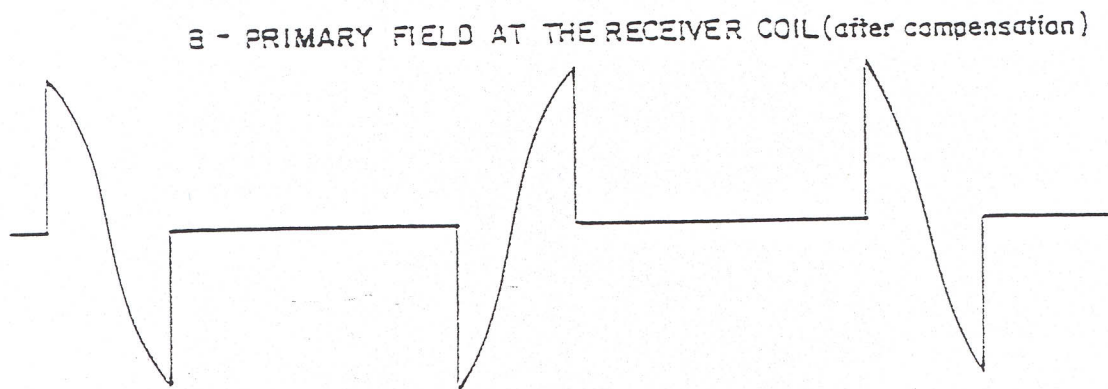
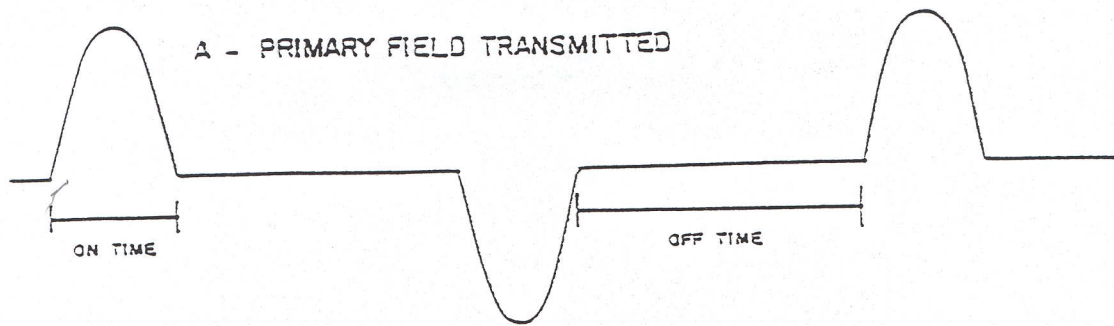


Figure 2

Appendix C

GEOTEM[®] Interpretation Notes

GEOTEM[®] INTERPRETATION

I. INTRODUCTION

The basis of the transient electromagnetic (EM) geophysical surveying technique relies on the premise that changes in the primary EM field produced in the transmitting loop will result in eddy currents being generated in any conductors in the ground. The eddy currents then decay to produce a secondary EM field which may be sensed as a voltage in the receiver coil.

GEOTEM (GEOterrex Transient ElectroMagnetic system) is an airborne transient (or time-domain) towed-bird EM system incorporating a high-speed digital receiver which records the secondary field response with a high degree of accuracy. Most often the total magnetic field is recorded concurrently.

Although the approach to GEOTEM interpretation varies from one survey to another depending on the type of data presentation, objectives and local conditions, the following generalizations may provide the reader with some helpful background information.

The main purpose of the interpretation is to determine the probable origin of the conductors detected during the survey and to suggest recommendations for further exploration. This is possible through an objective analysis of all characteristics of the different types of conductors and associated magnetic anomalies, if any. If possible the airborne results are compared to other available data. A certitude is seldom reached, but a high probability is achieved in identifying the conductive causes in most cases. One of the most difficult problems is usually the differentiation between surface conductors and bedrock conductors.

II. TYPES OF CONDUCTORS

A. Bedrock Conductors

The different types of bedrock conductors normally encountered are the following:

1. Graphites. Graphitic horizons (including a large variety of carbonaceous rocks) occur in sedimentary formations of the Precambrian as well as in volcanic tuffs, often concentrated in shear zones. They correspond generally to long, multiple conductors lying in parallel bands. They have no magnetic expression unless associated with pyrrhotite or magnetite. Their conductivity is variable but generally high.

2. Massive sulphides. Massive sulphide deposits usually manifest themselves as short conductors of high conductivity, often with a coincident magnetic anomaly. Some massive sulphides, however, are not magnetic, others are not very conductive (discontinuous mineralization), and some may be located among formational conductors so that one must not be too rigid in applying the selection criteria.

In addition, there are syngenetic sulphides whose conductive pattern may be similar to that of graphitic horizons but these are generally not as prevalent as graphites.

3. Magnetite and some serpentinized ultrabasics. These rocks are conductive and very magnetic.
4. Manganese oxides. This mineralization may give rise to a weak EM response.

B. Surficial Conductors

1. Beds of clay and alluvium, some swamps, and brackish ground water are usually poorly conductive to moderately conductive.
2. Lateritic formations, residual soils and the weathered layer of the bedrock may cause surface anomalous zones, the conductivity of which is generally low to medium but can occasionally be high. Their presence is often related to the underlying bedrock.

C. Cultural Conductors (Man-Made)

1. Power lines. These frequently, but not always, produce a conductive type of response on the GEOTEM record. In the case of direct radiation of its field, a power line is easily recognized by a GEOTEM anomaly which exhibits phase changes between different channels. In the case of a grounded wire, or steel pylon, the anomaly may look very much like a bedrock conductor.
2. Grounded fences or pipelines. These will invariably produce responses much like a bedrock conductor. Whenever they cannot be identified positively, a ground check is recommended.
3. General culture. Other localized sources such as certain buildings, bridges, irrigation systems, tailings ponds etc., may produce GEOTEM anomalies. Their instances, however, are rare and often they can be identified on the visual path recovery system.

III. ANALYSIS OF THE CONDUCTORS

The apparent conductivity alone is not generally a decisive criterion in the analysis of a conductor. In particular, one should note:

- its shape and size,
- all local variations of characteristics within a conductive zone,
- any associated geophysical parameter (e.g. magnetics),
- the geological environment,
- the structural context, and
- the pattern of surrounding conductors.

The first objective of the interpretation is to classify each conductive zone according to one of the three categories which best defines its probable origin. The categories are cultural, surficial and bedrock. A second objective is to assign to each zone a priority rating as to its potential as an economic prospect.

A. Cultural Conductors

The majority of cultural anomalies occur along roads and are accompanied by a response on the power line monitor. (This monitor is set to 50 or 60 Hz, depending on the local power grid.) Power lines are the most common source of the anomalies and many are recognized immediately by virtue of phase reversals or an abnormal rate of decay. A certain number yield normal GEOTEM anomalies which could be mistaken for bedrock responses. There are also some power lines which have no GEOTEM response whatsoever.

The power line monitor, of course, is of great assistance in identifying cultural anomalies of this type. It is important to note, however, that geological conductors in the vicinity of power lines may exhibit a weak response on the monitor because of current induction via the earth.

Fences, pipelines, communication lines, railways and other man-made conductors can give rise to GEOTEM responses, the strength of which will depend on the grounding of these objects.

Another facet of this analysis is the line-to-line comparison of anomaly character along suspected man-made conductors. In general, the amplitude, the rate of decay, and the anomaly width should not vary a great deal along any one conductor, except for the change in amplitude related to terrain clearance variation. A marked departure from the average response character along any given feature gives rise to the possibility of a second conductor.

In most cases a visual examination of the site will suffice to verify the presence of a man-made conductor. If a second conductor is suspected the ground check is more difficult to accomplish. The object would be to determine if there is (i) a change in the man-made construction, (ii) a difference in the grounding conditions, (iii) a second cultural source, or (iv) if there is, indeed, a geological conductor in addition to the known man-made source.

B. Surficial Conductors

This term is used for geological conductors in the overburden, either glacial or residual in origin, and in the weathered layer of the bedrock. Most surficial conductors are probably caused by clay minerals. In some environments the presence of salts will contribute to the conductivity. Other possible electrolytic conductors are residual soils, swamps, brackish ground water and alluvium such as lake or river-bottom deposits, flood plains and estuaries.

Normally, most surficial materials have low to intermediate conductivity so they are not easily mistaken for highly conductive bedrock features. Also, many of them are wide and their anomaly shapes are typical of broad horizontal sheets.

When surficial conductivity is high it is usually still possible to distinguish between a horizontal plate (more likely to be surficial material) and a vertical body (more likely to be a bedrock source) thanks to the asymmetry of the GEOTEM responses observed at the edges of a broad conductor when flying adjacent lines in opposite directions. The configuration of the system is such that the response recorded at the leading edge is more pronounced than that registered at the trailing edge. Figure 1 illustrates the "edge effect" and the resulting conductive pattern in plan view. In practice there are many variations on this very diagnostic phenomenon.

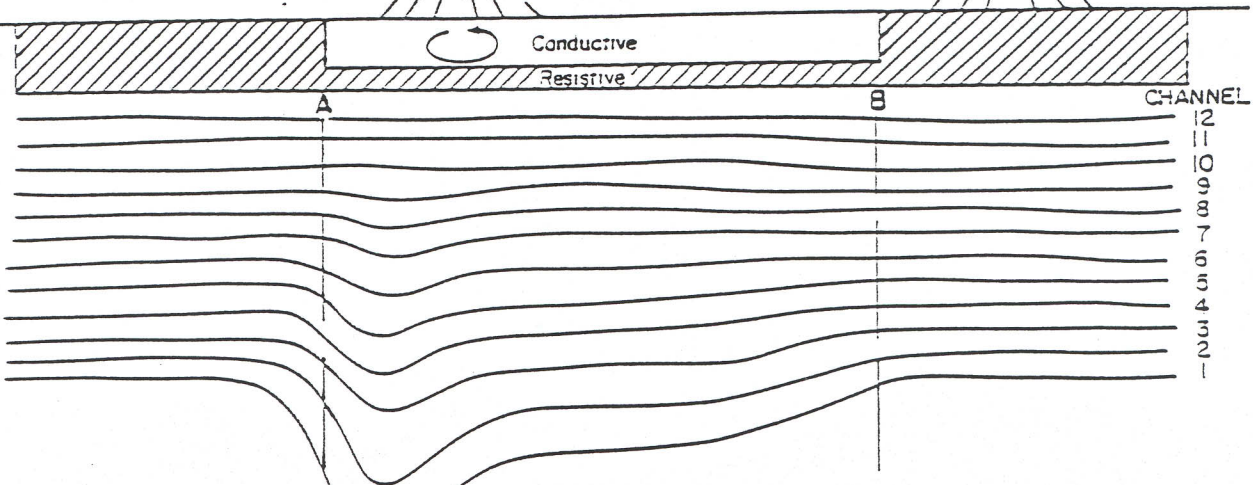
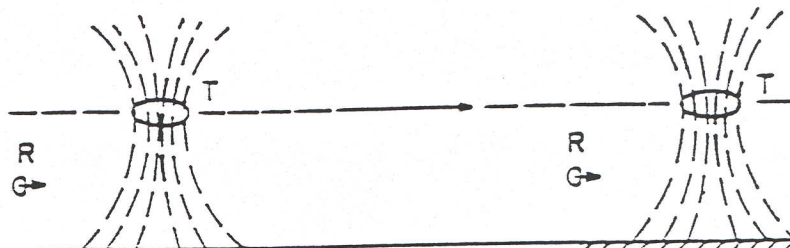
One of the more ambiguous situations as to the true source of the response is when surface conductivity is related to bedrock lithology as for example, surface alteration of an underlying bedrock unit. At times, it is also difficult to distinguish between a weak conductor within the bedrock (e.g. near-massive sulphides) and a surficial source.

In the search for massive sulphides or other bedrock targets, surficial conductivity is generally considered as interference but there are situations where the interpretation of surficial-type conductors is the primary goal. When soils, weathered or altered products are conductive, and in-situ, the GEOTEM responses are a very useful aid to geologic mapping. Shears and faults are often identified by weak, usually narrow, anomalies.

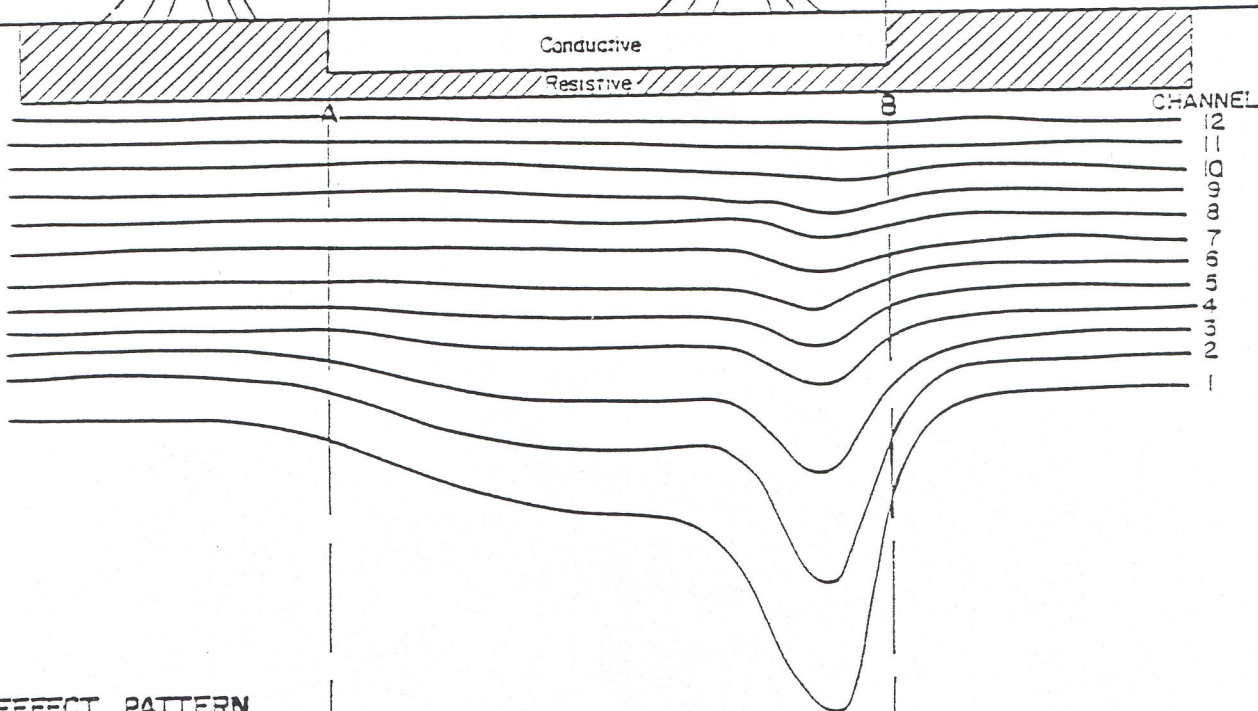
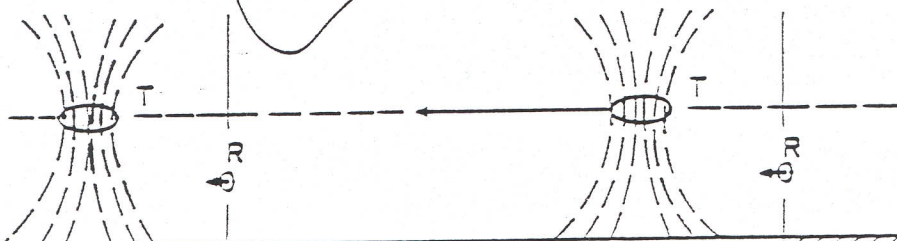
Analysis of surficial conductivity can be used in the exploration for such features as lignite deposits, kimberlites, paleochannels and ground water. In coastal or arid areas, surficial responses may serve to define the limits of fresh, brackish and salty water.

EDGE EFFECT

FLYING
FROM
A TO B



FLYING-
FROM
B TO A



EDGE EFFECT PATTERN

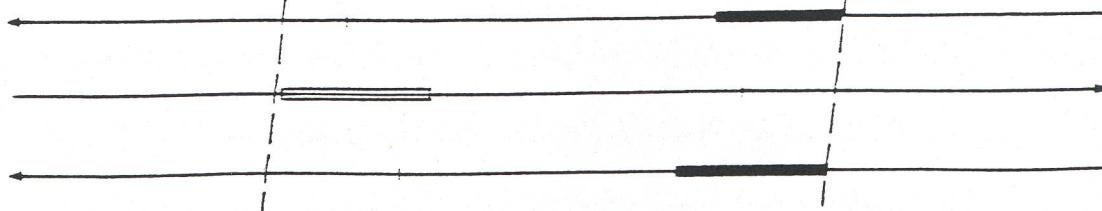


FIGURE 1

C. Bedrock Conductors

This category comprises those anomalies which cannot be classified according to the criteria established for cultural and surficial responses. It is difficult to assign a universal set of values which typify bedrock conductivity because any individual zone or anomaly might exhibit some, but not all, of these values and still be a bedrock conductor. The following criteria are considered indicative of a bedrock conductor:

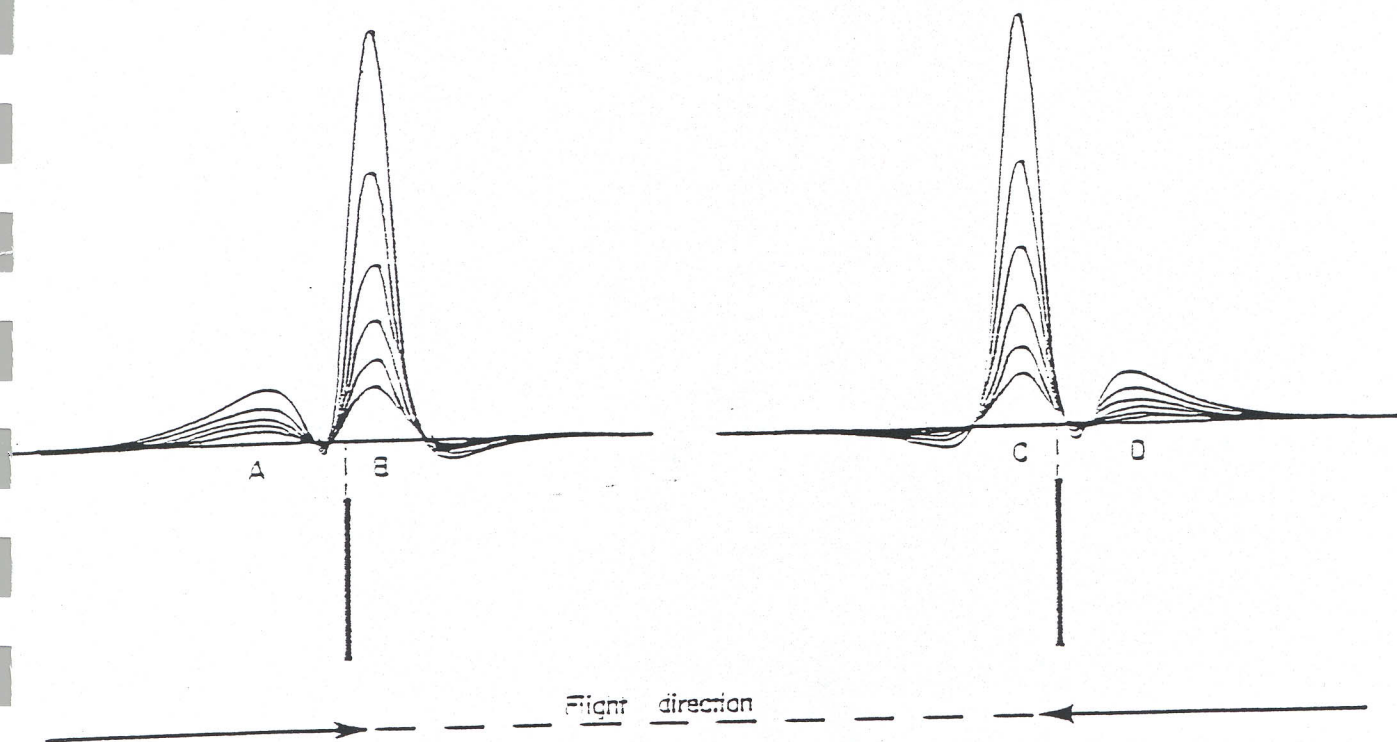
1. An intermediate to high conductivity identified by a response with slow decay, with deflections most often present in the later channels.
2. The anomaly should be narrow, relatively symmetrical, with a well-defined peak.
3. There should be no serious displacement of anomaly position or change in anomaly shape (other than mirror image) with respect to flight direction, except in the case of non-vertical dipping bodies. The alternating character of the response as a result of line direction can be diagnostic of conductor geometry. Figures 2 to 6 illustrate anomalies associated with different target models.
4. A small to intermediate amplitude. Large amplitudes are normally associated with surficial conductors. The amplitude varies according to the depth of the source.
5. A degree of continuity of the EM characteristics across several lines.
6. An associated magnetic response of similar dimensions. One should note, however, that those rocks which weather to produce a conductive upper layer will possess this magnetic association. In the absence of one or more of the characteristics defined in 1, 2, 3 and 4, the related magnetic response cannot be considered significant.

Most obvious bedrock conductors occur in long, relatively monotonous, sometimes multiple zones following formational strike. Graphitic material is usually the most probable source. Massive syngenetic sulphides extending for many kilometres are known in nature but, in general, they are not common. Long formational structures associated with a strong magnetic expression may be indicative of banded iron formations.

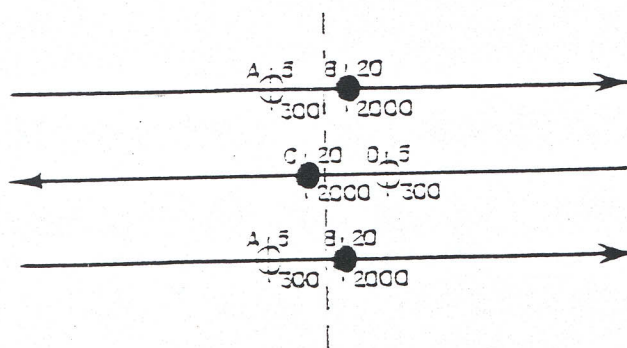
A bedrock conductor reflecting the presence of a massive sulphide would normally exhibit the following characteristics:

- a high conductivity,
- a good anomaly shape (narrow and well-defined peak),
- a small to intermediate amplitude,
- an isolated setting,

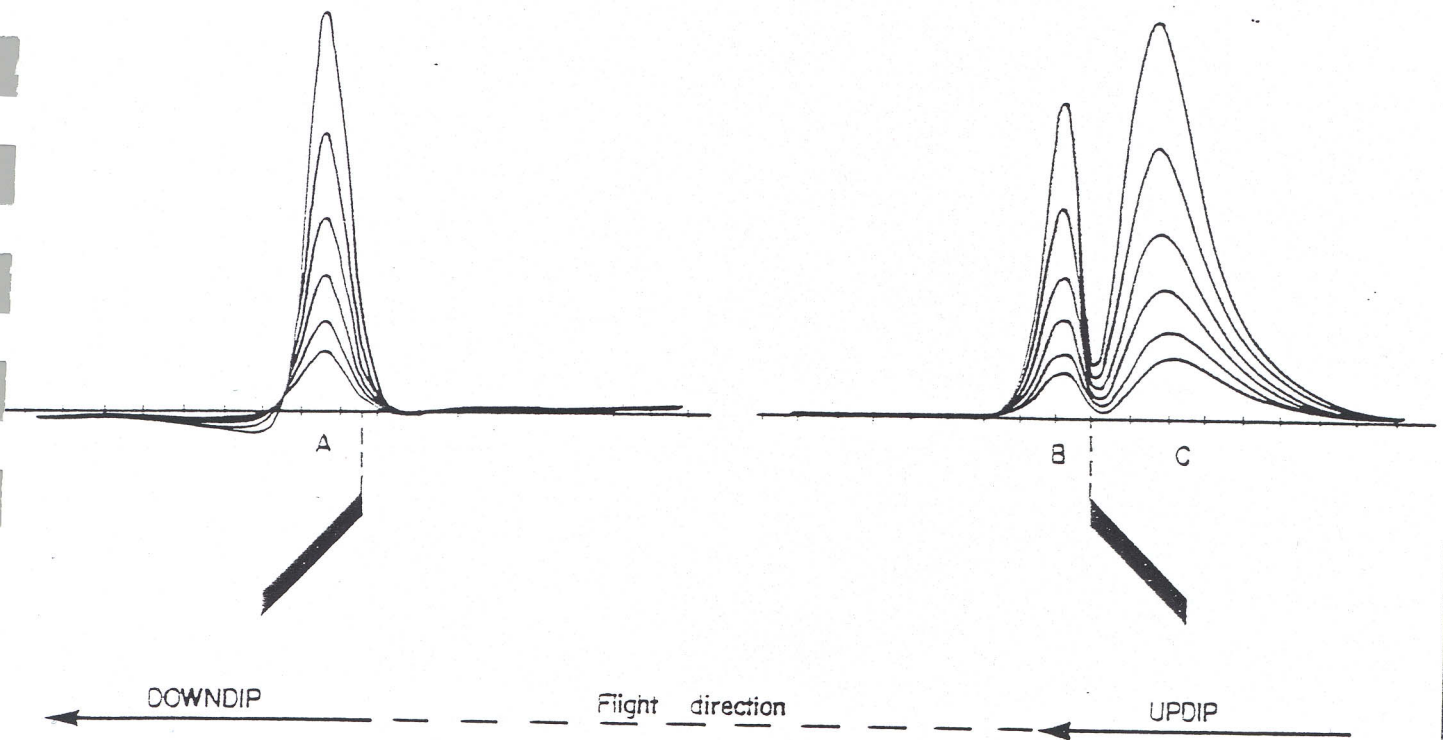
THE VERTICAL PLATE RESPONSE



ANOMALY MAP PRESENTATION (no lag applied)



THE DIPPING PLATE RESPONSE



ANOMALY MAP PRESENTATION (no lag applied)

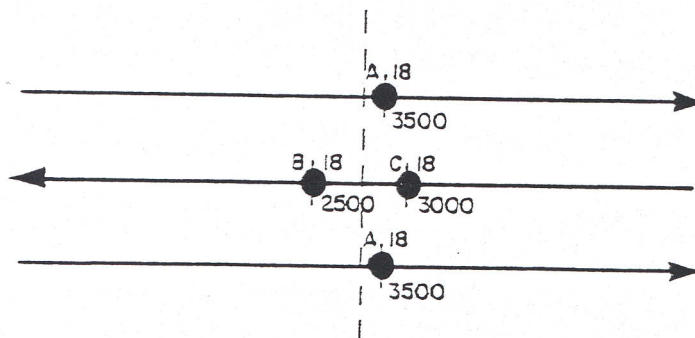
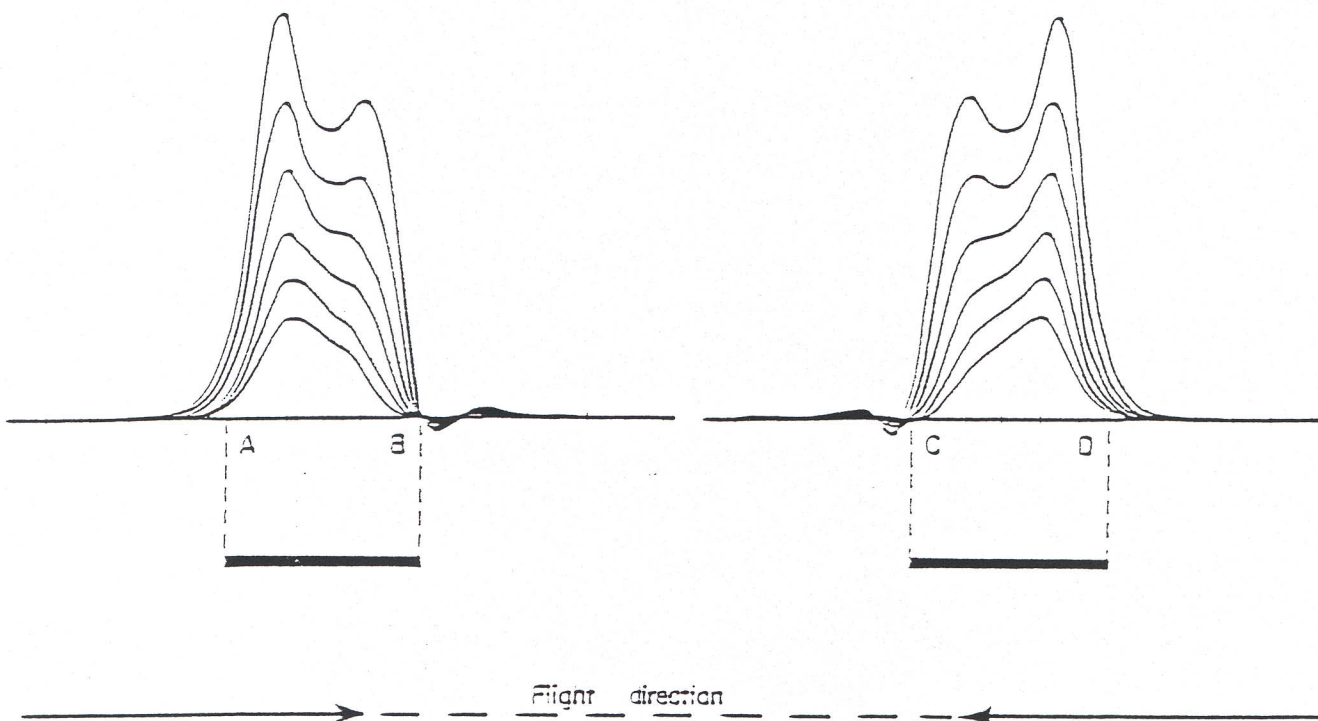


Figure 3

THE HORIZONTAL PLATE RESPONSE



ANOMALY MAP PRESENTATION (no lag applied)

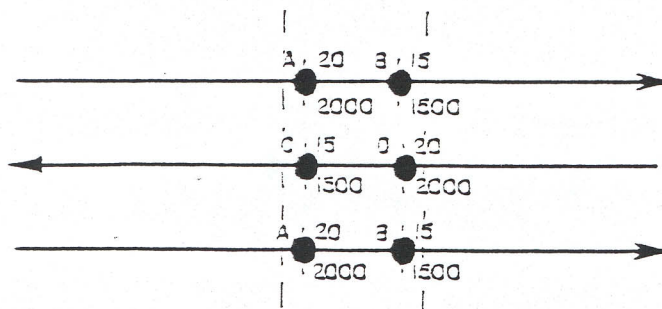
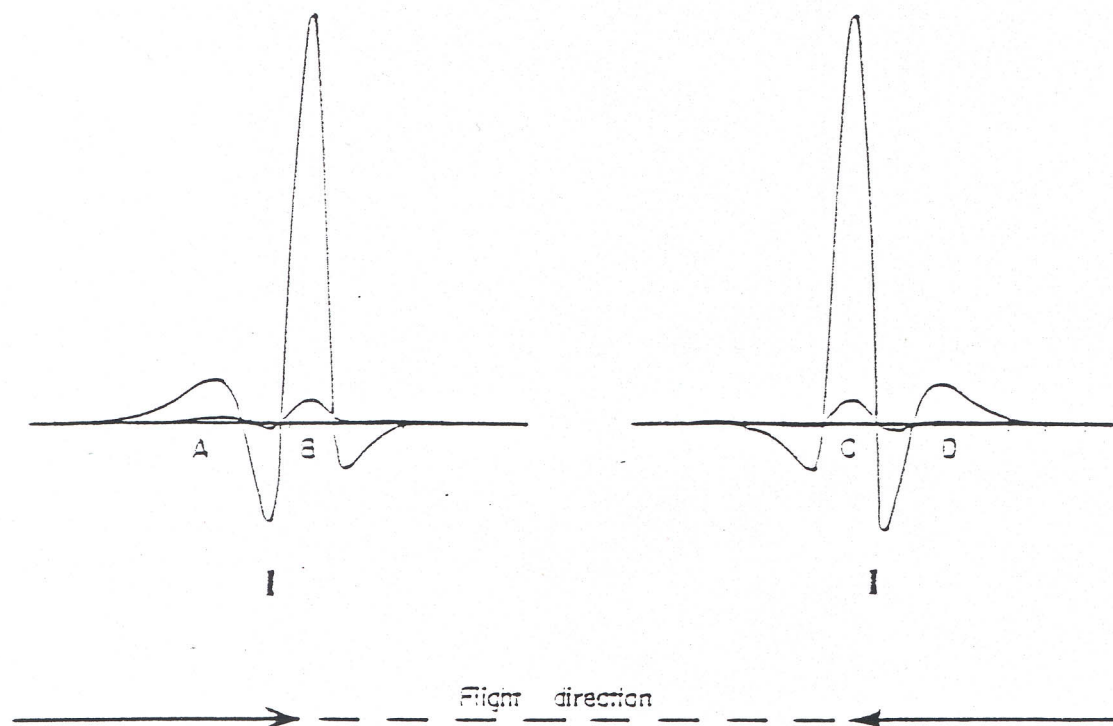


Figure 4

THE VERTICAL RIBBON RESPONSE



ANOMALY MAP PRESENTATION (no lag applied)

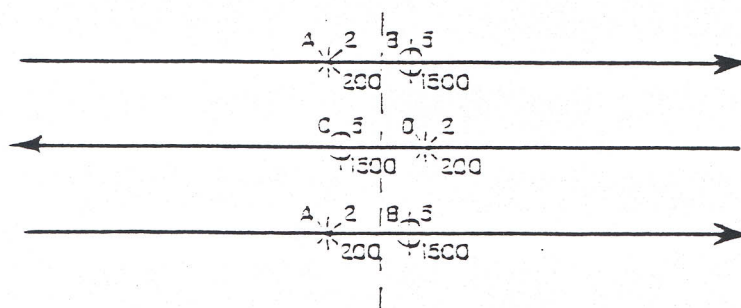
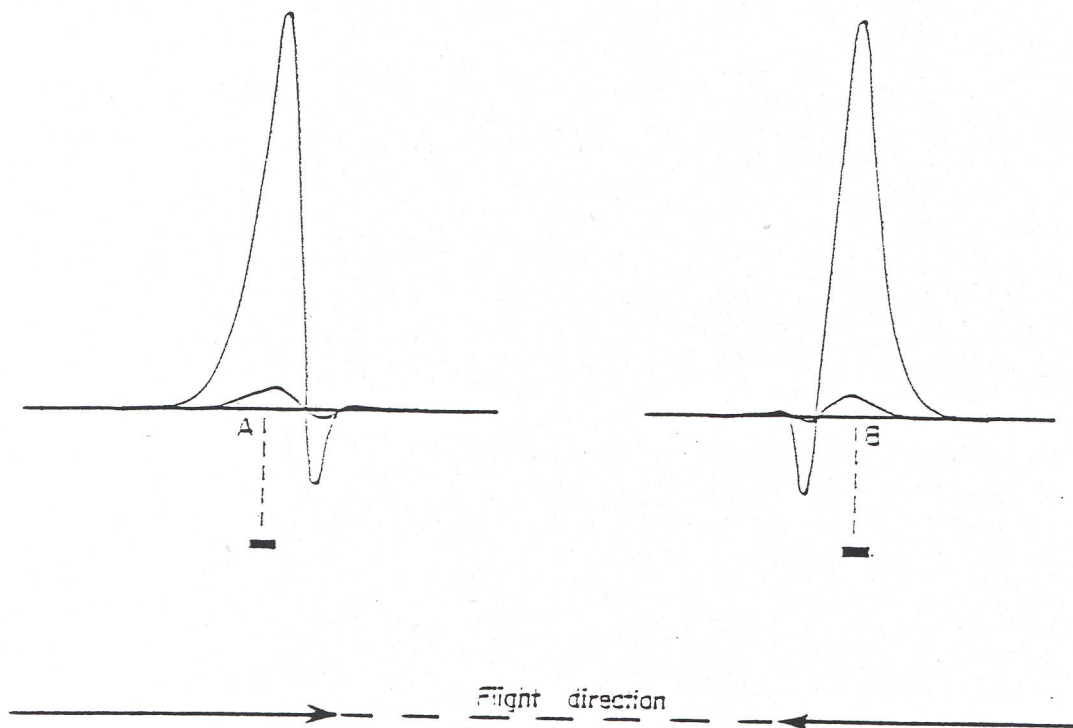


Figure 5

THE HORIZONTAL RIBBON RESPONSE



ANOMALY MAP PRESENTATION (no lag applied)

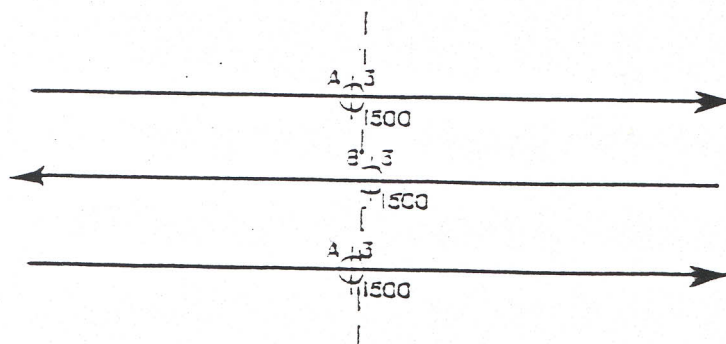


Figure 6

- a short strike length (in general, not exceeding one kilometre), and
- preferably, with a localized magnetic anomaly of matching dimensions.

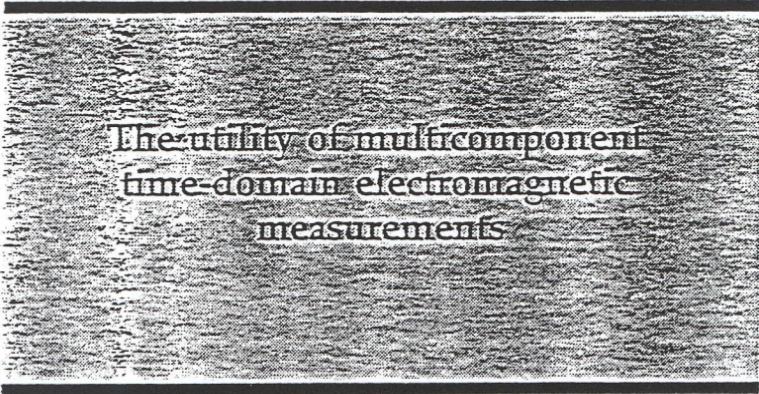
The selection of targets from within extensive (formational) belts is much more difficult than in the case of isolated conductors. Local variations in the EM characteristics, such as in the amplitude, decay, shape etc., can be used as evidence for a relatively localized occurrence. Changes in the character of the EM responses, however, may be simply reflecting differences in the conductive formations themselves rather than indicating the presence of massive sulphides and, for this reason, the degree of confidence is reduced.

Another useful guide for identifying localized variations within formational conductors is to examine the magnetic data compiled as isomagnetic contours. Further study of the magnetic data can reveal the presence of faults, contacts and other features which, in turn, help define areas of potential economic interest.

Finally, once ground investigations begin, it must be remembered that the continual comparison of ground knowledge to the airborne information is an essential step in maximizing the usefulness of the GEOTEM data.

Appendix D

**The Utility of Multicomponent Time-Domain
Electromagnetic Measurements**



The utility of multicomponent
time-domain electromagnetic
measurements

GEOTERREX

OTTAWA, CANADA

1994

Richard S. Smith¹ and Pierre B. Keating²

¹Geoterrrex, Ottawa, Ontario, Canada, K1G 3P5

FAX: 613-731-0453 TEL: 613-731-9571

²Geological Survey of Canada, Ottawa, Ontario, Canada.

ABSTRACT

Time-domain airborne electromagnetic systems historically measure the in-line horizontal (x) component. New versions of the hardware are designed to collect two additional components (the vertical (z) and horizontal lateral (y) components) to provide greater diagnostic information.

In areas where the geology is near horizontal, the z-component response provides greater signal to noise, particularly at late delay times. This allows the conductivity to be determined to greater depth. In a layered environment, the symmetry implies that the y component will be zero; hence a non-zero y component will indicate a lateral inhomogeneity.

Three components can be combined to give the energy envelope of the response. Over a vertical plate, this function has a single positive peak and no side lobes. The shape of the energy envelope is dependent on the flight direction, but less so than the x component.

In the interpretation of discrete conductors, the z-component data can be used to ascertain the dip and depth to the conductor using simple rules of thumb. When the profile line is perpendicular to the strike direction and over the center of the conductor, the y component will be zero; otherwise it will be a combination of the x and z components. The extent of contamination by the x and z components can be used to ascertain the strike direction and the lateral offset of the target respectively.

Having the z- and y-component data increases the total response when the profile line has not traversed the target. This increases the possibility of detecting a target located between adjacent flight lines or beyond a survey boundary.

INTRODUCTION

The acquisition of multiple-component electromagnetic (EM) data is becoming more commonplace. In some techniques, such as those which use the plane-wave assumption (MT, CSAMT and VLF) more than one component has been acquired as a matter of routine for some time (see reviews by Vozoff, 1990, 1991; Zonge and Hughes, 1991; McNeill and Labson, 1991). Other controlled-waveform finite-source systems which have acquired multiple component data are generally experimental, such as those described in the appendices of Spies and Frischknecht (1991).

Slingram EM systems, comprising a moving dipolar transmitter and a moving receiver, generally only measure one component of the response. The MaxMin system was designed to have the capability to measure a second (minimum coupled) component, but this does not appear to be used in practice. The only systems which have two receiver coils are those which measure the wavetilt or polarization ellipse (Frischknecht et al., 1991).

Historically, time-domain EM systems have been capable of collecting multicomponent data in a sequential manner by reorienting the sensor for each component direction. The usefulness of additional components is discussed by Macnae (1984) for the case of the UTEM system. Macnae concluded that as extra time was required to acquire the additional components, this time was better spent collecting more densely spaced vertical-component data. These data, which are less subject to spheric noise, could subsequently be converted to the horizontal components via the Hilbert transform operator because the measured response is a potential field. Multiple-component data was routinely collected by Newmont Exploration using their proprietary EMP system (no longer in use). Examples describing the interpretation of EMP data are given by Barnett (1984) and Boyd and Wiles (1984).

Recent instrument developments have been towards multicomponent systems. For example, commercially available ground systems such as the Geonics PROTEM,

the Zonge GDP-32 and the SIROTEM have been expanded to include multiple input channels which allow three (or more) components to be acquired simultaneously. There is also a version of the UTEM system with multiple channels currently being developed at Lamontagne Geophysics Ltd. The multichannel receivers require complimentary multicomponent sensors -- for ground based systems these have been developed by Geonics Ltd and Zonge Engineering and Research Organization.

Multicomponent borehole measurements are performed most efficiently with multicomponent borehole sensor probes. Prototype probes were developed at Biliden (Hodges et al., 1991) and by Lee (1986), but multicomponent measurements are now becoming more common with the release of probes for commercial use by Crone Geophysics and Exploration Ltd and Geonics. Three component UTEM and SIROTEM borehole sensors are also in development at Lamontagne and Monash University, respectively. Hodges et al. (1991) present an excellent discussion of techniques which can be used to interpret three-component borehole data.

Airborne systems such as frequency-domain helicopter electromagnetic methods acquire data using multiple sensors, but each receiver has a corresponding transmitter in a position of minimum or maximum coupling (Palacky and West, 1991); hence, these systems are essentially multiple single-component systems. The exception to this rule is the now superseded Dighem III system (Fraser, 1972) which used one transmitter and three receivers.

The only multicomponent airborne EM (AEM) system currently in operation is the SPECTREM system (Macnae, et al., 1991). This system, a proprietary development of the PROSPECT system (Annan, 1986), was originally designed to acquire the x, y and z components, but is apparently only collecting two components (x and z) at the time of writing. Other multicomponent systems currently in development are:

- i) the SALTMAP system,
- ii) a helicopter time-domain system (Hogg, 1986), and
- iii) a new version of the GEOTEM[®] system (GEOTEM is a registered

trademark of Geotrex).

Apart from a few type curves in Hogg (1986), there is little literature available which describes how to interpret data from these systems.

This paper is intended to give an insight into the types of responses expected with the new multicomponent AEM systems, and the information which can be extracted from the data. The insight could be of some assistance in interpreting data from multicomponent moving-source ground EM systems, should this type of data be acquired, but would not necessarily be applicable to fixed-source EM.

The use of multicomponent data will be discussed for a number of different applications. For illustration purposes, this paper will use the transmitter-receiver geometry of the GEOTEM system (Figure 1), which is comparable to the other fixed-wing geometries (SPECTREM and SALTMAP). The GEOTEM system is a digital transient EM system utilizing a bipolar half-sinusoidal current waveform [more details are in Annan and Lockwood (1991)]. The sign convention used in this paper is shown in Figure 1, with the y component being into the page.

SOUNDING IN LAYERED ENVIRONMENTS

In a layered environment, current flow is horizontal (Morrison et al., 1969) so the z component is much larger than the x component, particularly in resistive ground and/or at late delay times. At the same time, the spheric noise in the vertical (z) direction is five to ten times less (Macnae, 1984; McCracken et al., 1986), so the z component has a greater signal-to-noise ratio. Figure 2 shows theoretical curves over two different, but similar, layered earth models. One model is a half-space of 500 $\Omega\cdot\text{m}$ and the other is a 350 m thick layer of 500 $\Omega\cdot\text{m}$ overlying a highly resistive basement. In this plot the data have been normalized by the total primary field. The z component is six to ten times larger than the x component, and both curves are above the noise level, at least for part of the measured transient. For this plot, the spheric noise was assumed not to be contaminating the x component, so a 30 ppm

noise level would be typical. In order to distinguish between half-space and 350 m thick layer, it is not only necessary that each curve be above the noise level, the difference between the response of the two models must also be greater than the noise level. Figure 3, which is this difference, shows that only the z-component difference is above the noise level and hence able to distinguish the two conductivity models. Hence for the case shown, the z component is more useful than the x component for determining whether there is a resistive layer at 350 m depth. Because of the z-component signal is generally larger in a layered environment, levels this conclusion will also be true in general.

In practice, the receiver bird changes orientation, so part of the vertical component will be measured by the horizontal sensors. This could be corrected using positioning information and/or redundant information from the primary field. An alternative is to calculate and model the magnitude of the total field, as this is a quantity independent of the receiver orientation. This is what was done by Macnae et al. (1991) when calculating the conductivity depth sections for SPECTREM data.

The symmetry of the secondary field is such that if the EM bird is aligned radially with the transmitter, the y component will always be zero. In fact, the y component will be zero whenever the conductivity structure on both sides of the aircraft is the same. A non-zero y component is therefore useful in identifying off-line lateral inhomogeneities in the ground.

DISCRETE CONDUCTORS

Historically, airborne transient electromagnetic (TEM) data have been used for conductor detection. One of the reasons why the old INPUT system measured the x component of the response was that the response measured peaked when the receiver passed over the top of the conductor. The bottom part of Figure 4 shows the response over a vertical conductor, as calculated with the PLATE program (Dyck and West, 1984). As is standard practice, the data have been plotted at the receiver, so the x component peaks over the conductor. Note that there is also a peak at 200 m, just

before the transmitter passes over the conductor, and a trailing edge negative to the left of the conductor. The z component (dashed line) has two peaks and a large negative trough just before the conductor. Because of the symmetry, the y component (dotted line) is zero. All the peaks, troughs and negatives make the response of a single conductor complicated to display and hence interpret. The display can be simplified by calculating the "energy envelope" of the response. This quantity is the square root of the sum of the squares of each component and its spatial derivative. As such, it is similar to the analytic signal in magnetics, but as it is not "analytic" in the formal mathematical sense, it is termed the energy envelope. The energy envelope plotted on Figure 4 is almost symmetric, and would be a good quantity to present, in plan form, as contours, or as an image.

What little asymmetry remains in the energy envelope is a good indication of the coupling of the AEM system to the conductor and can be used to reduce the asymmetry of the individual curves. For example, the top part of Figure 4 shows the x and z component normalized by the energy envelope at each point. The size of the two x peaks and the two z peaks are now roughly comparable.

Dip determination

The response of a plate with a dip of 120° is shown on Figure 5. For the x and z components, the peak on the down dip side is larger. However, the z-component peaks remain identifiable over a larger range of dips and plotting the ratio of the peak sizes, as has been done with solid squares on Figure 6, shows that the ratio is very close to the tangent of the dip divided by 2. Hence, calculating the ratio of the peak amplitudes (R) will yield the dip (θ) using

$$\theta = 2 \tan^{-1}(R).$$

Depth determination

As the depth of the body increases, the distance between the two z-component peaks increases. As an example of this, Figure 7 shows the case of a plate 150 m

deeper than the plate of Figure 4. The peaks are now 450 m apart, as compared with 275 m on Figure 4. A plot of the peak-to-peak distances for a range of depths is shown on Figure 8 for plates with 60, 90 and 120° dips. The distribution follows a straight line and it can be seen that if the dip is within 30 degrees of vertical, the depth to the top of the body can be determined to within about 25 m, an error which is tolerable in airborne EM interpretation. More traditional methods for determining the depth (Palacky and West, 1973) use the rate of decay of the response in all the channels. Our method uses only one channel, allowing a depth for each delay time to be ascertained and, hence, it may be possible to track any migration of the current system in the conductor.

Strike and offset determination

The response shown in Figure 4 varies in cases when the plate has a strike different from 90° or the flight path is offset from the center of the plate.

Figure 9 shows the response for a plate with zero offset and Figure 10 is when the plate is offset by 150 m from the profile line. The z and x response are little changed from the no offset case, but the y response, which was zero, is now significant. In fact, the shape of the response curve appears to be the mirror image of the z response.

In the case when the plate strikes at 45°, the y component is similar in shape but opposite in sign to the x-component response (Figure 11).

These similarities can be better understood by looking at schematic diagrams of the secondary field from the plate. Figure 12 shows a plate and the field in section, with increasing offset denoted by moving the aircraft to the right. For zero offset the field is vertical (z only). As the offset increases, the field rolls over into the y component.

The case of variable strike is depicted in plan view on Figure 13 by leaving the plate stationary and changing the flight direction. As the strike changes from perpendicular, what was purely x component now rotates into the y component.

The y component (H_y) can thus be considered to be a mixture of x (H_x) and z (H_z) components, viz

$$H_y = C_{stk} H_x + C_{off} H_z,$$

an equation which is approximate only. The response for a variety of strike angles and offset distances has been calculated and in each case the y-component response has been decomposed into the x and z components by solving for the constants of proportionality C_{stk} and C_{off} .

A plot of C_{stk} for the case of zero offset and varying strike direction ζ is seen on Figure 14. The values determined from the data are plotted with solid squares and compared with the tan of 90° minus the strike angle. Because the agreement is so good, the formula

$$\zeta = 90 - \tan^{-1}(C_{stk})$$

can be used to determine the strike. This relation was first obtained by Fraser (1972).

When the strike is fixed at 90° , and the offset varies, the corresponding values obtained for C_{off} have been plotted with solid squares on Figure 15. Again, there is good agreement with the arctangent of C_{off} and the ζ angle between vertical and the line joining the profile line with the center of the plate. If the depth d is already obtained using the method described above, or by the method described in Palacky and West (1973), then the offset distance O can be obtained from the formula

$$\begin{aligned} O &= d \tan(\zeta) \\ &= d C_{off}. \end{aligned}$$

Lateral detectability

Figure 12 illustrates that the y component becomes relatively strong as the lateral displacement from the conductor is increased. Thus, if the y component is measured then the total signal will remain above the noise level at larger lateral displacements from the conductor. This has been illustrated by assuming a flat-lying conductor, here approximated by a wire loop circuit of radius 125 m (Figure 16). The x, y and z components of the response have been computed using the formulae for the

large-loop magnetic fields in Wait (1982). The results are plotted on Figure 16 as a function of increasing lateral displacement of the transmitter/receiver from the center of the conductor. The transmitter and receiver are separated in a direction perpendicular to the lateral displacement, so as to simulate the case when the system is maximal coupled to the conductor, but the flight line misses the target by an increasing amount. The effect of varying the conductance or measurement time has been removed by normalizing the response to the total response measured when the system is at zero displacement. At displacements greater than 80 m, the y component is clearly larger than any other component. If the same sensitivity and noise level is assumed for the x, y and z components, it is clearly an advantage to measure the y component to increase the chances of detecting the target when the flight line has not passed directly over the conductor.

CONCLUSIONS

The additional components (y and z) collected with multicomponent AEM data improve the interpretability of the data.

The z-component data enhances the ability of the AEM system to resolve layered structures. This is because of the reduced spheric noise and the increased signal. If all the components are employed to correct for coil rotation, then the data quality and resolving power is increased further, as individual components are not contaminated by another component. Having better signal-to-noise and greater fidelity in the data will allow deeper layers to be interpreted with confidence.

The y component is helpful in detecting when the conductivity structure has lateral inhomogeneities which are not symmetric about the flight line.

All components are used to calculate the energy envelope, which is a valuable quantity to image. The energy envelope has a single peak over a vertical conductor and two peaks over a dipping conductor, one at either end. The asymmetry in the response profiles for the individual components can be reduced by normalizing each

profile by the energy envelope.

All three components are of great use in determining the characteristics of discrete conductors. For example, the distance between the two peaks in the z-component profile can be employed to determine the depth. Also, the normalized ratio of the two z-component peaks helps to ascertain the dip of the conductor. The x component has been used in the past for these purposes, but is not as accurate, as it requires the data at all delay times, or an ability to identify a very small peak.

The y component can be utilized to extract information about the conductor which cannot be obtained from single component AEM data. The degree of mixing between the y and z components can give the lateral offset of the conductor (provided the depth is known), while the mixing between the y and x component gives the strike of a vertical conductor.

Finally, measuring the y component gives an enhanced ability to detect a conductor away from the profile line, either between lines or beyond the edge of a survey boundary.

REFERENCES

- Annan, A.P., 1986, Development of the PROSPECT I airborne electromagnetic system: *in* Palacky, G.J., Ed., Airborne resistivity mapping. Geol. Surv. Can. Paper 86-22, 63-70.
- Annan, A.P., and Lockwood, R., 1991, An application of airborne GEOTEM in Australian conditions: *Explor. Geophy.*, 22, 5-12.
- Barnett, C.T., 1984, Simple inversion of time-domain electromagnetic data: *Geophysics*, 49, 925-933.
- Boyd, G.W., and Wiles, C.J., 1984, The Newmont drill-hole electromagnetic pulse system - Examples from eastern Australia: *Geophysics*, 49, 949-956.
- Dyck, A.V., and West, G.F., 1984, The role of simple computer models in interpretations of wide-band drill-hole electromagnetic surveys in mineral exploration: *Geophysics*, 49, 957-980.
- Fraser, D.C., 1972, A new multicoil aerial electromagnetic prospecting system: *Geophysics*, 37, 518-537.
- Frischknecht, F.C., Labson, V.F., Spies, B.R., and Anderson, W.L., 1991, Profiling methods using small sources: *in* Nabighian M.N., Ed., Electromagnetic methods in applied geophysics, Volume 2, Applications, SEG Investigations in geophysics, no. 3, 105-270.
- Hodges, D.G., Crone, J.D., and Pemberton, R., 1991, A new multiple component downhole pulse EM probe for directional interpretation: *in* Proc. 4th Int. MGLS/KEGS Sym. on Borehole Geophy. for Min. Geotech. and Groundwater Appl., Toronto, August, 1991.
- Hogg, R.L.S., 1986, The Aerodat multigeometry, broadband transient helicopter electromagnetic system: *in* Palacky, G.J., Ed., Airborne resistivity mapping. Geol. Surv. Can. Paper 86-22, 79-89.
- Lee, J., 1986, A three component drill-hole EM receiver probe: M.Sc. thesis, Univ. of Toronto.
- Macnae, J.C., 1984, Survey design for multicomponent electromagnetic systems:

Geophysics, 49, 265-273.

Macnae, J.C., Smith, R.S., Polzer, B.D., Lamontagne, Y., and Klinkert, P.S., 1991,

Conductivity-depth imaging of airborne electromagnetic step-response data:

Geophysics, 56, 102-114.

McCracken, K.G., Oristaglio, M.L., and Hohmann, G.W., 1986, Minimization of noise

in electromagnetic exploration systems: Geophysics, 51, 819-832.

McNeill, J.D., and Labson, V., 1991, Geological mapping using VLF radio fields: *in*

Nabighian M.N., Ed., Electromagnetic methods in applied geophysics, Vol. 2,

Applications, SEG Investigations in geophysics, no. 3, 521-640.

Morrison, H.F., Phillips, R.J., and O'Brien, D.P., 1969, Quantitative interpretation

of transient electromagnetic fields over a layered earth: Geophy. Prosp., 17, 82-

101.

Palacky, G.J., and West, G.F., 1973, Quantitative measurements of Input AEM

measurements: Geophysics, 38, 1145-1158.

Palacky, G.J., and West, G.F., 1991, Airborne electromagnetic methods: *in* Nabighian

M.N., Electromagnetic methods in applied geophysics, Volume 2, Applications,

SEG Investigations in geophysics, no 3, 811-879

Spies, B.R., and Frischknecht, F.C., 1991, Electromagnetic sounding: *in* Nabighian

M.N., Electromagnetic methods in applied geophysics, Volume 2, Applications,

SEG Investigations in geophysics, no 3, 285-425.

Vozoff, K., 1990, Magnetotellurics: Principles and practise: Proc. Indian Acad. Sci.,

99, 441-471.

Vozoff, K., 1991, The magnetotelluric method: *in* Nabighian M.N., Electromagnetic

methods in applied geophysics, Volume 2, Applications, SEG Investigations in

geophysics, no 3, 641-711.

Wait, J.R., 1982, Geo-electromagnetism: Academic Press Inc.

Zonge K.L., and Hughes, L.J., 1991, Controlled source audio-magnetotellurics: *in*

Nabighian M.N., Electromagnetic methods in applied geophysics, Volume 2,

Applications, SEG Investigations in geophysics, no 3. 713-809.

FIGURE CAPTIONS

- Fig. 1. The geometric configuration of the GEOTEM[®] system. The system comprises a transmitter on the aircraft and a receiver sensor in a "bird" towed behind the aircraft. The z direction is positive up, x is positive behind the aircraft and y forms a right-hand coordinate system.
- Fig. 2. The response for a $500 \Omega\cdot\text{m}$ half-space (solid line) and a $500 \Omega\cdot\text{m}$ layer of thickness 350 m, overlying a resistive half-space (dashed line). The z -component responses are the two curves with the larger amplitudes and the two x -component response curves are six to ten times smaller than the corresponding z component. A noise level of 30 ppm is considered to be a typical in the absence of strong spherics.
- Fig. 3. The difference between the z and x components of the response for the two models of Figure 2. Only the z -component difference is above the noise level for any time and is, therefore, the only component capable of distinguishing between the responses of the two models.
- Fig. 4. (Bottom) The response of a 600 by 300 m plate 120 m below an aircraft flying from right to left. The plotting point for the response is below the receiver. The x -component response is the smaller amplitude solid line, the z component is the dashed line and the y -component response is the dotted line. The larger amplitude solid line is the energy envelope of all three components. (Top) The z and x components normalized by the energy envelope. These curves are for a delay time of 0.4 milliseconds after the transmitter current is turned off.
- Fig. 5. (Bottom) same as Figure 4, except the plate is now dipping at 120° . On the top graph note that the down-dip (left) peak on the normalized z -component response is now larger than the right peak.
- Fig. 6. The ratio of the peak amplitudes of the normalized z -component response (left/right), plotted with solid squares. The ratio plots very close to the tangent

of half the dip angle of the plate.

Fig. 7. The same as Figure 4, except the plate is now 270 m below the aircraft. Note that the distance between the z-component peaks is now much greater.

Fig. 8. The peak-to-peak distance as a function of plate depth for three different dip angles. A variation in dip of $\pm 30^\circ$ does not result in a large change in the peak-to-peak distance.

Fig. 9. The response of a 300 by 300 m plate traversed by a profile line crossing the center of the plate in a direction perpendicular to the plate (strike angle of the plate with respect to the profile line is 90°).

Fig. 10. Same as Figure 9, except the profile line has been offset from the center of the plate by -150 m in the y direction (equivalent to a 150m displacement of the plate).

Fig. 11. Same as Figure 9, except the profile line traverses the plate such that the strike angle of the plate, with respect to the profile line, is 45° .

Fig. 12. A schematic diagram of the plate and the magnetic flux of the secondary field (section view). For increasing offset from the center of the plate, the magnetic field at the receiver rolls over from the z to the y component.

Fig. 13. A schematic diagram of the plate and the magnetic flux of the secondary field (plan view). Here varying strike is depicted by an equivalent variation of the flight direction. As the flight direction rotates from a strike angle of 90° , the receiver rotates so as to measure a greater response in the y direction.

Fig. 14. The ratio of the components y to x (C_{stk}), plotted as a function of varying strike angle (solid squares). The data agree very closely with the cotangent of the strike angle.

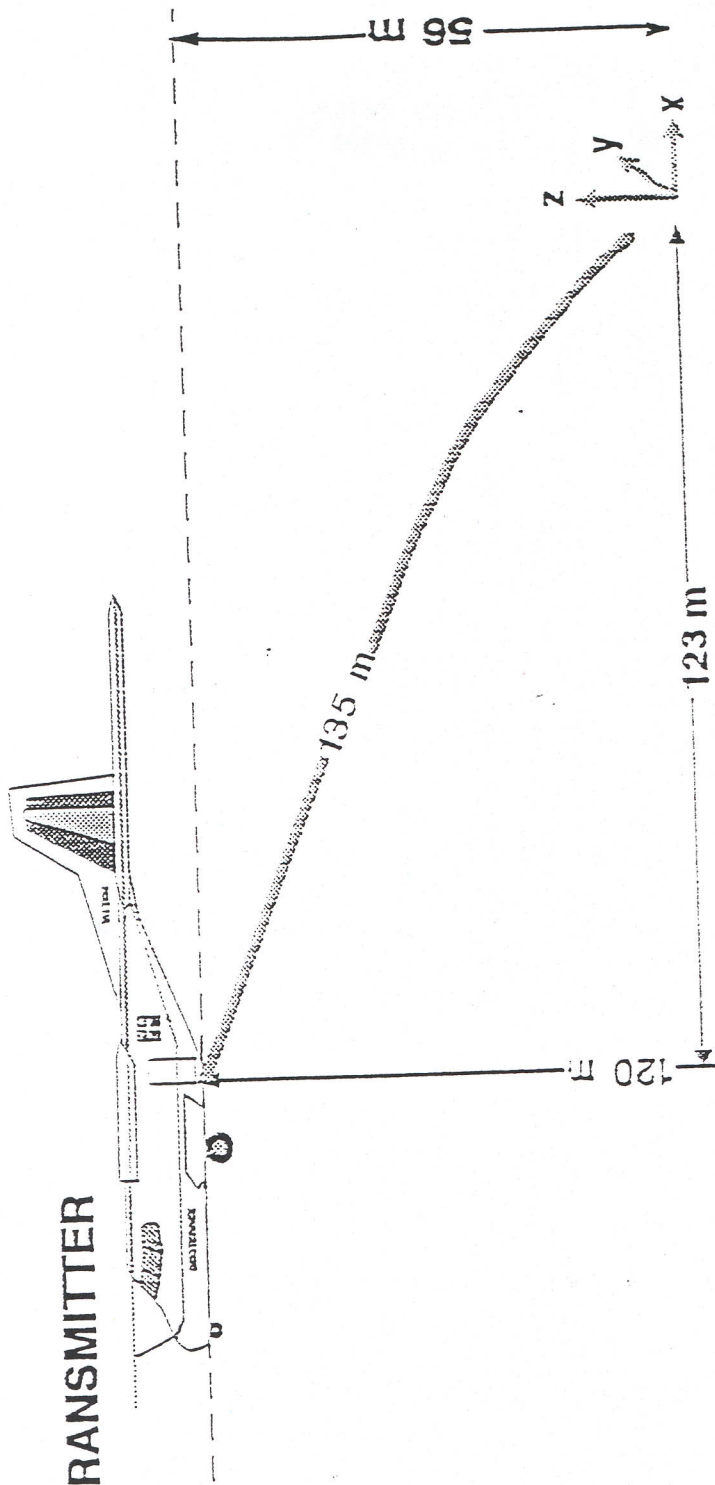
Fig. 15. The arctangent of the ratio of the components y to z (C_{off}), plotted as a function of varying offset (solid squares). There is good agreement with the angle of the profile line from the center of the plate (measured in degrees from the vertical).

Fig. 16. Plan view of a grey circular flat-lying conductor, radius 125 m. The AEM

system is offset a distance d from the center of the conductor along a radial line where the transmitter and receiver couple strongly to the body. The traverse direction of the system is from the bottom to the top of the figure.

Fig. 17. The normalized response of the EM system plotted as a function of increasing offset distance. The x component falls off most rapidly and the y component most slowly with offset distance.

TRANSMITTER

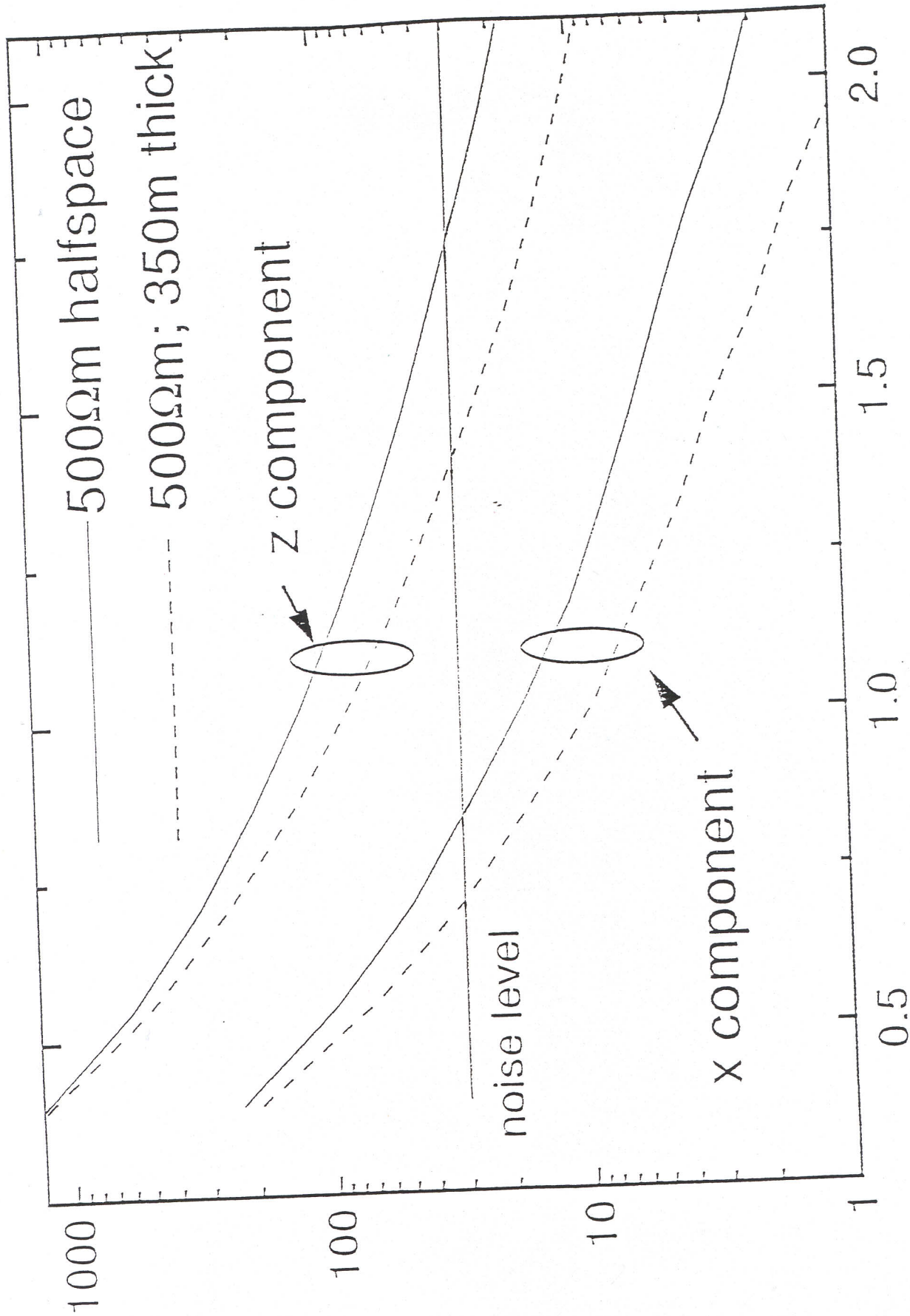


3 AXIS RECEIVER

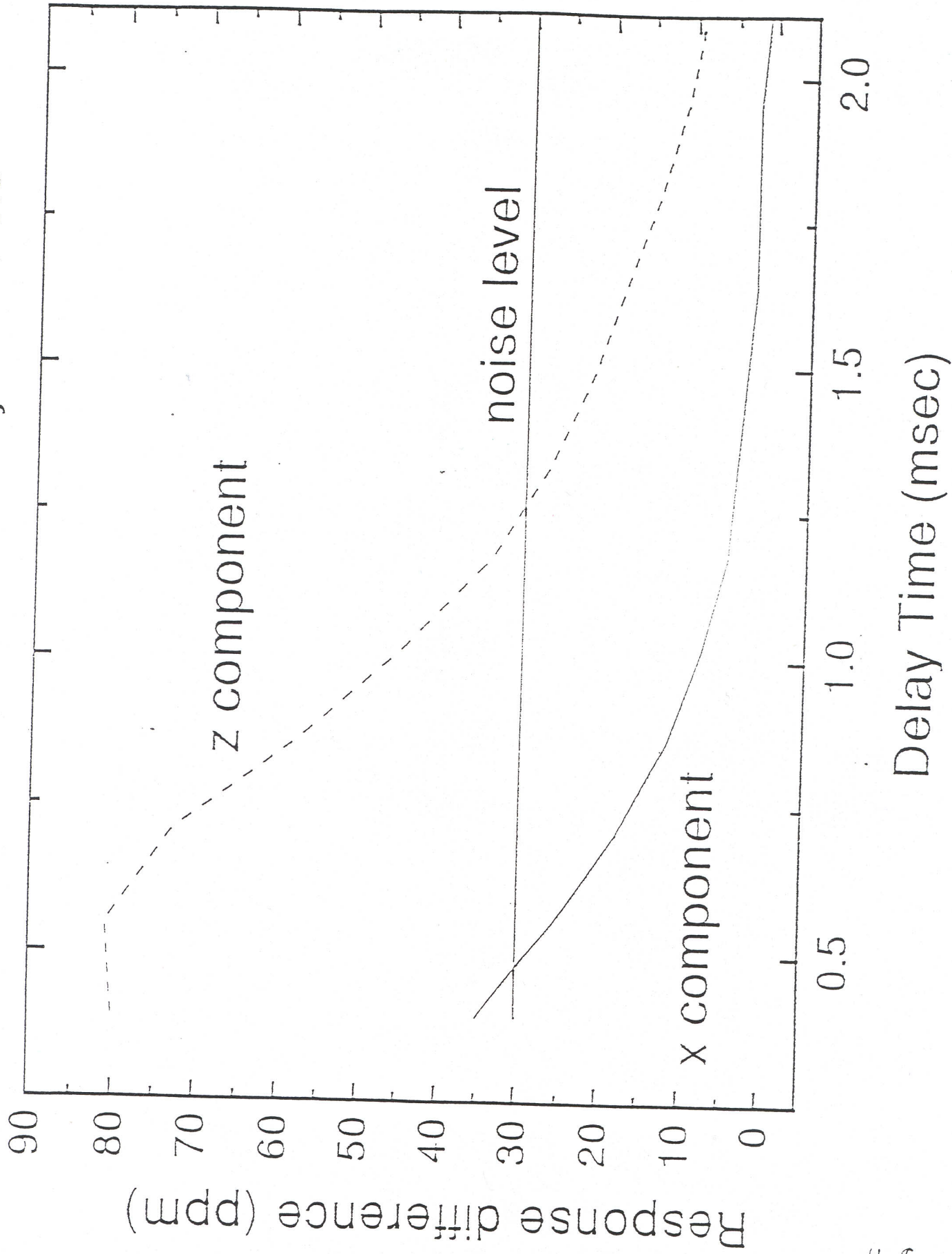
Smith & Keating

FIG-1

Response (ppm)

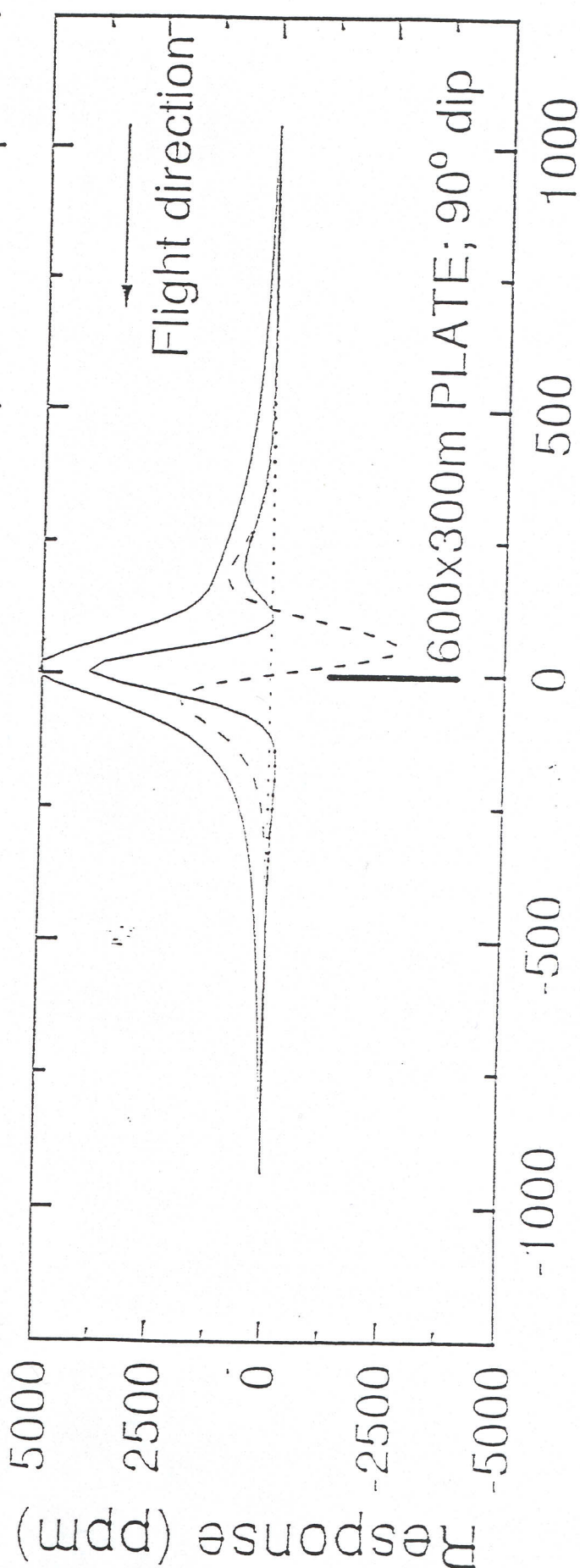
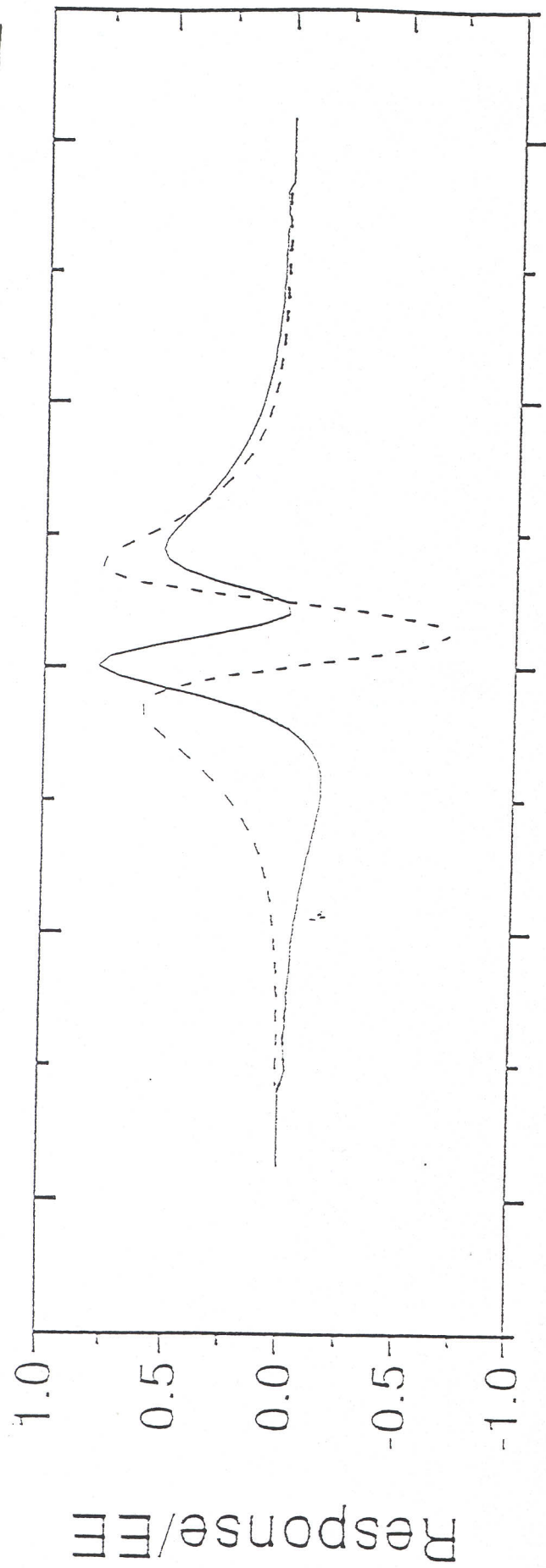


Delay Time (msec)

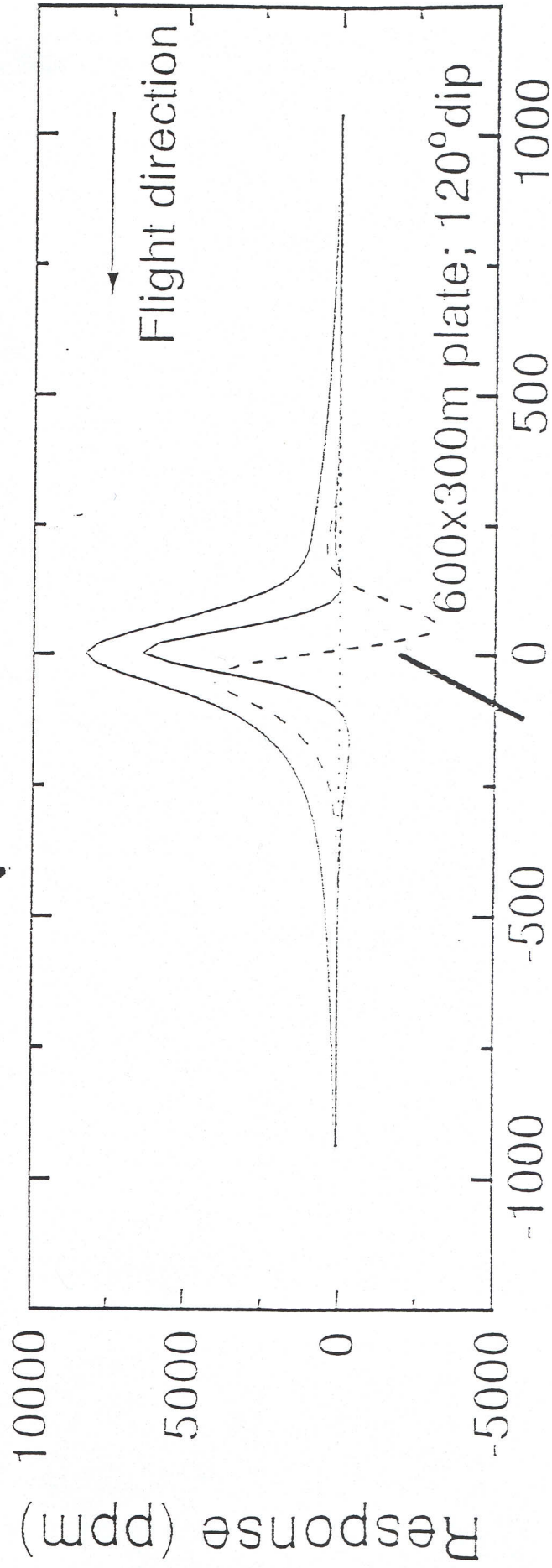
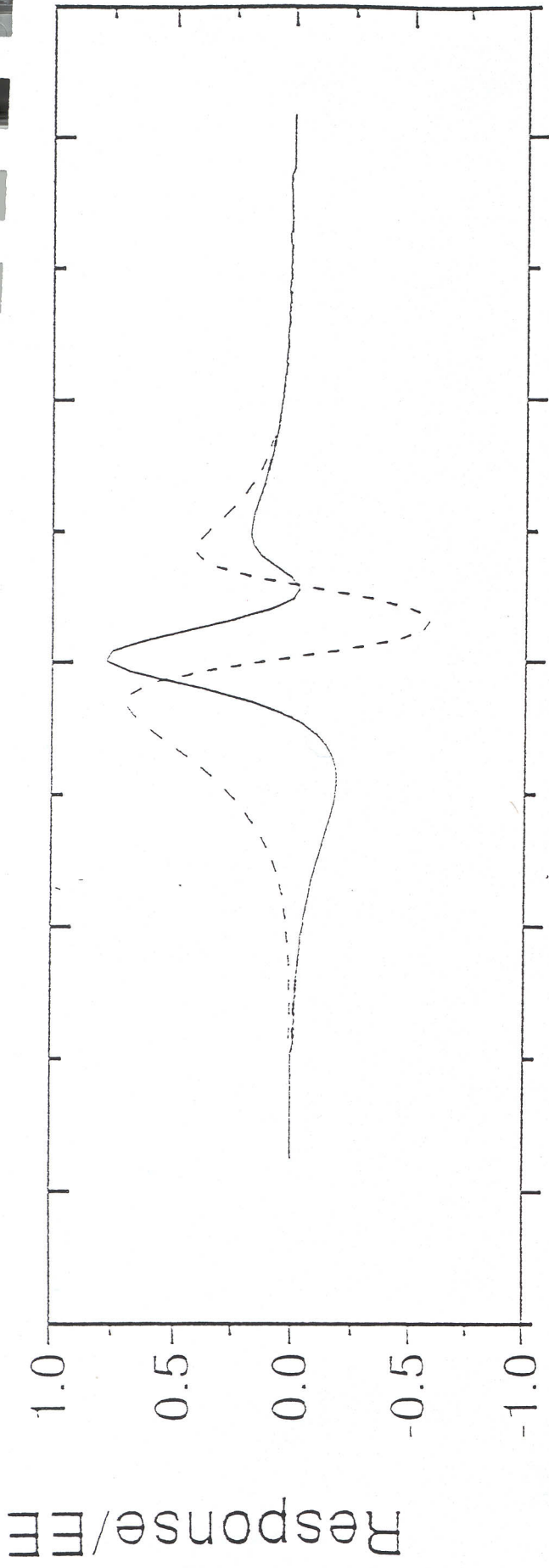


Smith, R.
Keating

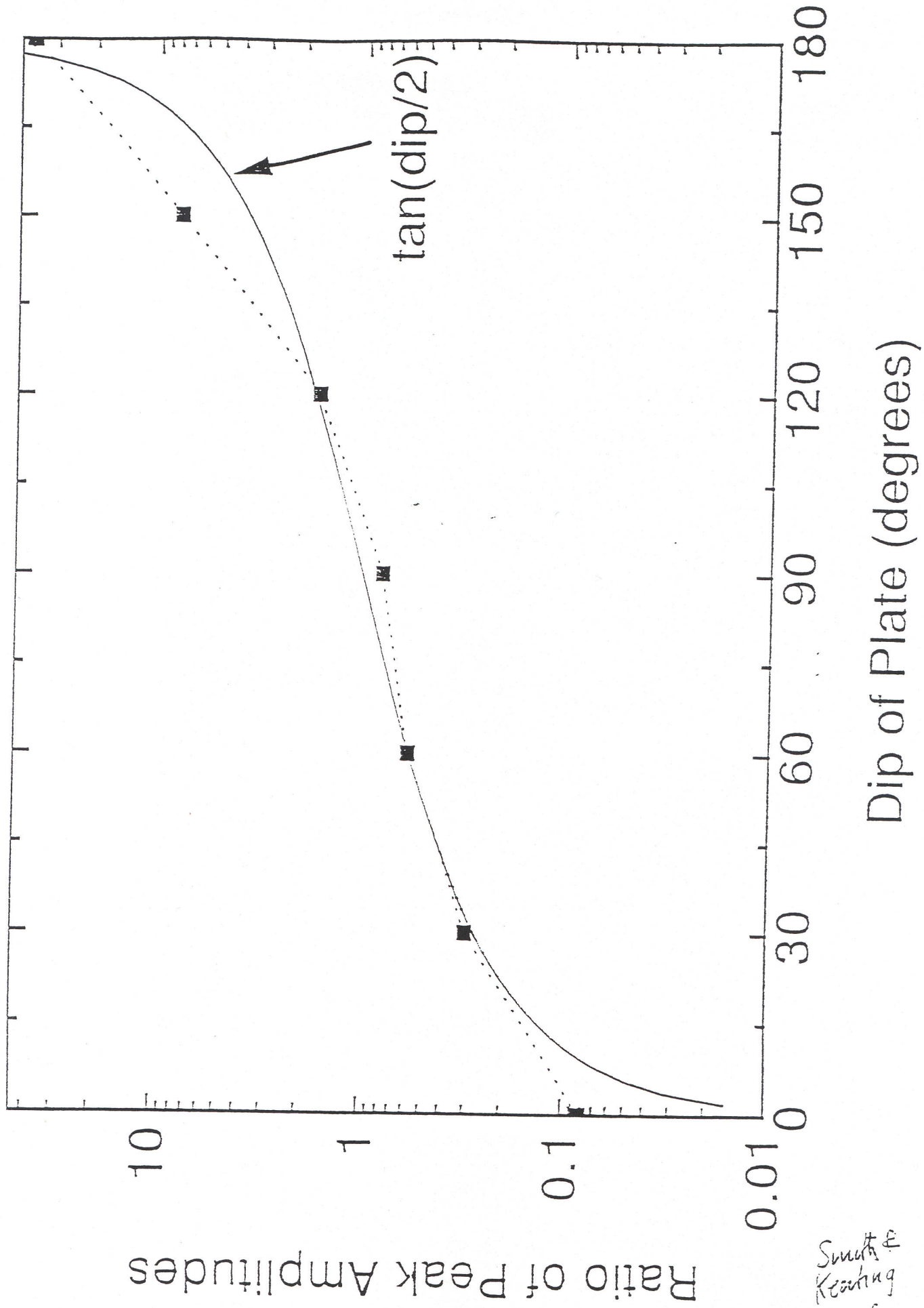
FIG 3



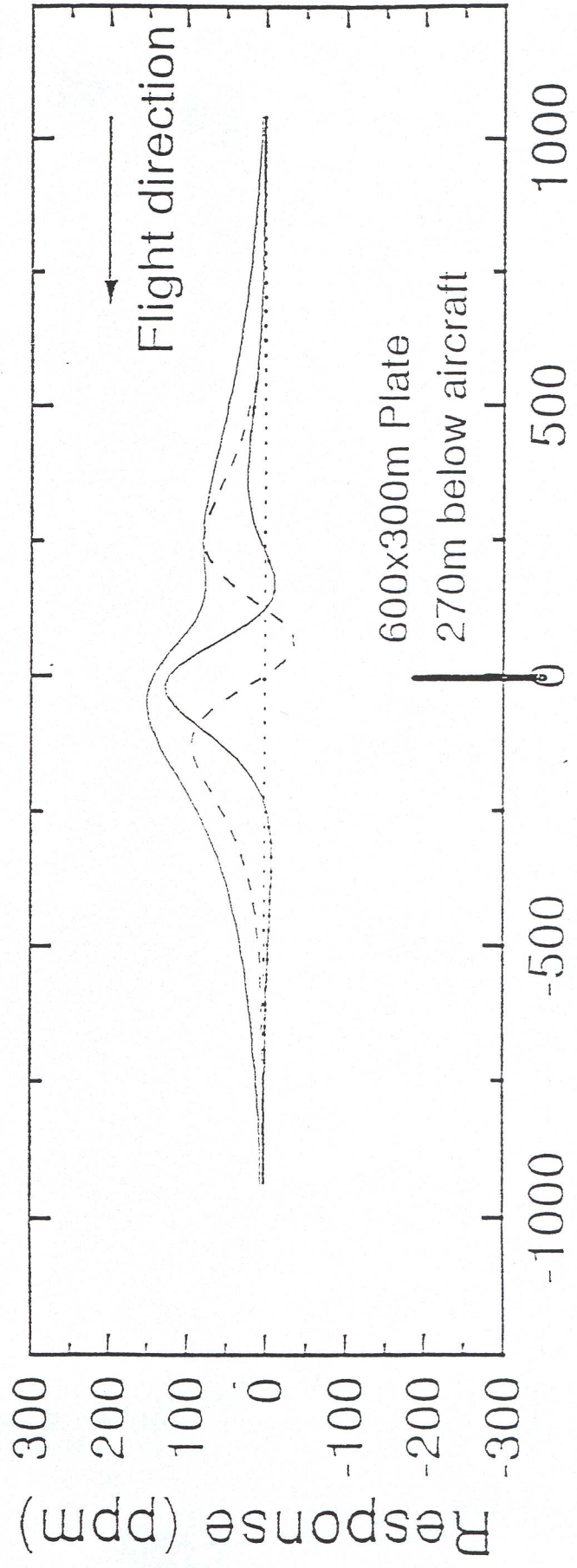
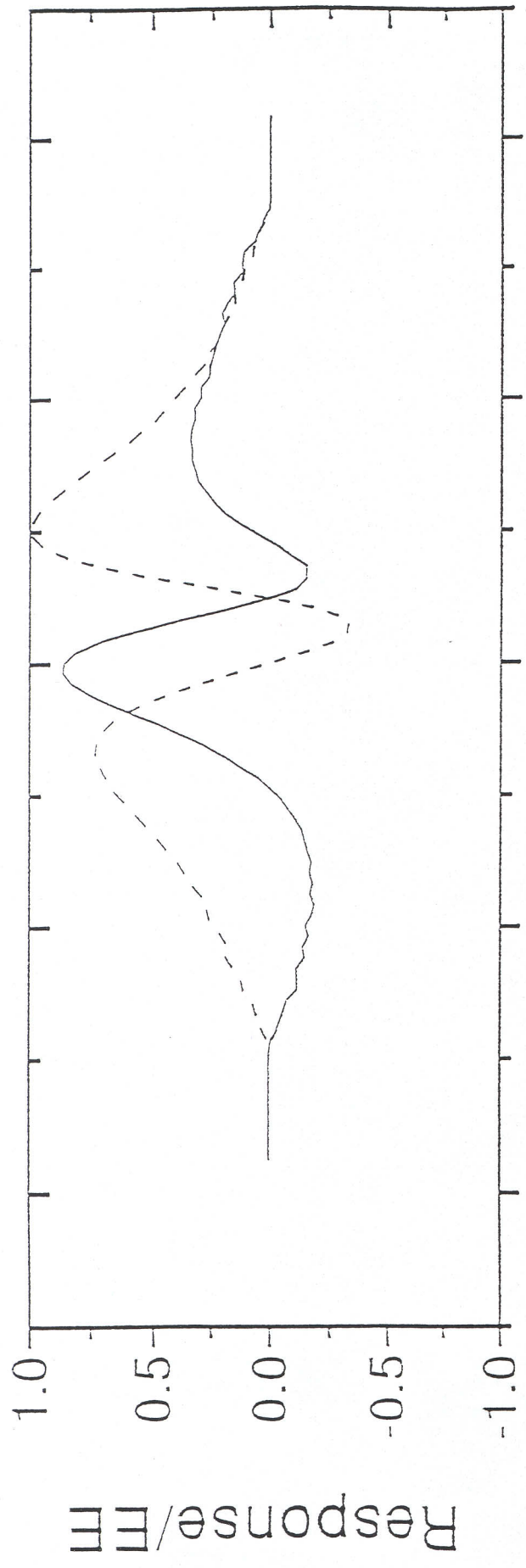
Smith &
Kearney
Fig 4



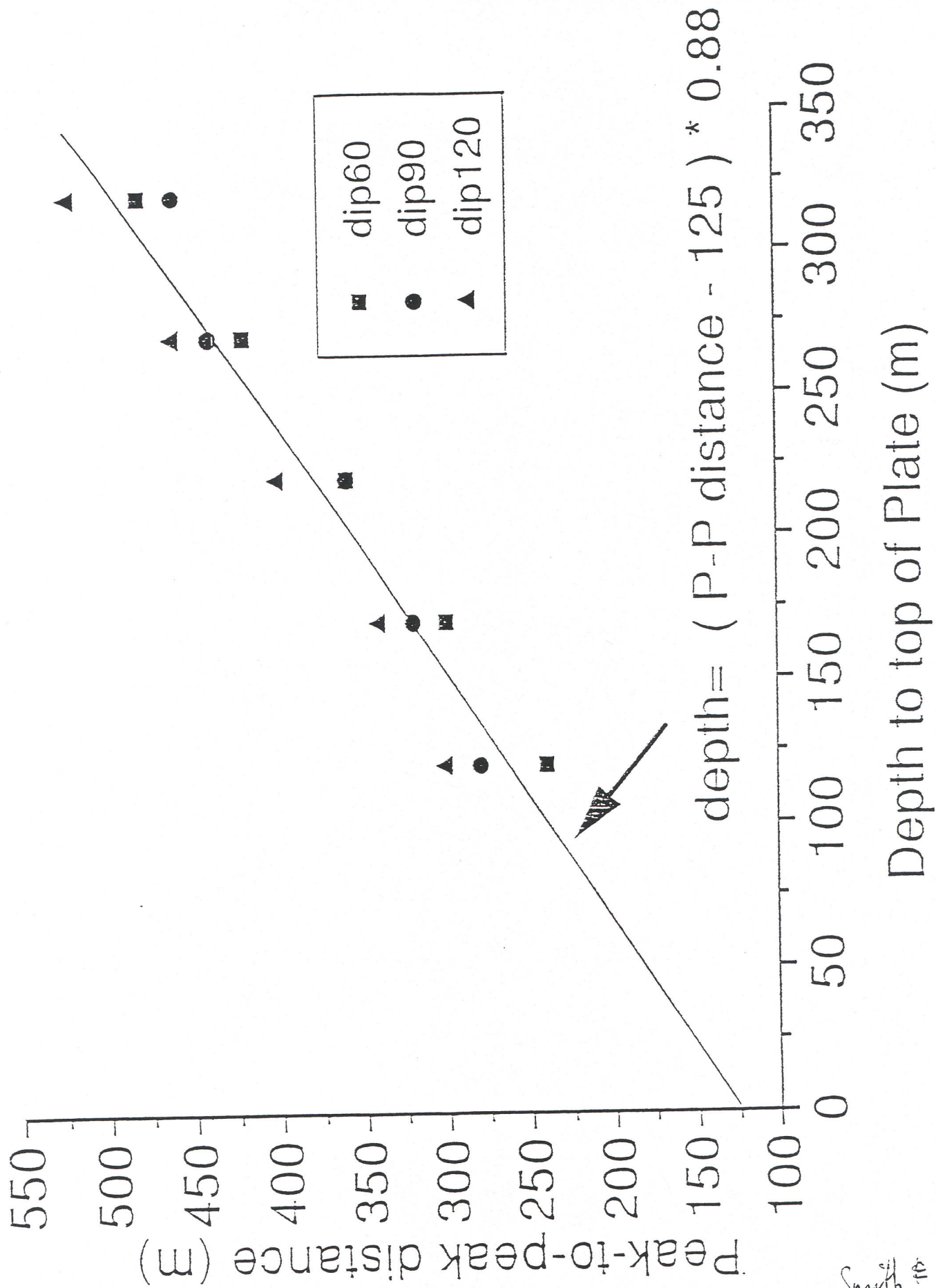
Smith &
Keating
Fig 5



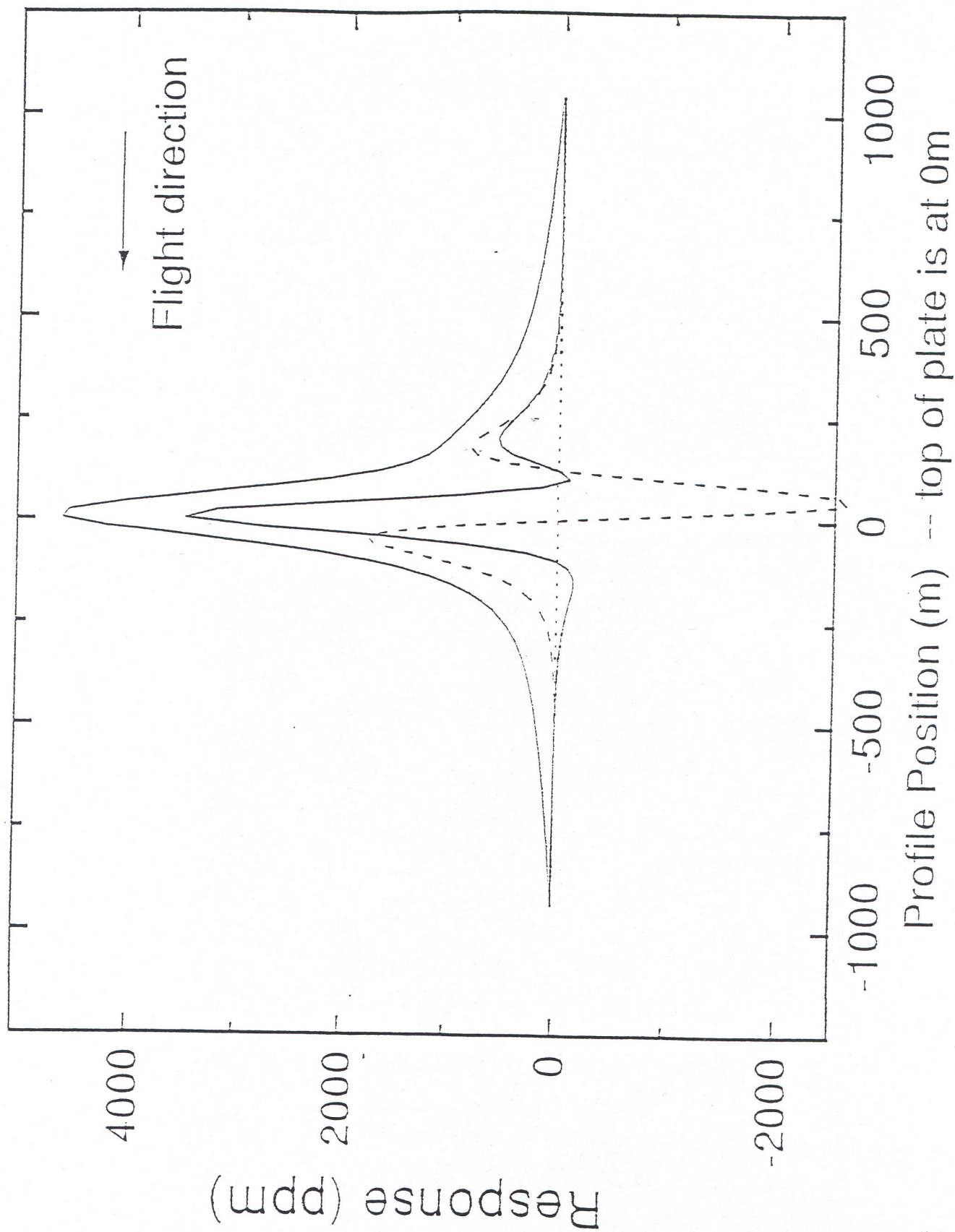
Smith &
Keating
Fig 6



Smith &
Keating
Fig 7

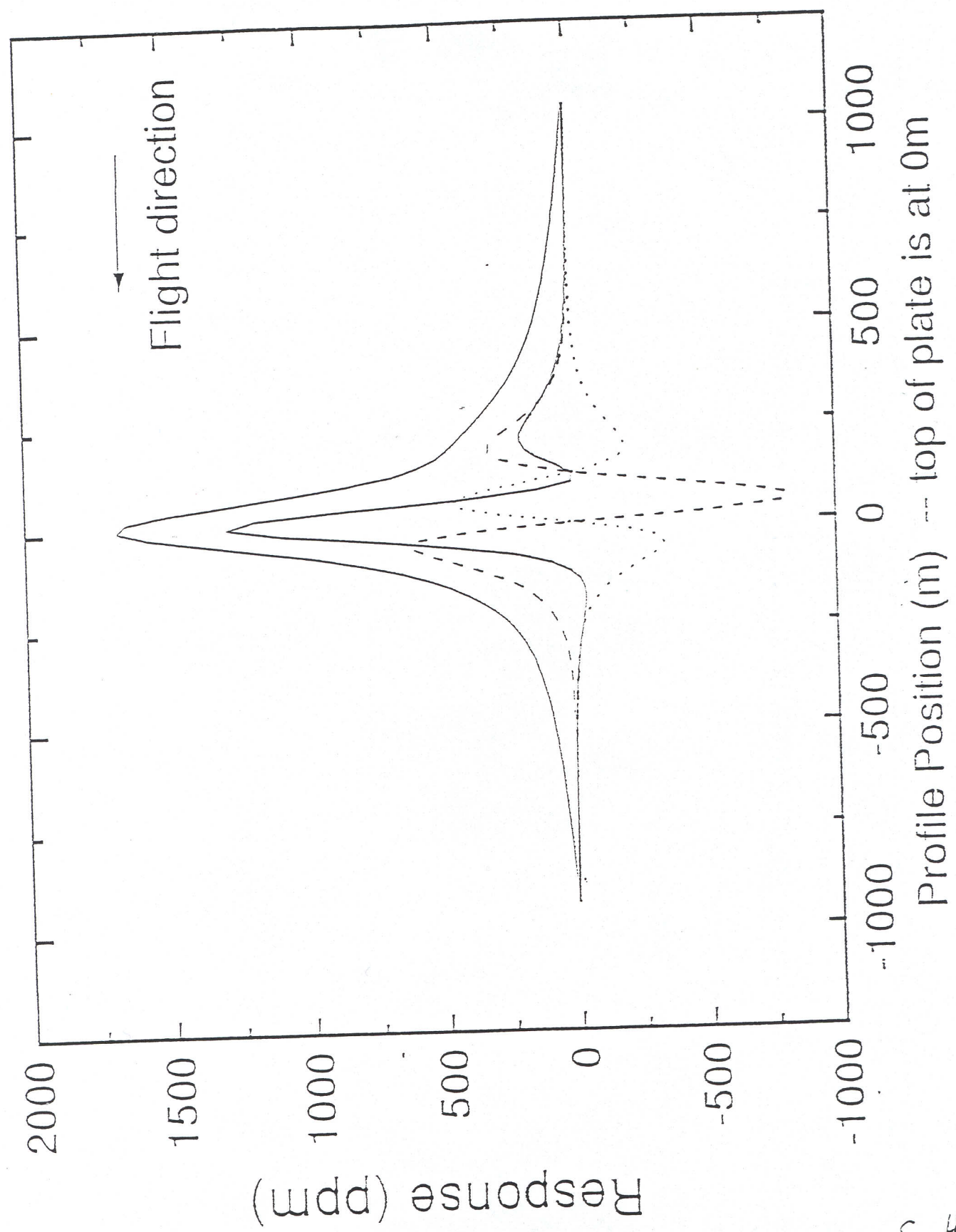


Profile line offset by 0m



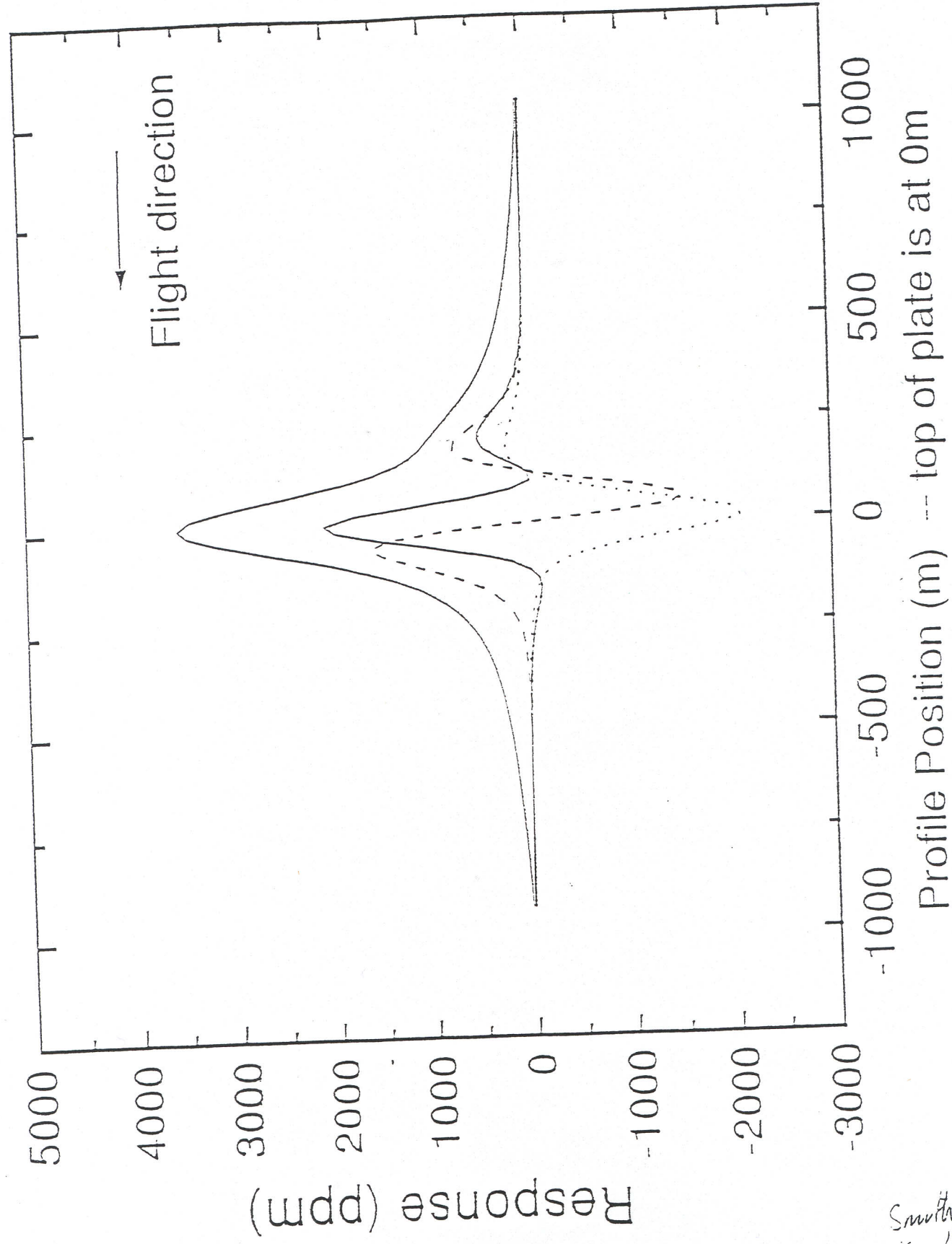
Smith
Kearney
FIG 9

Profile line onset by -150m



Smith &
Kearney
FIG 10

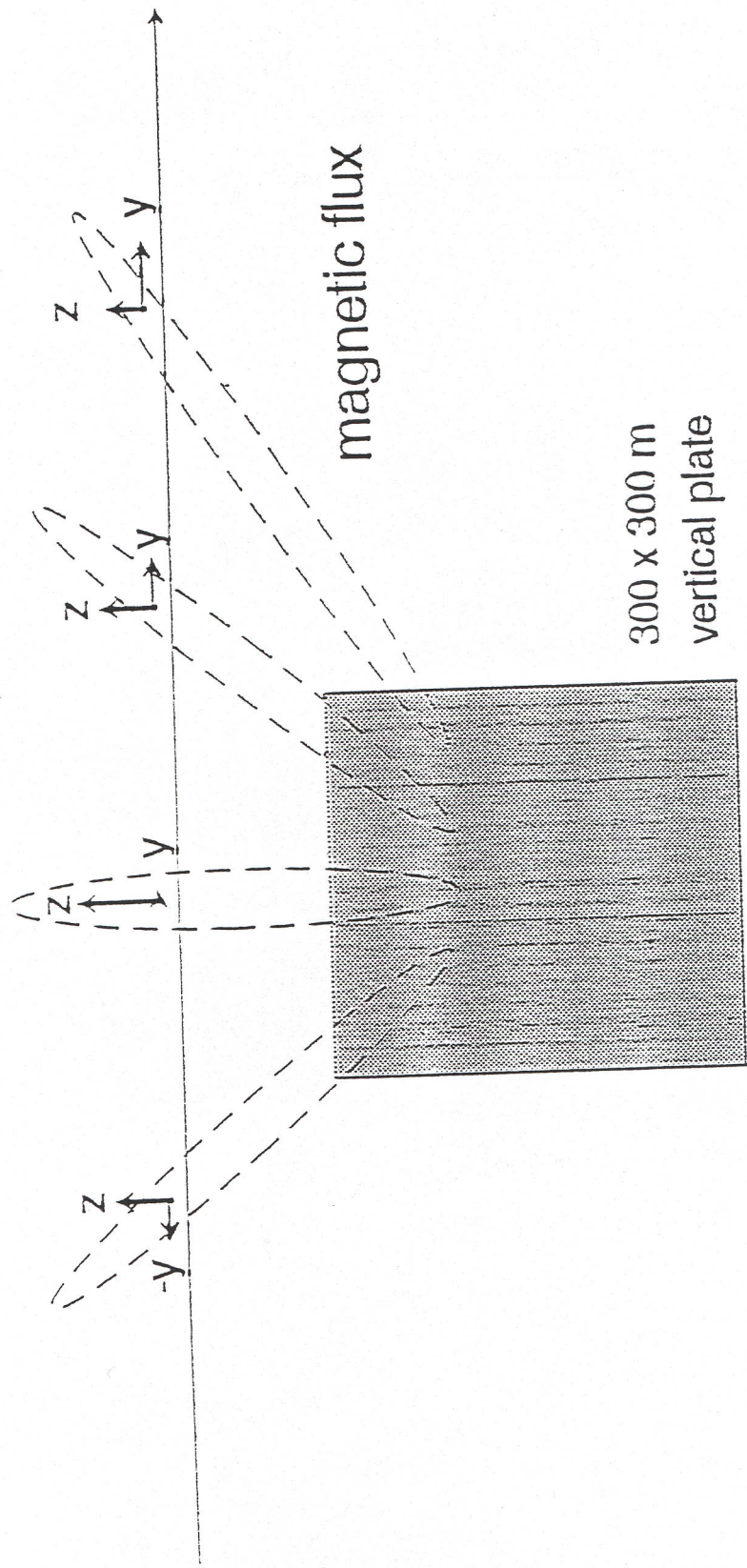
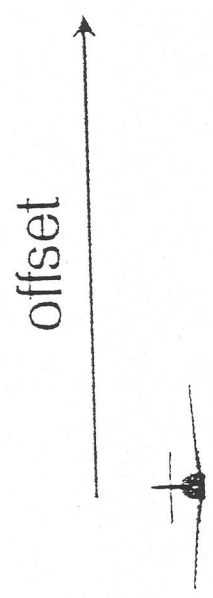
Plate strikes at 45°



Smith & Keating

FIG 11

SECTION

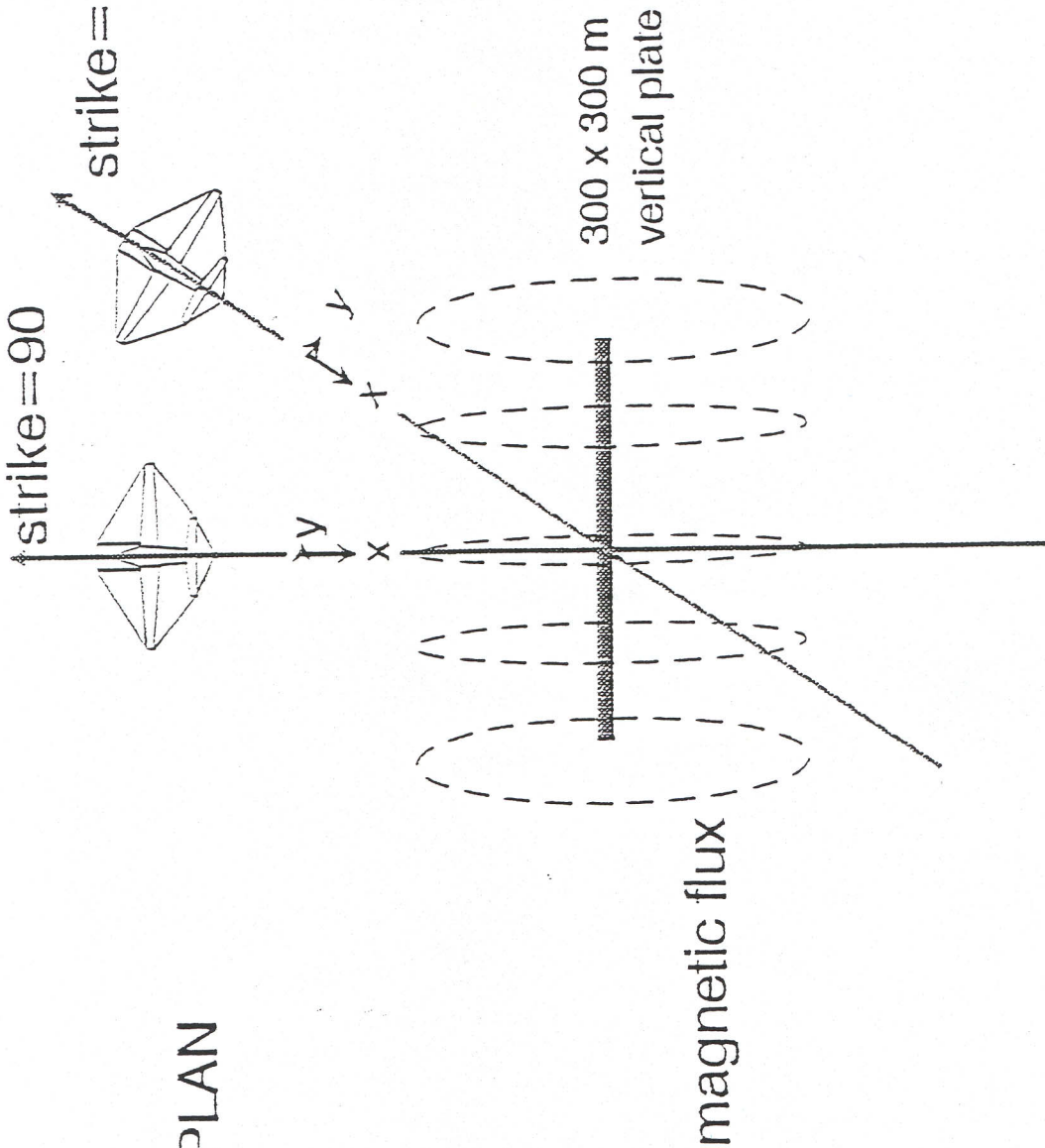


Smith &
Keating
FIG-12

strike=90

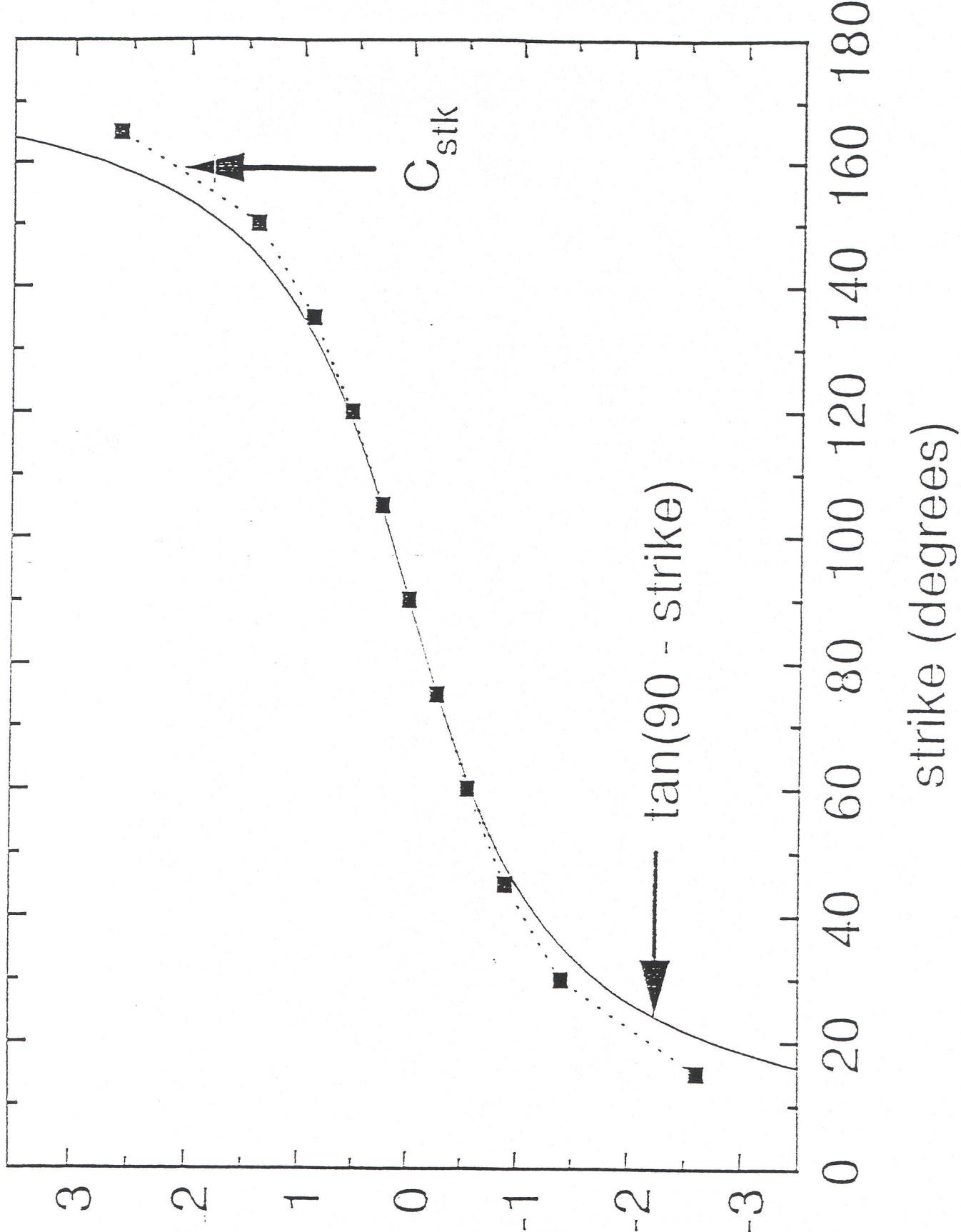
strike=120

PLAN



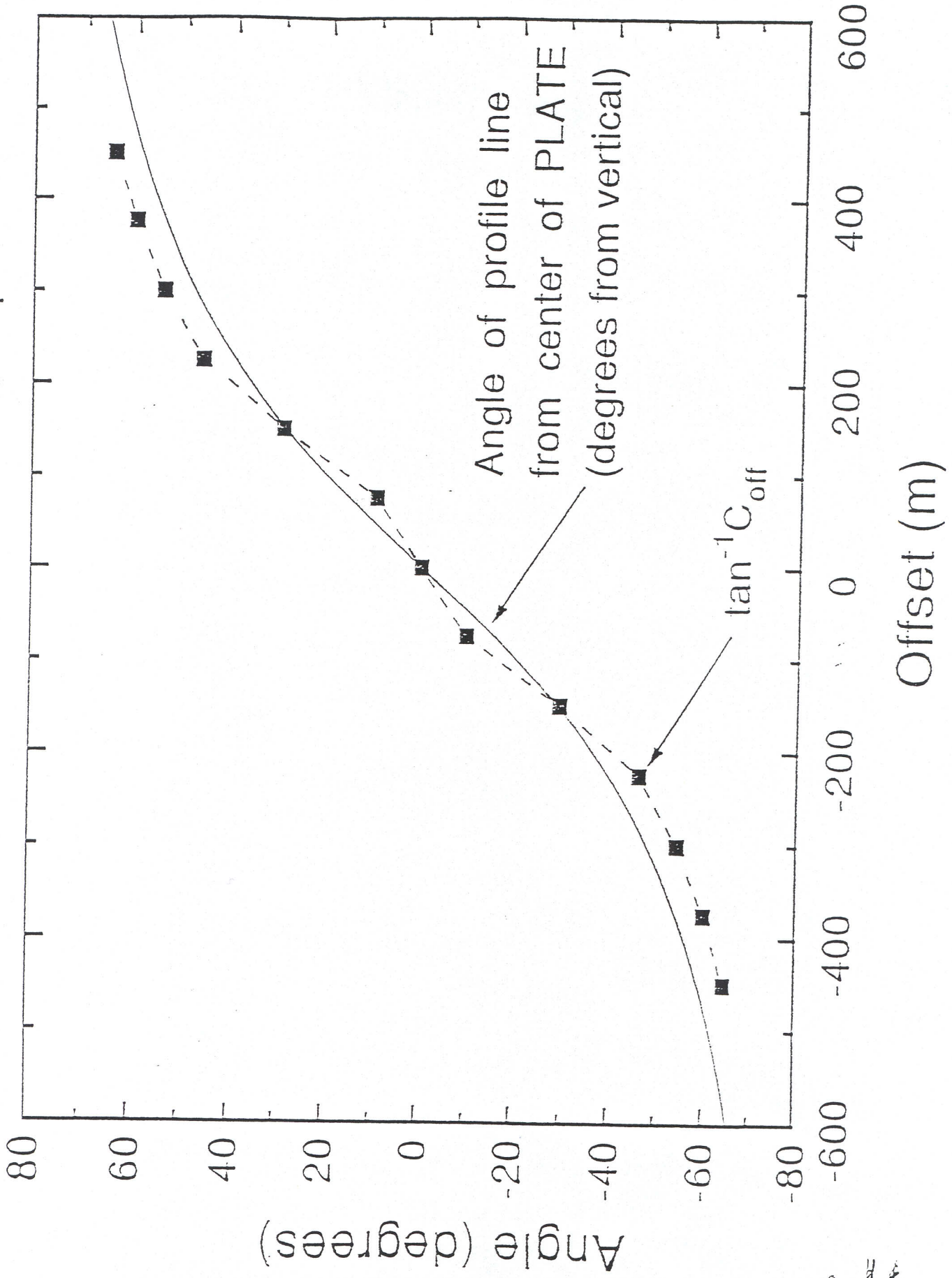
Smith &
Kraton
Fig 13

300 x 300 m Plate, 120m depth

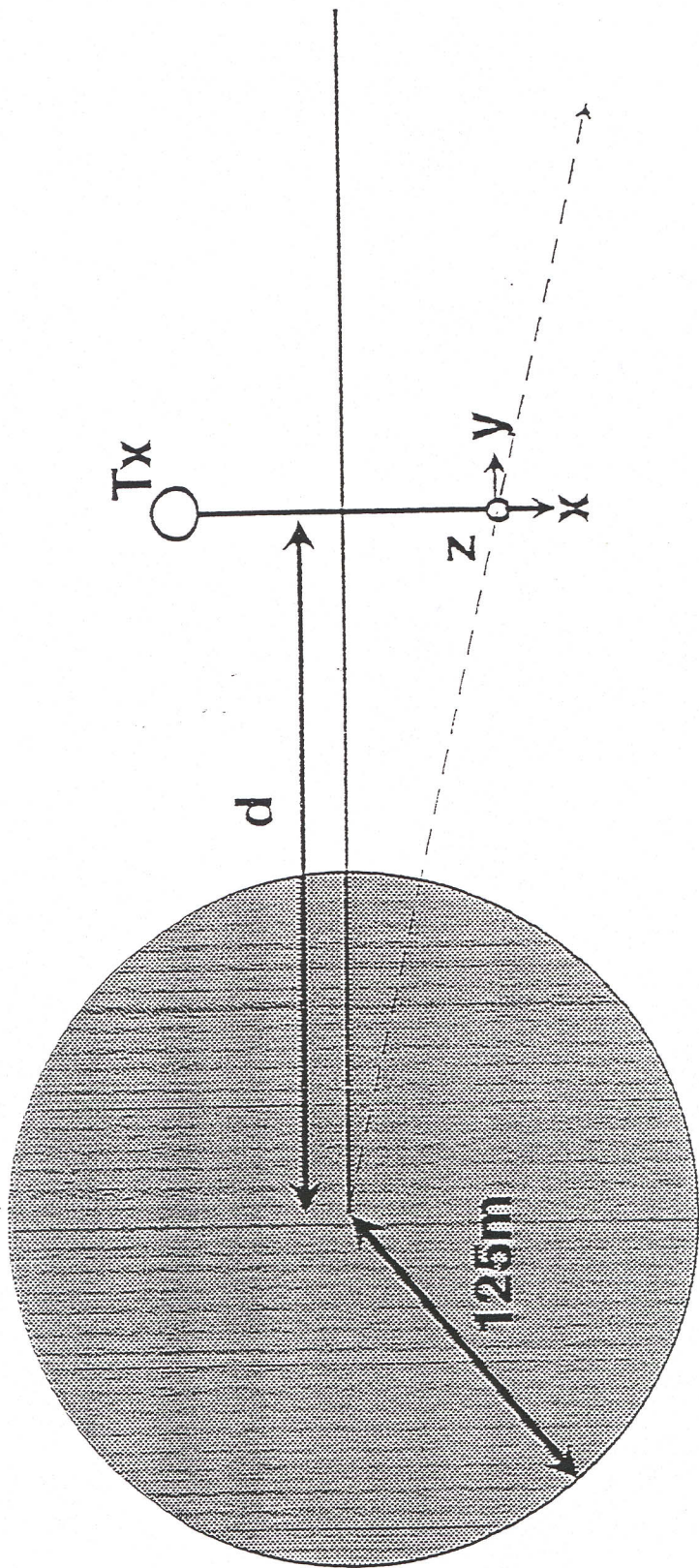


Smith
Keating
Fig 14

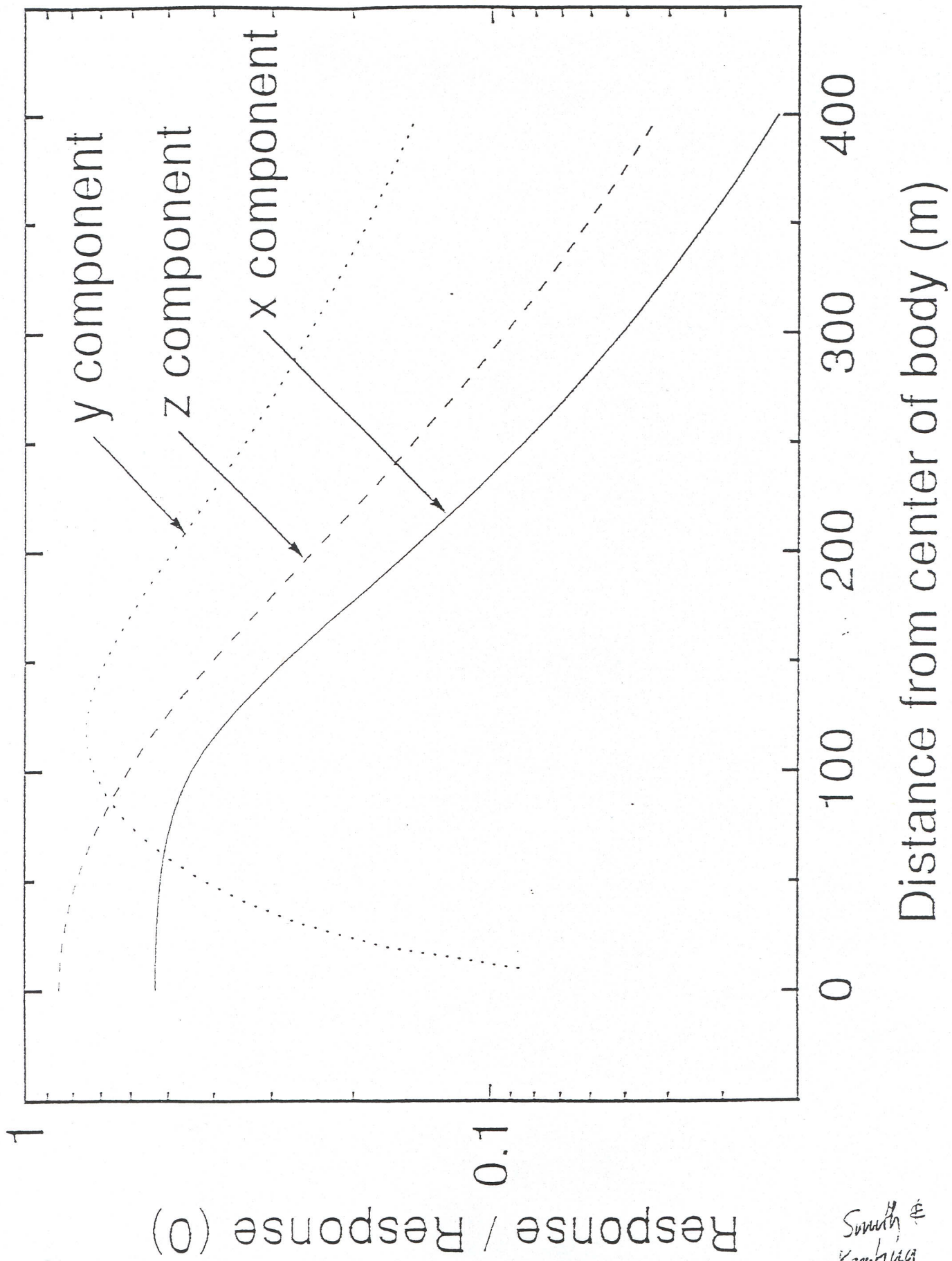
Plate 300 x 300 m at 120m depth



Smith & Keating
FIG-15



Smith &
Kearney
FIG 16



Smith &
Keebung
FIG 17.

Appendix E

Multicomponent GEOTEM[®] Modelling

Multicomponent GEOTEM modelling

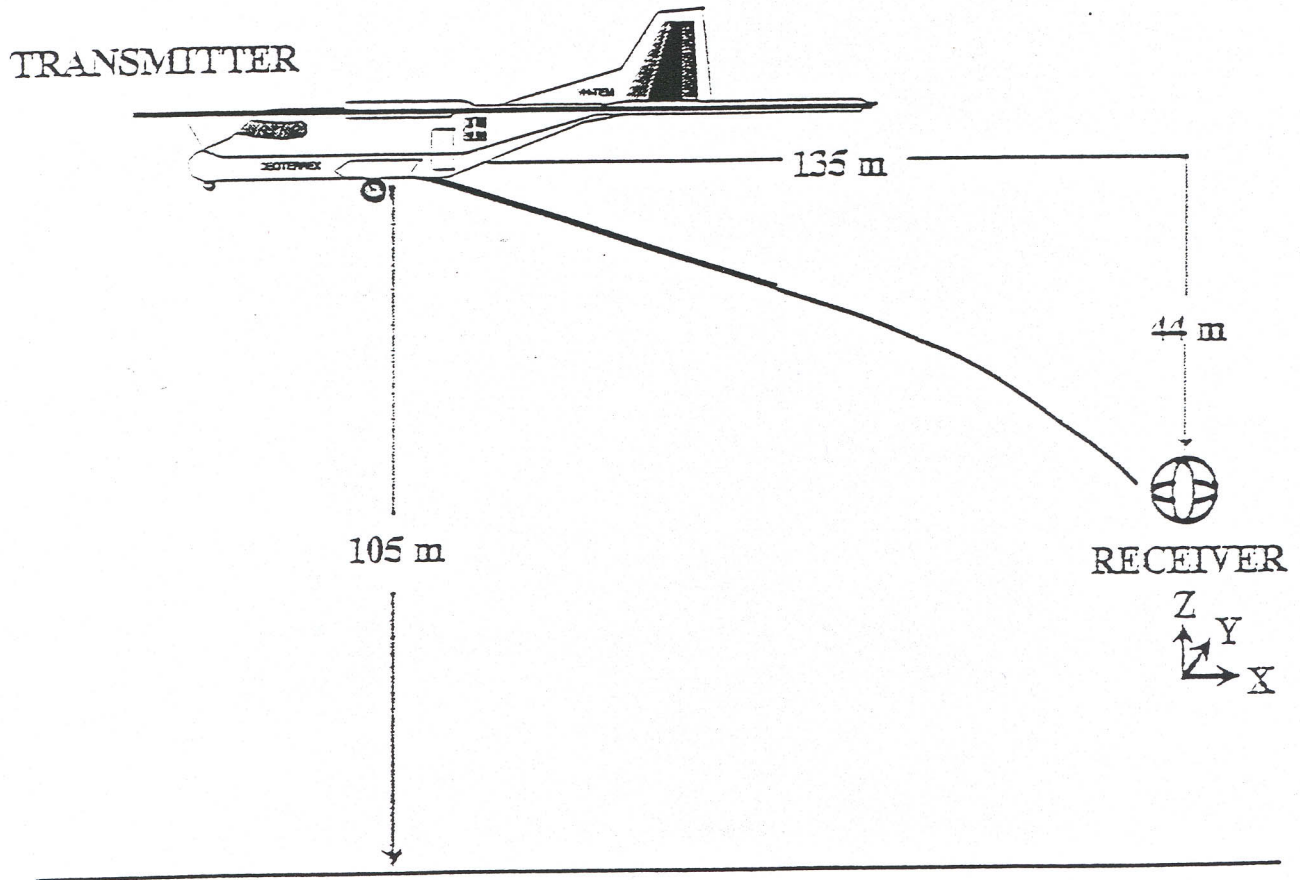
The PLATE program has been used to generate synthetic responses over a number of plate models with varying depth of burial (0, 150 and 300m) and dips (0, 45, 90 and 135 degrees). The geometry assumed for the GEOTEM system is shown on the following page, and the transmitter waveform on the subsequent page. For simplicity, only six receiver gates have been calculated and plotted.

In all cases the plate has a strike length of 600 m, with a strike direction into the page. The width of the plate is 300 m. As the flight path traverses the centre of the plate, the y component is zero and has not been plotted.

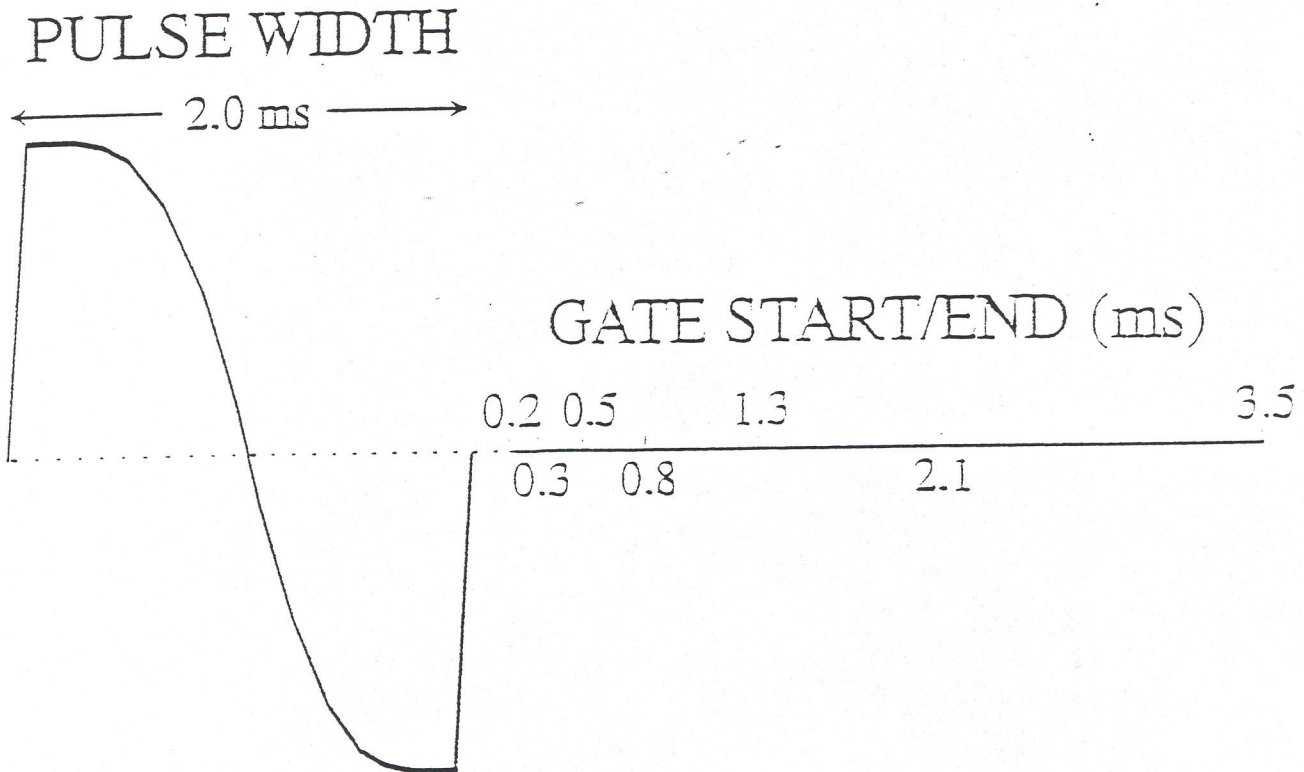
The conductance of the plate is 20 S. In cases when the conductance is different, an indication of how the amplitudes may vary can be obtained from the nomogram included.

In the following plots all components are normalized to the total primary field.

GEOTEM Geometry for modelling



Transmitter Waveform and Receiver sampling



Nomogram

ppm / (ppm for 20 S case)

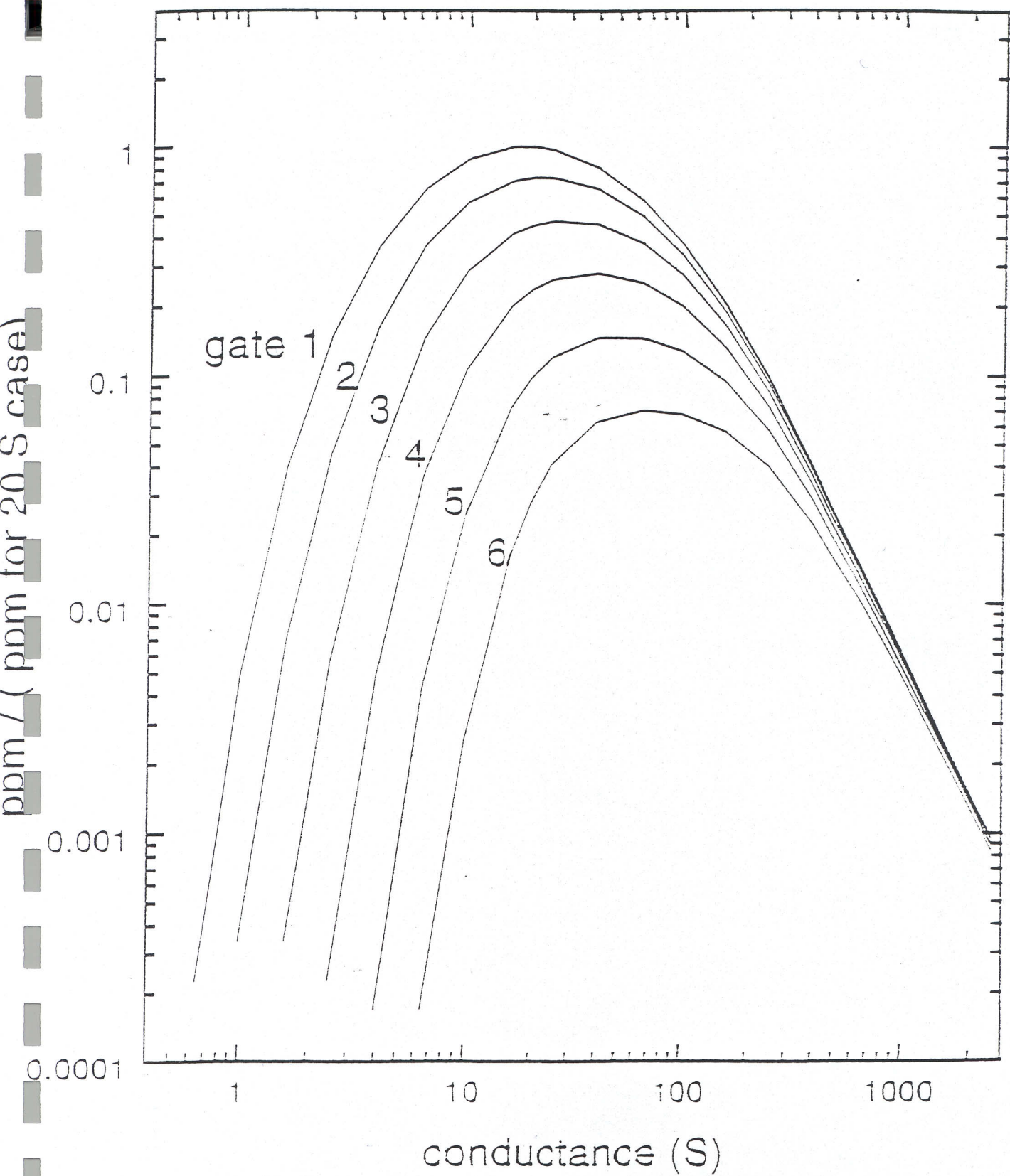


Plate: depth =0; dip =0

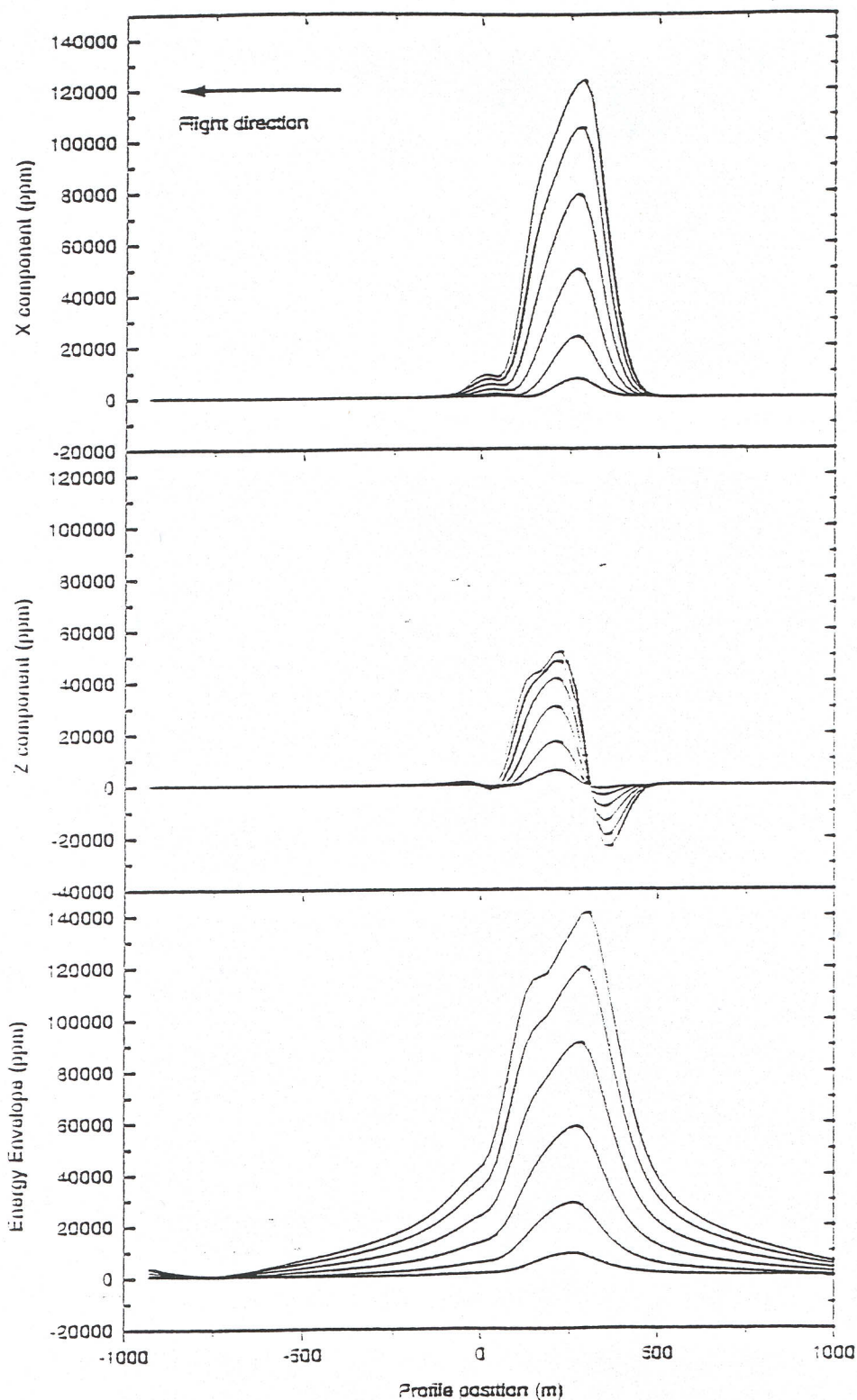


Plate: depth = 150; dip = 0

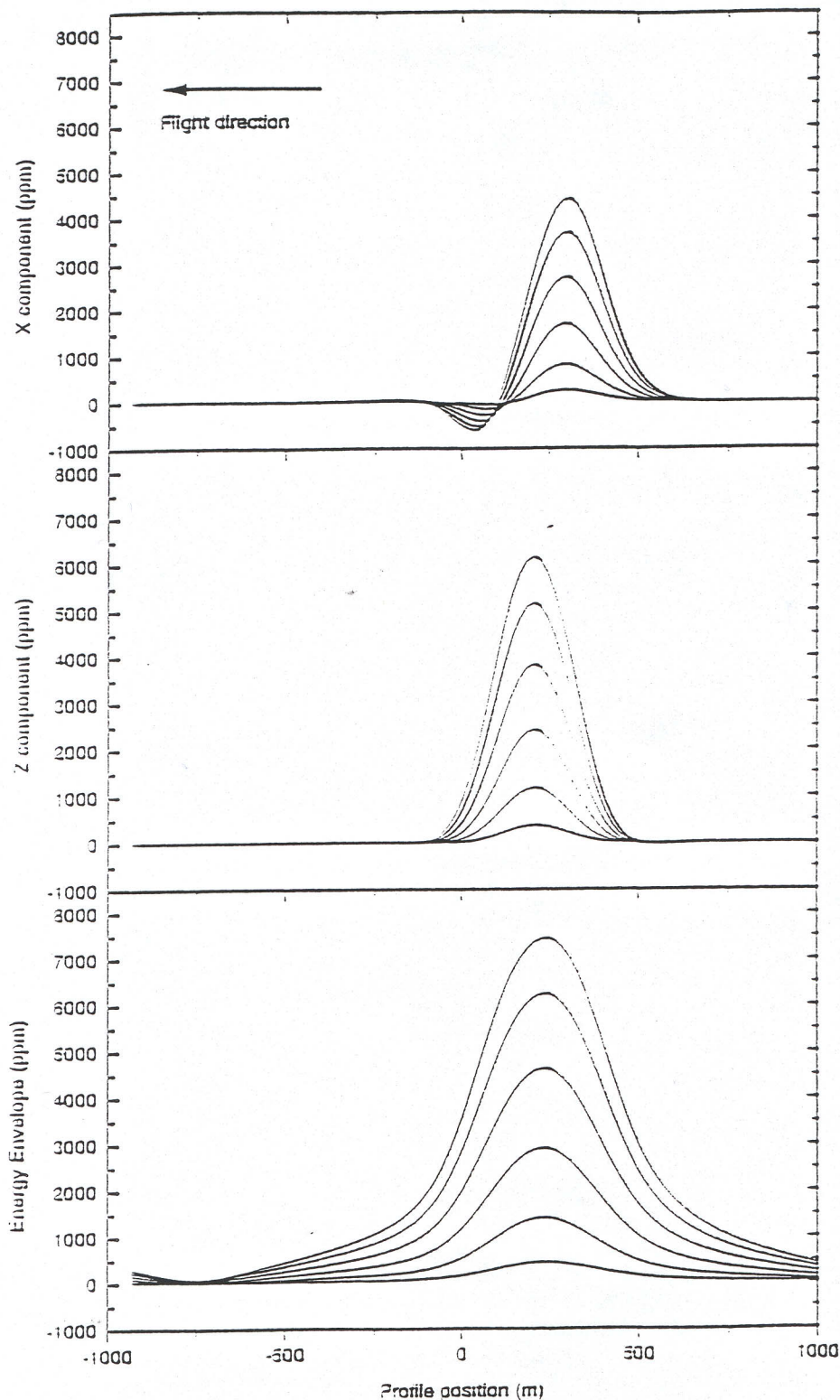


Plate: depth =300; dip =0

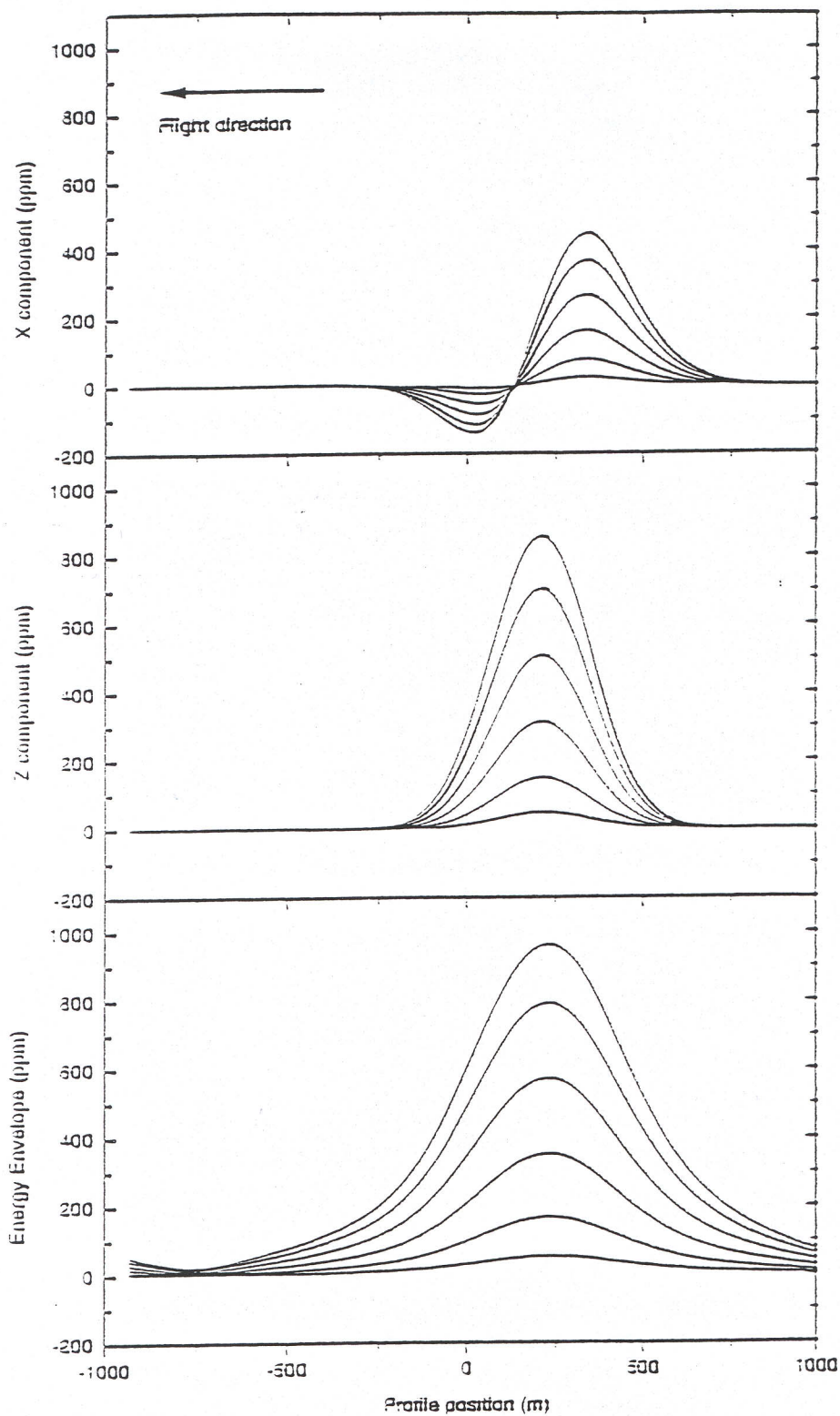


Plate: depth =0; dip =45

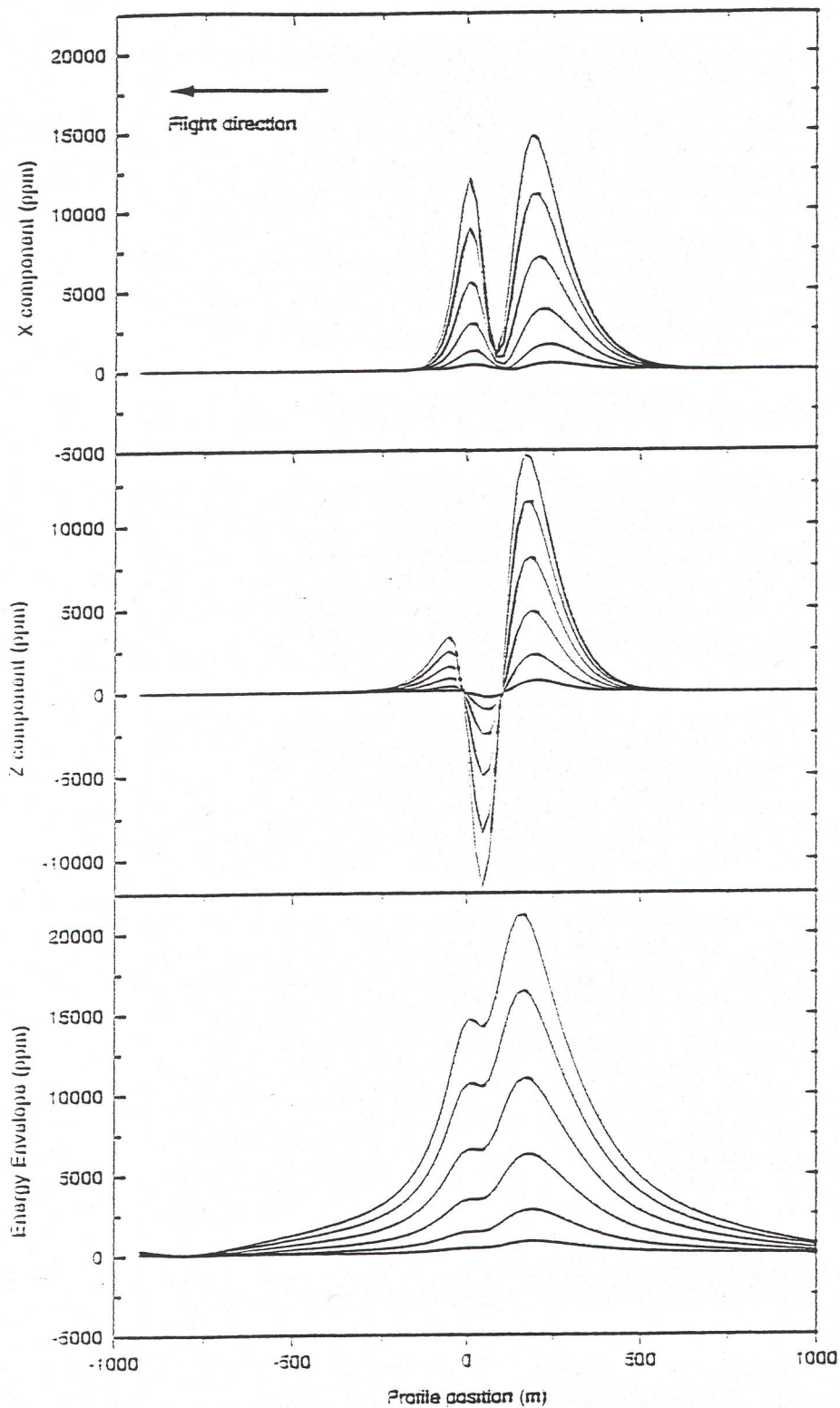


Plate: depth =150; dip =45

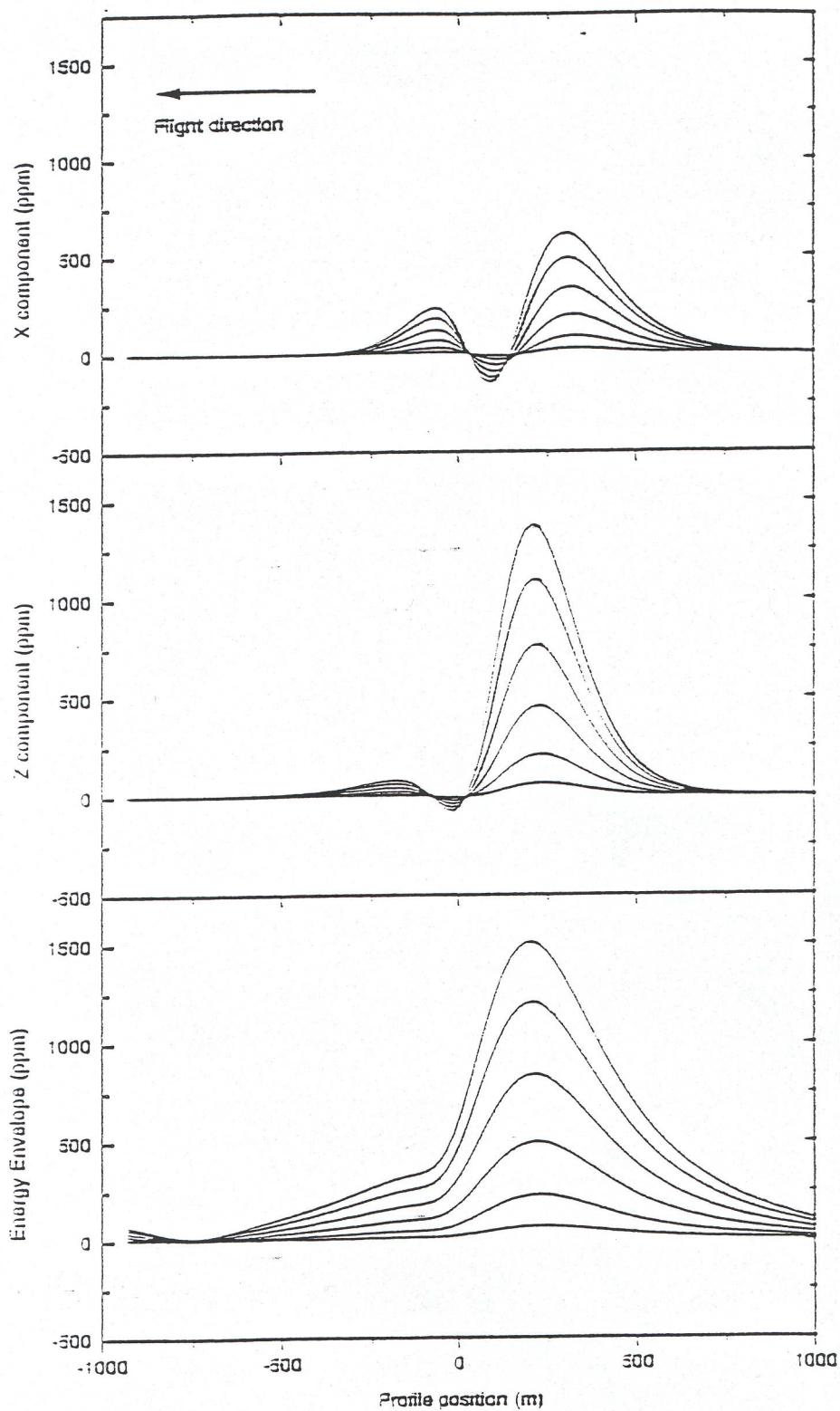


Plate: depth =300; dip =45

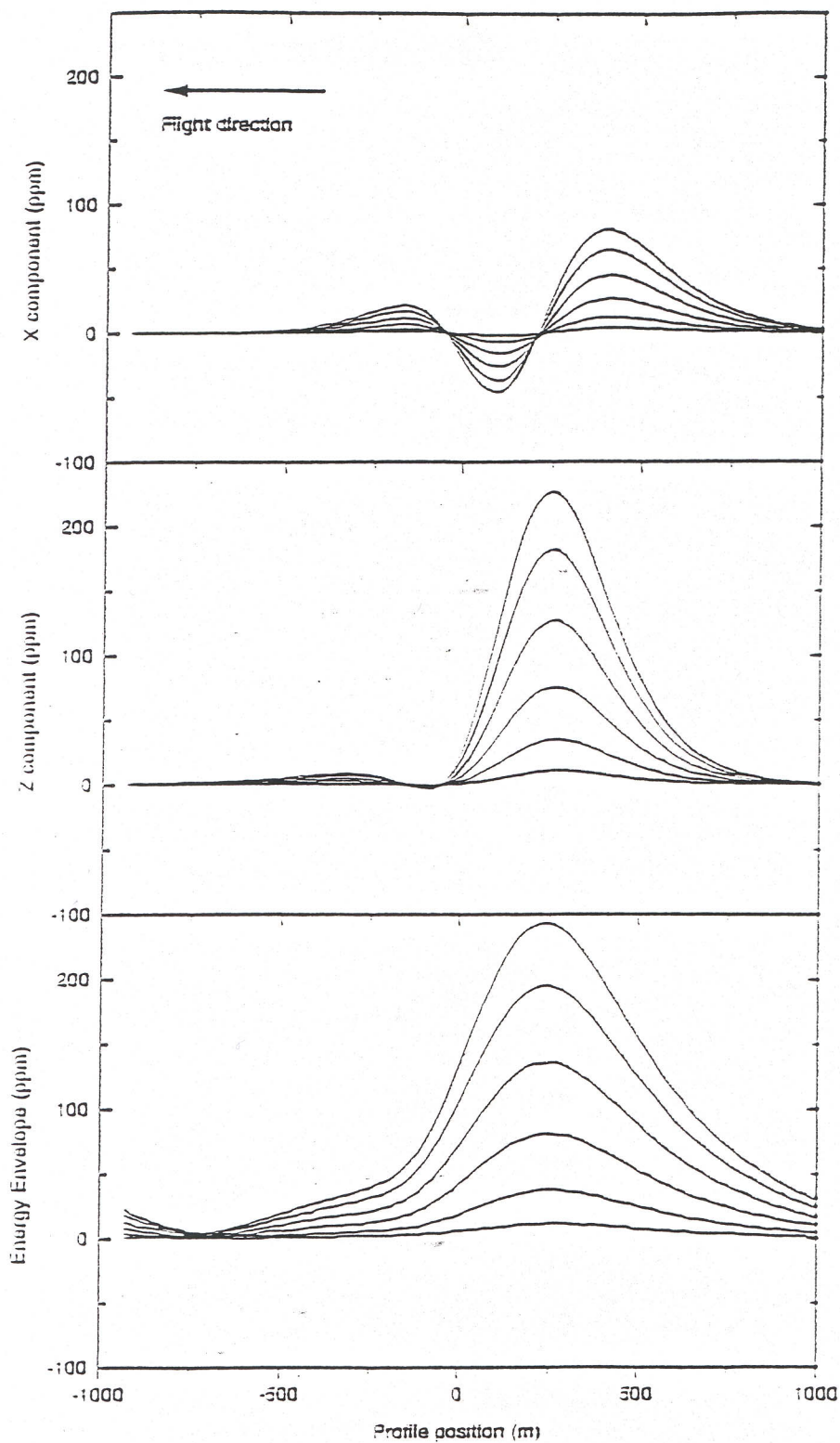


Plate: depth = 0; dip = 90

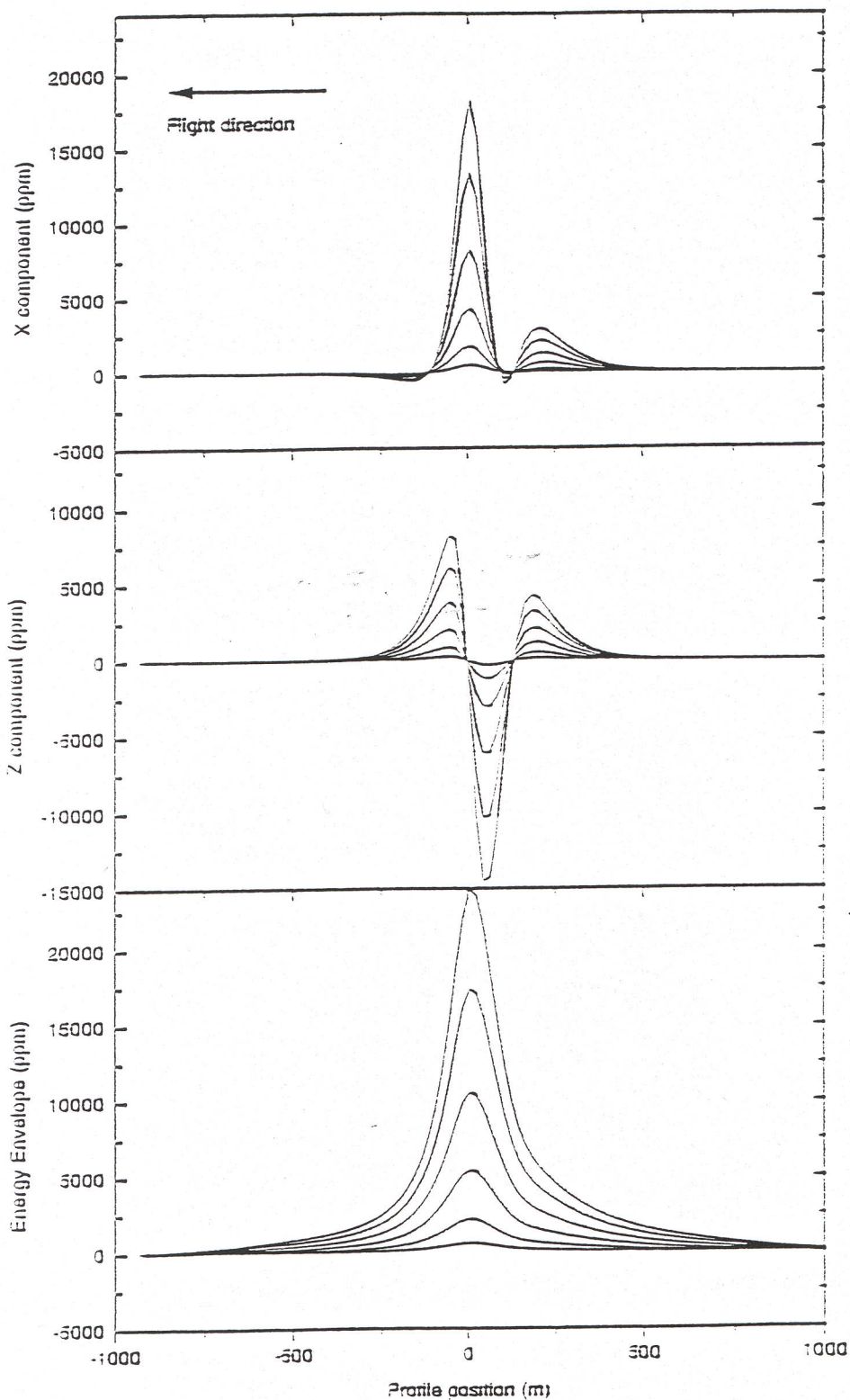


Plate: depth =150; dip =90

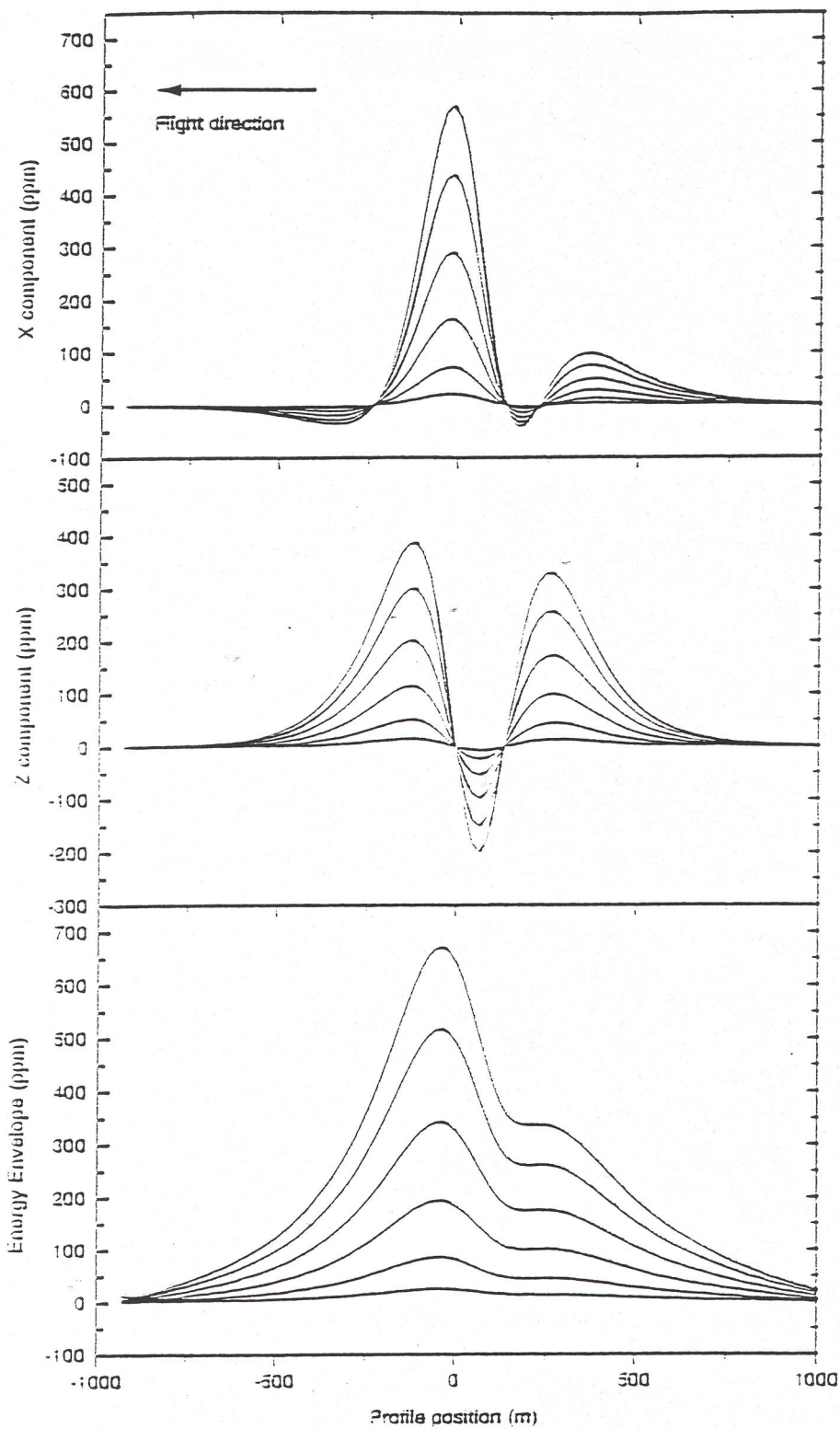


Plate: depth = 300; dip = 90

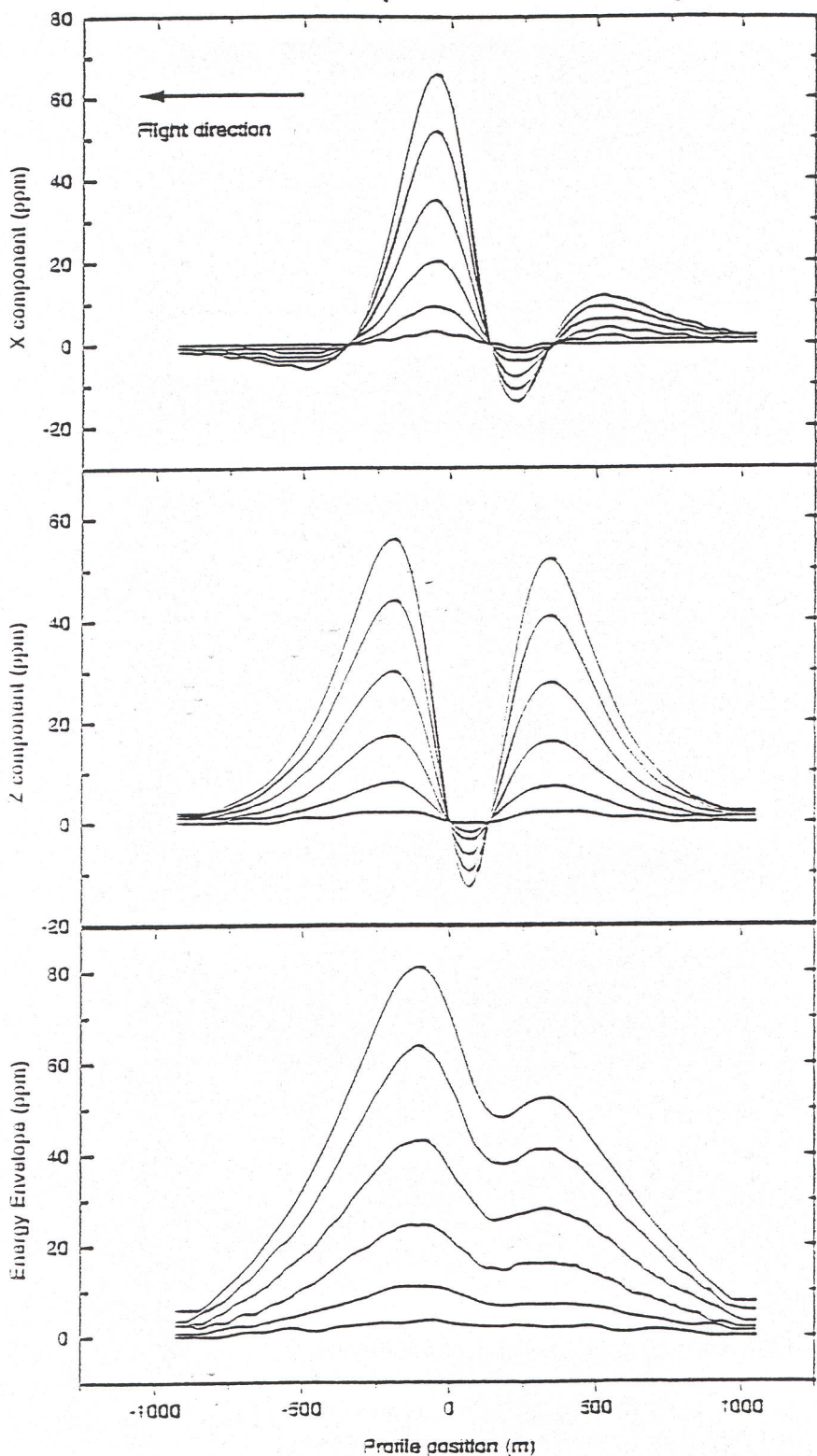


Plate: depth = 0; dip = 135

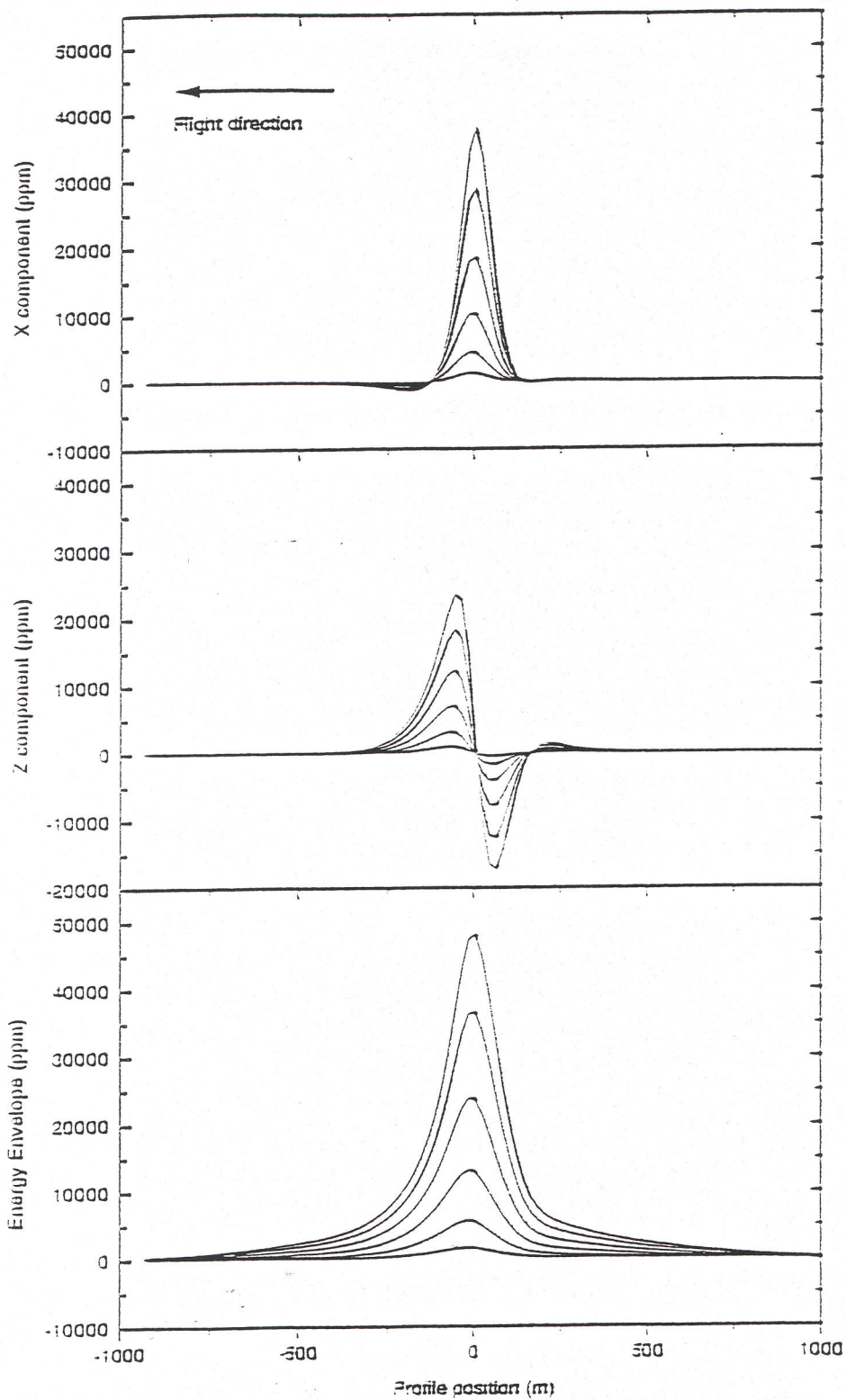


Plate: depth =150; dip =135

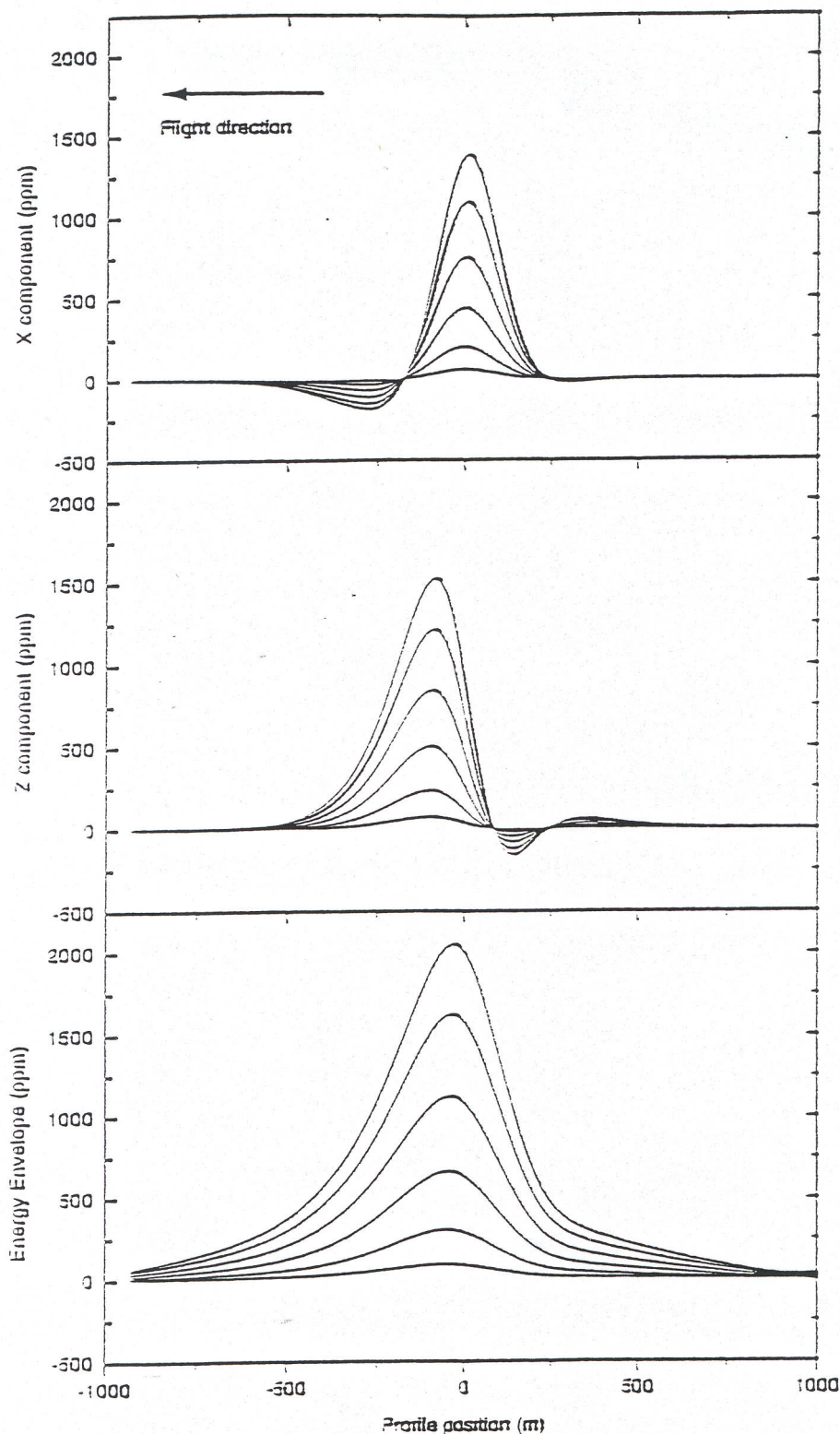
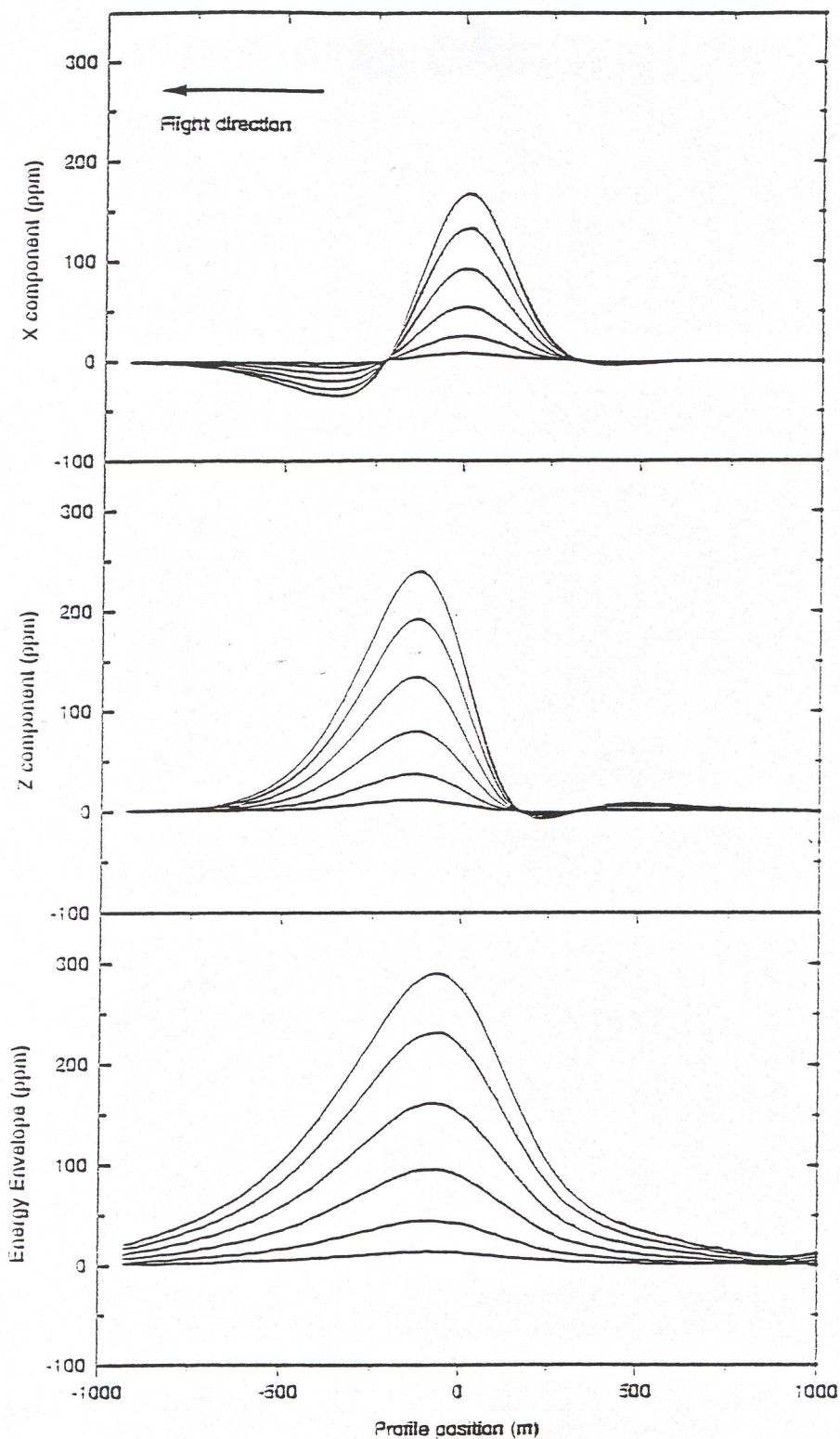


Plate: depth =300; dip =135



Appendix F

Archive Format Description

GPS ACCURACY CHECK

Flown at the Sierra Vista airport
March 14,1997

File : gpscheck.001

ASCII coded 13 I 10

Record length = 130 + CR = 131

One record per bloc

FORMAT

CHARACTERS	VARIABLE	UNITS
1-10	Line identifier	Line x 100 + part
11-20	Fiducial	Seconds
21-30	GPS Latitude (WGS84)	DD.ddddddd
31-40	GPS Longitude (WGS84)	DD.ddddddd
41-50	GPS Latitude (Clarke 1866)	DD.ddddddd
51-60	GPS Longitude (Clarke 1866)	DD.ddddddd
61-70	UTM Easting (Clarke 1866)	metres
71-80	UTM Northing (Clarke 1866)	metres
81-90	GPS Elevation	metres x 100
91-100	GPS Acquired time	Sec x 100
101-110	GPS UTC Time	Sec x 10
111-120	GPS Satellite designator	n.a.
121-130	GPS PDOP	n.a.
131-131	CR	

Data is archived as one sample per second.

LINE-ID DIR FST-FID LST-FID TAPE BLOCK REC SAMPLES

1	0	52362	60430	1	1	1	8069
2	0	61045	62380	1	8070	1	1336

* * * * * ARCFLT COMPLETED * * * * *

MAG & EM LAG CHECK

Flown near the Sierra Vista airport

March 14,1997

File : magemlag.001

ASCII coded 5 I 10

Record length = 50 + CR = 51

One record per bloc

FORMAT

CHARACTERS	VARIABLE	UNITS
1-10	Line identifier	Line x 100 + part
11-20	Fiducial	Seconds
21-30	Raw x-coil channel 11	ppm
31-40	Raw Magnetics	nT x 100
41-50	Distance	metres
51-51	CR	

Data is archived as ten samples per second.

LINE-ID DIR FST-FID LST-FID TAPE BLOCK REC SAMPLES

101	3	59708	59748	1	1	1	401
201	1	59838	59878	1	402	1	401
301	3	59974	60024	1	803	1	501
401	1	60115	60155	1	1304	1	401

* * * * * ARCFLT COMPLETED * * * * *

ALTIMETER CALIBRATION CHECK

Flown at the Sierra Vista airport
March 14,1997

File : altcal.001

ASCII coded 7 I 10

Record length = 70 + CR = 71

One record per bloc

FORMAT

CHARACTERS	VARIABLE	UNITS
1-10	Line identifier	Line x 100 + part
11-20	Fiducial	Seconds
21-30	UTM Easting (Clarke 1866)	metres
31-40	UTM Northing (Clarke 1866)	metres
41-50	Radar altimeter	feet
51-60	Barometric altimeter	feet
61-70	GPS Elevation	metres x 100
71-71	CR	

Data is archived as one sample per second.

LINE-ID DIR FST-FID LST-FID TAPE BLOCK REC SAMPLES

1 0 66722 68081 1 1 1 1360

* * * * * ARCFLT COMPLETED * * * * *

Appendix G

Contents of CDT grids

CONTENT OF THE CONDUCTIVITY-DEPTH-TRANSFORM GRIDS

X values = Distance along the flight line.

The grid spacing will vary slightly from one line to the next reflecting the change in the average flying speed along each line.

The number of grid cells along the line is defined by the length of the line in metres, divided by the scale and multiplied by 1000, and this value rounded up to the nearest multiple of 64.

eg. For a line which has a length of 25,500 metres, and created for a scale of 1/50,000, the number of grid cells will be:

$$(25,500 / 50,000) \times 1000 = 510$$

$$\text{and } 510/64 = 7.969 \text{ rounded up to } 8 \times 64 = 512$$

The actual grid spacing in the X direction will then be the length of the line divided by the number of grid cells determined.

$$\text{eg. } 25,500 / 512 = 49.805 \text{ m}$$

Y values = Depth values.

For the desired maximum depth of investigation, 128 rows are allocated, resulting in a fixed Y direction cell size equal to the desired maximum depth divided by 128.

$$\text{eg. } 600 \text{ m} / 128 = 4.688 \text{ m}$$

Z values = Computed resistivity values, based on a layered earth model.

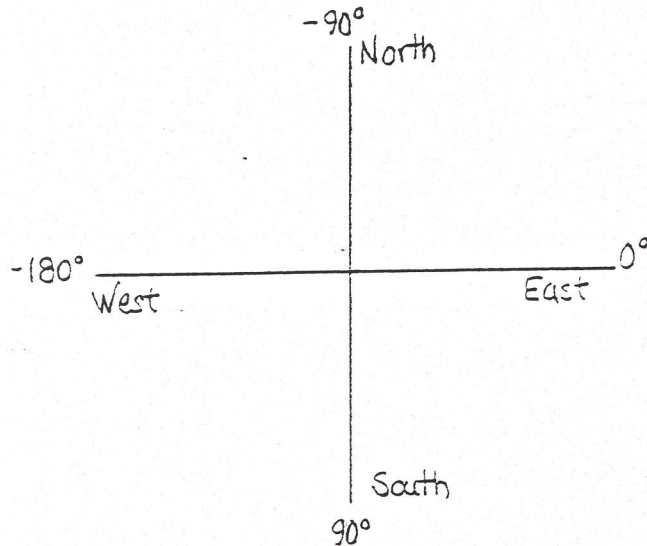
These values are actually stored as $(\log_{10}$ of conductivity in Siemens/m) multiplied by 1000.

The conversion to resistivity in ohm-m is then:

$$\text{Antilog}_{10}(\text{value}/1000)^{-1}$$

$$\text{eg. } -2500 = (\text{Antilog}_{10}-2.5)^{-1} = 316 \text{ ohm-m}$$

Grid rotation angle : This angle is the heading of the flight line based on a Cartesian notation, and therefore will change by 180° for reciprocal line directions.



Example from line 619 of the Cochiti Block:

Length of line is 27.767 Km

Maximum depth of investigation is 1300 metres below the reference datum, selected to be 2500 metres above sea level.

Horizontal scale 1/100,000

Content of the CDT grid file

Number of rows (Y direction)	128
Number of columns (X direction).....	320
X grid spacing	86.772 m
Y grid spacing	10.156 m
Z multiplier	0.001
Min value	-4.003
Max value	-0.731

The number of columns and X grid spacing are defined by :

$$\text{length of line (27767 m)} \times \text{scale (100,000)} \times 1000 = 277.67$$

$$\text{then, } 277.67/64 = 4.339 \text{ rounded-up to } 5$$

$$\text{and } 5 \times 64 = 320 \text{ columns}$$

$$\text{grid spacing is then equal to length of line (27767 m) / 320 = 86.772 m}$$

The Y grid spacing is defined by :

$$\text{Depth of investigation (1300 m) / 128 rows} = 10.156 \text{ m}$$

The true data range is :

$$\text{Minimum of } -4.003 = \text{Antilog}_{10} -4.003^{-1} = 10069 \text{ ohm-m}$$

$$\text{Maximum of } -0.731 = \text{Antilog}_{10} -0.731^{-1} = 5.38 \text{ ohm-m}$$

Correction of CDT grids for Topography

The CDT grids have traditionally been created with the depth information relative to surface, with surface represented as a horizontal line (top of the CDT grid). In areas of generally flat terrain, this representation is acceptable. However, in more rugged areas, this representation can be misleading and result in false interpretation of the results, if one is not careful; i.e. what may appear to be a steeply dipping layer may actually be a horizontal layer passing under a steep hill, since the surface reference at this point is not horizontal, but rising sharply.

For this reason, the surface reference of the CDT grids has been reprojected to the true terrain surface. The grid file must still however have a horizontal datum reference, which in this case has now been chosen as a datum slightly above the highest barometric elevation reached over the survey block. This is taken into account at the creation of the CDT grid, since the desired maximum depth of investigation must now be specified from the barometric datum chosen and not from surface. This will explain what may at first appear to be an "overly optimistic" depth of investigation.

When viewing the "Terrain corrected" CDT grids, the blank area between the top of the section and the first layer of real values represents air. The contour of the first layer of real values defines the ground surface and should match the true topography (this has been computed by the programme from the radar and barometric altimeter data).

The following parameters were used for the present survey

<u>Area</u>	<u>Barometric reference</u>	<u>Max. depth of investigation</u>
Rio Rancho	2200 metres	1100 metres
Rio Puerco	2300 metres	1000 metres
Cochiti	2500 metres	1300 metres

Appendix H

Sample parameter table file

SAMPLE PARAMETER FILE

'D0012706.0' = Name of original saved parameter table file

125.00000000000000 = Horizontal TX-RX separation in meters

50.00000000000000 = Vertical TX-RX separation in meters

30.00000000000000 = Base Frequency in Hertz

130.20833333333333 = Sample Interval in micro-seconds

20 Time Gates, First and Last Sample number:

20	2	3
----	---	---

19	4	13
----	---	----

18	14	23
----	----	----

17	24	33
----	----	----

16	34	34
----	----	----

15	35	35
----	----	----

14	36	37
----	----	----

13	38	39
----	----	----

1	40	41
---	----	----

2	42	44
---	----	----

3	45	47
---	----	----

4	48	51
---	----	----

5	52	56
---	----	----

6	57	62
---	----	----

7	63	69
---	----	----

8	70	77
---	----	----

9	78	86
---	----	----

10	87	98
----	----	----

11	99	112
----	----	-----

12	113	128
----	-----	-----

128 Samples. X,Y,Z,T waveforms in microVolts:

1	14675	-661	11897	-688
---	-------	------	-------	------

2	911262	-55983	519035	-11901
---	--------	--------	--------	--------

3	1709430	-97688	925387	-56506
---	---------	--------	--------	--------

4	1734052	-99747	926706	-104344
---	---------	--------	--------	---------

5	1678316	-96873	895411	-150269
---	---------	--------	--------	---------

6	1602132	-92483	854211	-194091
---	---------	--------	--------	---------

7	1509451	-87169	804378	-235407
---	---------	--------	--------	---------

8	1401621	-80936	746414	-273788
---	---------	--------	--------	---------

9	1279878	-73861	681078	-308837
---	---------	--------	--------	---------

10	1145721	-66110	609107	-340321
----	---------	--------	--------	---------

11	1000696	-57762	531412	-367955
----	---------	--------	--------	---------

12	846485	-48785	448744	-391584
----	--------	--------	--------	---------

13	684608	-39421	362102	-410950
----	--------	--------	--------	---------

14	516946	-29800	272327	-425877
----	--------	--------	--------	---------

15	345374	-19827	180536	-436222
----	--------	--------	--------	---------

16	171568	-9810	87633	-441932
17	-2335	242	-5354	-442942
18	-174755	10184	-97481	-439249
19	-343675	20008	-187766	-431010
20	-507725	29471	-275230	-418308
21	-664577	38592	-359027	-401298
22	-813421	47189	-438367	-380204
23	-952399	55138	-512352	-355309
24	-1079856	62515	-580304	-326896
25	-1195149	69228	-641614	-295291
26	-1296663	75058	-695566	-260876
27	-1383818	80104	-741808	-224051
28	-1455587	84228	-779835	-185260
29	-1511438	87446	-809328	-144896
30	-1551011	89742	-830104	-103391
31	-1573907	91078	-841936	-61170
32	-1488026	86300	-782325	-19005
33	-261690	12288	-113731	2076
34	-48090	4235	-22433	542
35	-11557	1072	-6349	475
36	-11458	819	-6482	588
37	-11079	789	-6212	602
38	-9577	714	-5394	615
39	-8567	634	-4827	631
40	-7813	633	-4387	637
41	-7099	505	-3937	654
42	-6482	520	-3582	652
43	-6022	435	-3287	659
44	-5575	385	-3056	659
45	-5003	448	-2791	661
46	-4819	367	-2584	662
47	-4439	324	-2439	664
48	-4140	330	-2192	671
49	-3901	258	-2113	665
50	-3676	305	-1949	674
51	-3445	274	-1831	667
52	-3258	248	-1685	664
53	-3009	194	-1603	670
54	-2926	232	-1494	661
55	-2682	216	-1425	662
56	-2620	204	-1355	656
57	-2539	165	-1240	665
58	-2296	160	-1207	663
59	-2245	173	-1153	650
60	-2122	170	-1056	651

61	-2028	163	-1035	652
62	-1949	124	-983	658
63	-1840	133	-924	649
64	-1743	154	-863	634
65	-1666	114	-825	644
66	-1648	125	-805	648
67	-1530	120	-773	643
68	-1482	117	-710	644
69	-1443	150	-710	642
70	-1318	137	-652	646
71	-1354	92	-658	642
72	-1316	94	-618	643
73	-1229	146	-589	639
74	-1195	107	-568	640
75	-1154	113	-523	642
76	-1068	112	-558	632
77	-1030	77	-494	628
78	-1102	69	-477	635
79	-994	65	-456	638
80	-976	95	-428	631
81	-997	1	-448	630
82	-835	148	-402	628
83	-805	23	-412	633
84	-943	129	-402	637
85	-770	47	-366	629
86	-772	101	-383	627
87	-799	80	-354	629
88	-750	49	-339	620
89	-774	99	-344	628
90	-718	87	-304	633
91	-701	70	-307	628
92	-717	61	-330	622
93	-619	93	-269	619
94	-694	51	-293	621
95	-617	72	-275	620
96	-614	104	-247	620
97	-643	59	-283	619
98	-593	55	-264	620
99	-624	72	-252	623
100	-562	54	-254	624
101	-589	64	-251	624
102	-494	38	-194	625
103	-590	39	-240	619
104	-545	67	-210	619
105	-518	36	-205	611

106	-522	68	-186	615
107	-380	69	-224	620
108	-620	4	-190	617
109	-479	84	-181	610
110	-443	27	-206	611
111	-460	49	-169	622
112	-417	34	-187	607
113	-451	57	-153	619
114	-433	77	-164	613
115	-400	44	-132	611
116	-412	55	-194	611
117	-381	62	-159	609
118	-399	42	-141	610
119	-361	65	-144	610
120	-342	70	-154	617
121	-349	48	-106	614
122	-363	72	-144	607
123	-344	34	-131	603
124	-418	64	-153	607
125	-340	41	-124	609
126	-364	29	-127	608
127	-342	75	-139	613
128	-334	47	-127	609

**CONVERSION FACTORS TO NORMALIZE THE EM DATA
FROM PV/M² to PPM**

FLIGHT N°	X-COIL	Z-COIL
1	0.0248	0.0335
2	0.0359	0.0496
3	0.0350	0.0491
5	0.0354	0.0483
6	0.0337	0.0544
7	0.0352	0.0528
8	0.0352	0.0538
9	0.0347	0.0566
11	0.0324	0.0609
12	0.0346	0.0528
13	0.0344	0.0549
14	0.0329	0.0636
15	0.0320	0.0667
16	0.0326	0.0659
17	0.0326	0.0651
18	0.0318	0.0659

Note:

1. The conversion factors should be applied as multipliers.
2. Flight 1 was a test flight flown with 90 Hz/2 ms, hence the difference between it and the other flights flown with 30 Hz/4 ms.

Appendix J

Production Log

BASE: ALBUQUERQUE, NEW MEXICO							JOB NO: 319				
Date	Flt.	Km.	Total Km.	Balance	Hr./Flt.	Total Hours	REMARKS	Elec. Operator	Oper. Day	Daily Average Km.	Km/Hour
Feb. 18	-	0.0	0.0	3,763.0		0.0	Ground station setup - Pilot flight training. Grounded - disabled pilot. Pilot flight training.				ERR
Feb. 19	-	0.0	0.0	3,763.0	0.0	0.0		1	0.0	ERR	
Feb. 20	-	0.0	0.0	3,763.0	0.0	0.0		2	0.0	ERR	
Feb. 21	-	0.0	0.0	3,763.0	0.0	0.0	Grounded - awaiting replacement pilot. Survey test @ 90 Hz - RioRancho. Survey test @ 30 Hz - RioRancho.		3	0.0	ERR
Feb. 22	1	112.9	112.9	3,650.1	1.5	1.5		R.P. + J.M.	4	28.2	75.2
Feb. 23	2	56.8	169.7	3,593.3	1.6	3.1		R.P.	4	42.4	54.7
Feb. 24	3	396.1	565.8	3,197.2	3.0	6.1	Survey @ 30 Hz - RioRancho. Wx out - extremely high winds. Wx out - high winds.	R.P. + J.M.	5	113.2	92.7
Feb. 25	-	0.0	565.8	3,197.2	0.0	6.1		6	94.3	92.7	
Feb. 26	-	0.0	565.8	3,197.2	0.0	6.1		7	80.8	92.7	
Feb. 27	4	0.0	565.8	3,197.2	1.0	7.1	Backup EM bird test flight. Grounded awaiting flying permit. Grounded awaiting flying permit.	R.P.	8	70.7	79.7
Feb. 28	-	0.0	565.8	3,197.2	0.0	7.1		9	62.9	79.7	
Mar. 1	-	0.0	565.8	3,197.2	0.0	7.1		10	56.6	79.7	
Mar. 2	5	558.8	1,124.6	2,638.4	3.6	10.7	Survey - RioRancho. Survey - RioRancho. Survey - RioRancho.	R.P. + J.M.	11	102.2	105.1
Mar. 3	6	485.6	1,610.2	2,152.8	2.9	13.6		R.P. + J.M.	11	146.4	118.4
Mar. 4	7	428.6	2,038.8	1,724.2	2.9	16.5		J.M.	12	169.9	123.6
Mar. 5	8	287.5	2,326.3	1,436.7	3.0	19.5	Survey - RioRancho. Survey - Cochiti. Flight scrubbed - bad mag. Electronics test flight.	J.M.	12	193.9	119.3
Mar. 6	9	0.0	2,326.3	1,436.7	3.8	23.3		J.M.	13	178.9	99.8
Mar. 7	10	0.0	2,326.3	1,436.7	1.0	24.3		R.P.	13	178.9	95.7
Mar. 8	11	63.5	2,389.8	1,373.2	1.3	25.6	Survey - Cochiti. Flight aborted - high winds. Survey - Cochiti. Survey - Cochiti.	R.P.	14	170.7	93.4
Mar. 9	12	317.0	2,706.8	1,056.2	3.5	29.1		D.P.	15	180.5	93.0
Mar. 10	13	394.8	3,101.6	661.4	3.3	32.4		D.P. & J.M.	16	193.9	95.7
Mar. 11	14	345.1	3,446.7	316.3	3.0	35.4	Survey - Cochiti. Survey - Cochiti/RioRancho. Survey - RioPuerco.	D.P. & J.M.	17	202.7	97.4
Mar. 12	15	253.9	3,700.6	62.4	3.1	38.5		D.P. & J.M.	17	217.7	96.1
Mar. 13	16	62.4	3,763.0	(0.0)	2.2	40.7		D.P.	17	221.4	92.5
Mar. 14	17	120.0	3,883.0	(120.0)	2.1	42.8	Survey - additional lines. Survey - additional lines.	D.P. & J.M.	18	215.7	90.7
Mar. 15	18	112.0	3,995.0	(232.0)	1.9	44.7		D.P.	19	210.3	89.4